^{13}C metabolic flux analysis of industrial Chinese hamster ovary (CHO) cell cultures

By

Allison Grace McAtee Pereira

Dissertation

Submitted to the Faculty of the

Graduate School of Vanderbilt Engineering

in partial fulfillment of the requirements

for the degree of

DOCTOR OF PHILOSOPHY

in

Chemical Engineering

December 15, 2018

Nashville, Tennessee

Approved:

Jamey D. Young, Ph.D.

Matthew Lang, Ph.D.

John T. Wilson, Ph.D.

Robert Carnahan, Ph.D.

To my family, for their constant love and support.
And, to my daughter, Grace—may you always know that you are capable of anything.

"It is not the critic who counts; not the man who points out how the strong man stumbles, or where the doer of deeds could have done them better. The credit belongs to the man who is actually in the arena, whose face is marred by dust and sweat and blood; who strives valiantly; who errs, who comes short again and again, because there is no effort without error and shortcoming; but who does actually strive to do the deeds; who knows great enthusiasms, the great devotions; who spends himself in a worthy cause; who at the best knows in the end the triumph of high achievement, and who at the worst, if he fails, at least fails while daring greatly, so that his place shall never be with those cold and timid souls who neither know victory nor defeat."

— *Theodore Roosevelt*

ACKNOWLEDGEMENTS

The last six and a half years at Vanderbilt have been an exciting time in my life and I owe my success to the support of countless people. First, I want to thank my advisor, Jamey Young, for his mentorship and guidance in my professional and personal development. I am thankful for his immense patience with me as I discovered what it means to be a scientific researcher and his extreme faith in me as we adventured into a new realm of metabolic engineering. The Young Lab has always been a family and I am so thankful I was welcomed in with open arms.

I would also like to thank the other members of my committee Matthew Lang, John Wilson, and Robert Carnahan for their continued support over the years of my dissertation projects. Their unique sets of expertise guided my ever-evolving projects and ultimately led to the completion of this dissertation. I am also thankful for the collaborators, both on and off Vanderbilt's campus, who have helped steer my projects during my time here. Dr. Carnahan and Tracy Cooper from the Vanderbilt Antibody and Protein Resource (VAPR) CORE provided invaluable insight into CHO cell culture transfection methods. Dr. Josh Fessel provided invaluable insight into mitochondrial metabolism and his lab provided training and materials vital to move my project forward. From Johns Hopkins University, the Betenbaugh lab has provided much supporting work and brainstorming throughout my tenure at Vanderbilt. Each of my projects presented within this dissertation were in collaboration with pharmaceutical companies. Specifically, I would like to thank Kristen Douglas of Genentech, Jason Walther of Sanofi, and Kevin Smith of Janssen.

My time at Vanderbilt would not have been the same without the support, collaboration, and friendship of the members of the Young Lab both past and present. I have had the great honor to work with every graduate student and post-doc to enter into the Young Lab to date. I am

very thankful for Taylor Murphy, Rob Egnatchick, Alex Leamy, Casey Duckwall, Lara Jazmin, Young Mi Whang, and Neil Templeton for helping me transition into the laboratory and being invaluable resources on everything from lab protocols to everything flux analysis during their time in the lab. Specifically, I'm extraordinarily thankful for Neil Templeton's help and guidance as I began my research projects in the lab. Much of what I learned in the lab as far as techniques and protocols I owe to his teachings. Thanks to my classmate Adeola Adebiyi, who entered the lab and underwent the induction to metabolic flux analysis with me and to Martha Wall for the invaluable MATLAB assistance and tool development that helped my work tremendously during my time in the lab. I genuinely appreciate the time I've spent in the Young Lab and the conversations I've had with Ian Cheah, Mohsin Rahim, Sarah Sacco, and Amy Zheng. I will never be able to thank Clint Hasenour enough for the invaluable conversations he took the time to have with me pertaining to my projects during his time in the lab. I am immensely grateful to Irina Trenary and her assistance on all things during my tenure in the Young Lab. Her assistance enabled me to continue performing experiments while pregnant and get data while I was home on maternity leave.

I am eternally grateful for all of the friendships I have made during my time living in Nashville. My cohort including Will Erwin, Christoph Klein, Andrew Summers, Joe Webb, Adeola Adebiyi, and Holly Zarick was such a family to me for the first several years of the program and I will never forget the homework sessions on the porch and the many conversations in the first-year office. Finally, I will be forever grateful for the community of friends I made during this time of my life—Anne Talley, Sonia Brady, Nikki Reinemann, Lara Jazmin, Holly Zarick, Meredith Moore, May Ou, and many others in the Vanderbilt ChBE department and community for their friendship and support.

Finally, I lived a lot of life during my stint in Nashville. This will forever be the city where I met my husband, George, became a mother to my daughter, Grace, and adopted my fur-baby, Aria. My family has been incredibly supportive of me throughout my years pursuing my PhD. My mom, Robin McAtee, has always encouraged me to pursue my dreams and through her example of attaining her own PhD, I knew it could be done. Her dissertation defense was the first I attended as a teenager and it was a full-circle moment to have her attend my dissertation defense so many years later. My father, Brent, sisters, Brandi and Abby, and all of my extended family has provided me with the love, support, and the shoulders to lean on during rough times responsible for getting me through this process. They have always encouraged me to pursue my dreams and provided nothing but love and support—and for that, I am eternally thankful.

I would also like to acknowledge the National Science Foundation (NSF) for funding the work presented here. I was funded through an NSF GRFP (graduate research fellowship program) award and our collaboration with Janssen was funded by an NSF GOALI grant (CBET-1604426).

TABLE OF CONTENTS

Page

DEDICATION……ii

ACKNOWLEDGEMENTS……iii

LIST OF TABLES……..ix

LIST OF FIGURES……xi

LIST OF ABBREVIATIONS…….……xvii

Chapter

1 INTRODUCTION 1

1.1 References 4

2 BACKGROUND AND SIGNIFICANCE 6

2.1 Chinese hamster ovary cells in biomanufacturing 6
2.2 Energy metabolism and protein production 9
2.3 ^{13}C metabolic flux analysis allows for the quantification of energy metabolism 12
2.4 References 20

3 ^{13}C MFA of industrial CHO cells overexpressing the global metabolic regulator PGC-1α..... 27

3.1 Summary 27
3.2 Introduction 28
3.3 Materials and methods 31
3.3.1 Generation of cell lines 31
3.3.2 Characterization of stable PGC-1α overexpressing lines 33
3.3.3 Generation and characterization of stable empty vector (EV) overexpressing lines …..... 33
3.3.4 Total RNA isolation and quantitative real-time PCR 34
3.3.5 Cell culture and isotope labeling experiment..... 34
3.3.6 Determination of growth and extracellular exchange rates 35
3.3.7 Oxygen consumption measurements 36
3.3.8 Gas chromatography-mass spectrometry (GC-MS) measurements..... 36
3.3.9 ^{13}C isotopically non-stationary metabolic flux analysis (INST-MFA)..... 36
3.3.10 Statistical analysis..... 37
3.4 Results..... 37
3.4.1 Stable PGC-1α lines exhibit higher PGC-1α mRNA levels than parental control line..... 37
3.4.2 PGC-1α lines consume more oxygen than the control 38
3.4.3 Net growth rates of all PGC-1α lines except C1 are similar to the parental control.. 38

3.4.4 PGC-1α lines exhibit higher volumetric titers and qP than the control 40
3.4.5 PGC-1α lines consume both glucose and lactate at higher rates than the control. 40
3.4.6 PGC-1α lines have higher oxidative metabolic fluxes than control 41
3.4.7 EV overexpressing cell lines 41
3.5 Discussion 43
3.6 Future Directions 46
3.7 Appendix 48
3.8 References 58

4 ^{13}C FLUX ANALYSIS REVEALS THAT REBALANCING MEDIUM AMINO ACID COMPOSITION CAN REDUCE AMMONIA PRODUCTION WHILE PRESERVING CENTRAL CARBON METABOLISM OF CHO CELL CULTURES. 63

4.1 Summary 64
4.2 Introduction 64
4.3 Materials and methods 67
4.3.1 Media 67
4.3.2 Cell Culture 67
4.3.3 Parallel ^{13}C Labeling Studies 68
4.3.4 Analytical Techniques 69
4.3.5 Metabolic Flux Analysis 70
4.3.6 Statistical Analysis 71
4.4 Results 71
4.4.1 Ammonia production was reduced in LA medium without altering growth, viability, or mAb specific productivity 71
4.4.2 Glutamine, but not glucose, uptake was reduced in LA medium 73
4.4.3 Alanine production is associated with ammonia accumulation 74
4.4.4 Glycolysis and PPP fluxes were not significantly altered in LA medium 75
4.4.5 CAC fluxes were not significantly altered in LA medium, despite variations in anaplerotic contributions from certain amino acids 76
4.5 Discussion 77
4.6 Appendix 80
4.7 References 105

5. ^{13}C METABOLIC FLUX ANALYSIS IN LABELING CHO CELL STATIONARY GROWTH PHASE 111

5.1. Summary 111
5.2. Background and Introduction 112
5.3. Materials and Methods 115
5.3.1. Cell Culture 115
5.3.2. Analytical techniques 116
5.3.3. ^{13}C Metabolic flux analysis 117
5.3.4. Statistical analysis 118
5.4. Results 119
5.4.1. CHO cells overexpressing anti-apoptotic genes survive longer with higher VCDs . …..... 119

5.4.2. Anti-apoptotic gene overexpression altered extracellular CHO cell fluxes during stationary phase 121
5.4.3. Anti-apoptotic gene overexpression led to trends in increased mitochondrial metabolism 122
5.5. Discussion 123
5.6. Appendix 126
5.7. Reference 130

6. ^{13}C FLUX ANALYSIS IN DETERMINING OXIDATIVE PENTOSE PHOSPHATE PATHWAY ACTIVITY IN INDUSTRIAL CHINESE HAMSTER OVARY (CHO) CELL LINES 134

6.1. Summary 135
6.2. Background and Introduction 135
6.3. Materials and Methods 139
6.3.1. Cell Culture 139
6.3.2. Analytical techniques 140
6.3.3. ^{13}C Metabolic flux analysis 140
6.3.4. Statistical analysis 141
6.4. Results 141
6.5. Discussion and Future Directions 143
6.6. Appendix 146
6.7. References 151

7. CONCLUSIONS 154

7.1. Future Directions 155
7.2. Contribution 157
7.3. References 174

LIST OF TABLES

Table 3-1 Experimental timeline of ^{13}C labeling experiments. Days 5-8 are shaded to indicate presence of^{13}C glucose in the cell culture medium. The ^{13}C glucose bolus fed on day 5 initiated the labeling experiment (time = 0 hours), and samples were withdrawn and cold quenched at multiple time points to measure ^{13}C enrichments of intermediate metabolites. 35

Table A-3-1 Model goodness-of-fit assessment metrics as determined by INCA software and the best-fit model for each cell line. 48

Table A-3-2 Precursor requirements for growth. 48

Table A-3-3 Flux maps with 95% confidence intervals indicated by lower bound (LB) and upper bound (UB). 51

Table 4-1 Relative amino acid composition of Low Ammonia (LA) medium. Values indicate fold-changes relative to CM. 67

Table A- 4-1 Flux maps of the three media conditions with 95% confidence intervals; CM=control medium, LA=low ammonia medium, LA+=low ammonia medium with added ammonia. LB-lower bound of 95% confidence interval, UB-upper bound of 95% confidence interval. An '.e' indicates an extracellular metabolite pool; '.m' indicates a mitochondrial metabolite pool; '.u' indicates an unlabeled metabolite pool; and a '.l' indicates a labeled metabolite pool. 80

Table A- 4-2 Growth (day^{-1}) and antibody (nmol/Mcell/day) fluxes for the three media conditions. 82

Table A- 4-3 Metabolite fragments measured by GC-MS for analysis of intracellular metabolite labeling. 83

Table A- 4-4 Model goodness-of-fit assessment. 84

Table A- 4-5 Pyruvate contribution to anaplerosis. PC=pyruvate carboxylase, ME=malic enzyme, PC-ME=difference between PC and ME fluxes (i.e., net anaplerotic flux from pyruvate). CM=control medium, LA=low ammonia medium, LA+=low ammonia medium with added ammonia. SE=standard error of flux estimate, LB=lower bound of 95% confidence interval, UB=upper bound of 95% confidence interval, CI=confidence interval. 85

Table A- 4-6. Biomass composition. 86

Table A- 4-7 Antibody composition (mol/mol). 87

Table 5-1 Description of each cell line studied. Genes overexpressed in each cell line and ^{13}C tracer fractional enrichment data for each cell line are detailed below. 117

Table A- 5-1 Model goodness-of-fit assessment, where SSR is the sum of squares residual. .. 126

Table A- 5-2 Precursor requirements for growth. 127

Table A- 5-3 Flux maps of each cell line with overall flux value in (mmol/10Bcells/day) with 95% confidence intervals reported as a lower bound (LB) and upper bound (UB) for each reported flux value. 128

Table A- 5-4 Metabolite fragments measured by GC-MS for analysis of intracellular metabolite labeling..... 129

Table 6-1 Metabolic model used for ^{13}C MFA with carbon rearrangements shown as lowercase letters. H6P represents six-carbon molecules G6P and F6P. T3P represents three-carbon molecules DHAP and GAP. P5P represents five-carbon Ru5P, R5P, and X5P. Lac.u is unlabeled lactate..... 141

Table A- 6-1 Model goodness-of-fit assessment metrics as determined by INCA software and the best fit model at each time point. *indicates lack of fit in the model. 146

Table A- 6-2 Flux values at Day 0. Fluxes are reported as a percent of glucose uptake rate. ... 146

Table A- 6-3 Flux values at Day 1. Fluxes are reported as a percent of glucose uptake rate. ... 147

Table A- 6-4 Flux values at Day 2. Fluxes are reported as a percent of glucose uptake rate. ... 147

Table A- 6-5 Flux values at Day 3. Fluxes are reported as a percent of glucose uptake rate. ... 147

Table A- 6-6 Flux values at Day 3.5. Fluxes are reported as a percent of glucose uptake rate. 148

Table A- 6-7 Flux values at Day 4. Fluxes are reported as a percent of glucose uptake rate. ... 148

Table A- 6-8 Flux values at Day 6. Fluxes are reported as a percent of glucose uptake rate. ... 148

Table A- 6-9 Flux values at Day 8. Fluxes are reported as a percent of glucose uptake rate. ... 149

Table A- 6-10 Flux values at Day 10. Fluxes are reported as a percent of glucose uptake rate. 149

Table A- 6-11 Flux values at Day 12. Fluxes are reported as a percent of glucose uptake rate. 149

LIST OF FIGURES

Figure 2-1 The role of glutamine synthetase (GS). GS allows for the synthesis of glutamine from glutamate and is not expressed at high endogenous levels in CHO cells. 8

Figure 2-2 ^{13}C metabolic flux analysis (MFA) allows researchers to peek inside the black box to elucidate metabolic phenotype beyond that described by extracellular analysis alone. On the left, inputs and outputs can be quantified; however, it is impossible to define intracellular metabolic fluxes without further information due to the large number of unknown fluxes. ^{13}C MFA applies ^{13}C tracers to provide such information. V_i indicates an individual flux value; A-G represent generic intracellular metabolites. 11

Figure 2-3 ^{13}C metabolic flux analysis workflow. (A) Stably labeled ^{13}C isotopic substrate (e.g., glucose) is fed to cell cultures. (B) Intracellular metabolites are analyzed for ^{13}C incorporation. (C) Intracellular metabolite ^{13}C labeling is simulated from an established network of metabolic reactions. (D) These simulated labeling data are compared to the experimentally measured labeling data. (E) From the lack of fit between the simulated and measured isotopic data, the fluxes of the reaction network are adjusted, and (F) the process detailed in steps (C)-(E) are repeated until the lack of fit is minimized to a statistically acceptable level. 13

Figure 2-4 Comparison of stationary metabolic flux analysis (MFA) and isotopically nonstationary (INST)-MFA. The left panel shows conventional MFA while the right panel shows INST-MFA based on the analysis of samples collected prior to isotopic steady state. 15

Figure 2-5 Discerning the split of glycolysis and pentose phosphate pathway metabolic activity. The mass isotopomer distribution of pyruvate if generated purely through glycolysis or the PPP is shown. Any linear combination of the two can exist as cells generally utilize both pathways simultaneously. Linear regression can be used to determine the actual split ratio of glycolysis/PPP by fitting the experimental data to a mathematical model that accounts for the stoichiometry and atom rearrangements caused by the metabolic network..... 17

Figure 3-1 Role of PGC-1α as a master regulator of mitochondrial biogenesis. PGC-1α can be induced by CREB and activated by a variety of post-translational modifications including SIRT1 deacetylation and AMP kinase dependent phosphorylation. Active PGC-1α is a transcriptional co-activator which allows transcription factors such as NRF-1 to promote the nuclear expression of numerous mitochondrial genes including TFAM—a mitochondrial transcription factor that initiates expression of the mitochondrial genome resulting in mitochondrial biogenesis. 29

Figure 3-2 Recombinant PGC-1α mRNA levels reported as fold changes over control expression. Expression levels were normalized to expression of the housekeeping gene, HPRT, on day seven of the fed-batch experiment as indicated in **Table 1**. Means +/- SEM plotted, n=2. 38

Figure 3-3 Oxygen uptake rates (OURs) of the four PGC-1α CHO cell lines compared to the C2869Acontrol line. Means +/- SEM reported, n=2; **** indicates significant difference from the control, α <0.0001; ** α<0.01..... 39

Figure 3-4 (A) Growth curves over the full duration of the experiment. (B) Net growth rates calculated during stationary growth phase (days 5-8). (C) Death rates of each line during stationary growth phase. The gross growth rate reported in **Figure A-1** was calculated by adding the death rates in (C) to the net growth rates in (B). Means +/- SEM reported, n=4; **** indicates significant difference from control, α<0.0001..... 39

Figure 3-5 (A) mAb titer profiles, (B) final volumetric mAb titer measured on day eight of the experiment, and (C) cell specific productivity (qP) of each line. Means +/- SEM shown, n=4; *** indicates significant difference from control, α <0.001, **** α <0.0001..... 40

Figure 3-6 (A) Glucose uptake rate (GUR) and (B) lactate uptake rate (LUR) of each cell line. Means +/- SEM shown, n=4; ** indicates significant difference from control, α <0.01, *** α <0.001, **** α <0.0001..... 41

Figure 3-7 Metabolic flux maps during stationary growth phase. The magnitude of each reported net carbon flux corresponds with the color and the width of the corresponding arrow. The mitochondrial oxidative citric acid cycle fluxes are boxed for emphasis..... 42

Figure A-3-1 Gross growth rates during stationary growth phase. Gross growth was used in the ^{13}C MFA experimental analysis as it accounts for total biomass generation. Means +/- SEM plotted, n=4; *** indicates significant difference from control, α <0.001. 49

Figure A-3-2 Specific growth rates during exponential growth phase. The control line (C2869A) and line C1 trend together while the remaining PGC-1α lines experience significantly decreased rates of growth during exponential phase, days zero through five of the experiment. Means +/- SEM plotted, n=4; *** indicates significant difference from control, α <0.001, **** α <0.0001..... 49

Figure A-3-3 Viability profiles of the cultures. Mean +/- SEM reported; n=4..... 50

Figure A-3-4 Anti- PGC-1α Western Blot (WB) of the selected PGC-1α lines and parental line (leftmost lane). C1 appeared to express a different PGC-1α isoform than the other lines. Anti-PGC-1α antibody should detect both recombinant and endogenous PGC-1α. Intact PGC-1α should be detected at 113 kDa, NT- PGC-1α at 37 kDa, and PGC-1α4 at 29.1 kDa. 50

Figure A-3-5 Average percent enrichments (APEs) of intracellular metabolites over the course of the experiment. Isotopic steady state is reached when the fractional enrichment does not change over time. These data prompted the conclusion that isotopic steady state was not obtained. Therefore, INST-MFA was used to regress fluxes in the stationary phase CHO cell cultures studied here..... 52

Figure A-3-6 Average percent enrichments (APEs) of intracellular metabolites over the course of the experiment (continued). Isotopic steady state is reached when the fractional enrichment does not change over time. These data prompted the conclusion that isotopic steady state was not obtained. Therefore, INST-MFA was used to regress fluxes over time in the CHO cell cultures studied here. 53

Figure A-3-7 Average percent enrichments (APEs) of intracellular metabolites over the course of the experiment (continued). Isotopic steady state is reached when the fractional enrichment does not change over time. These data prompted the conclusion that isotopic steady state was not obtained. Therefore, INST-MFA was used to regress fluxes over time in the CHO cell cultures studied here. 54

Figure A-3-8 Flux results of selected intracellular fluxes. Means +/- SEM reported, n=2. 55

Figure A-3-9 Characterization of twelve of the twenty PGC-1a stable lines generated from mini-pool selection. The other eight lines were not measured due to their lack of PGC-1a mRNA expression (measured via RT qPCR), and three with no mAb expression are not included here. The gray bars are the lines chosen for the ^{13}C MFA study described in this chapter. Mean +/- SEM, n=2; grown in batch and measured during stationary growth phase. 55

Figure A-3-10 Comparison of EV- and PGC-1α stable lines specific productivities (qP) in descending order normalized to the C2869A control line. Other lines are denoted as indicated by the accompanying table. These experiments were performed in batch growth and measurements were taken over stationary phase. N=2. 56

Figure A- 3-11 Comparison of EV- and PGC-1α stable lines mAb volumetric titers in descending order. All values are normalized to the respective control, C2869A. All lines are displayed as indicated in the accompanying table. 56

Figure A- 3-12 ΔGUR and ΔLUR of EV and PGC-1a lines plotted in descending order. The ΔGUR and ΔLUR values were calculated by subtracting the GUR and LUR of the respective control. Cultures were grown in batch culture and measurements taken during stationary growth phase. 57

Figure 4-1 Experimental design. Cells were passaged approximately every three days. Parallel labeling experiments with [1,2-$^{13}C_2$]glucose and [U-$^{13}C_5$]glutamine took place during passage 4 (P4). Culture samples collected from P3 flasks were used to determine dry cell weight..... 69

Figure 4-2 (A) Growth curve and (B) Percent viability of CHO cells cultured in the three media variants. Data indicate mean values +/- SEM, n=4..... 72

Figure 4-3 (A) Ammonia production rate and (B) mAb specific productivity of cultures in the experimental media conditions. Data indicate mean fluxes +/- SEM, n=4. ****α<0.0001; ***α<0.001; **α<0.01..... 72

Figure 4-4 (A) Glucose uptake rate (GUR) and glutamine uptake rate (QUR). (B) Excretion rates of alanine, aspartate, glutamate, and glycine. Data indicate mean fluxes +/- SEM, n=4. ****α<0.0001; *α<0.05. 74

Figure 4-5 (A) Central carbon metabolic map with enzymes of interest labeled. Arrow width represents flux in carbon moles for the CM condition. (B) Glycolytic fluxes, (C) pentose phosphate pathway (PPP) fluxes, and (D) citric acid cycle (CAC) fluxes during P4. Data indicate mean fluxes +/- SEM, n=4. 75

Figure 4-6 Anaplerotic fluxes through glutamate dehydrogenase (GDH) and aspartate transaminase (AST). In our flux model, GDH flux represents total anaplerosis from glutamate to alpha-ketoglutarate, while AST represents total anaplerosis from aspartate to oxaloacetate. Data indicate mean fluxes +/- SEM, n=4. 76

Figure A- 4-1 Average percent enrichments (APEs) of pyruvate and lactate for CM fed cells labeled with [1,2-$^{13}C_2$]glucose. 89

Figure A- 4-2 APEs of pyruvate and lactate for LA fed cells labeled with [1,2-$^{13}C_2$]glucose. ... 90

Figure A- 4-3 APEs of pyruvate and lactate for LA+ fed cells labeled with [1,2-$^{13}C_2$]glucose.. 91

Figure A- 4-4 APEs of malate and glutamate for CM fed cells labeled with [U-$^{13}C_5$]glutamine. 92

Figure A- 4-5 APEs of alanine, glycine, serine, aspartate, and asparagine for CM fed cells labeled with [U-$^{13}C_5$]glutamine. 93

Figure A- 4-6 APEs of malate and glutamate for LA grown cells labeled with [U-$^{13}C_5$]glutamine..... 94

Figure A- 4-7 APEs of alanine, glycine, serine, aspartate, and asparagine for LA grown cells labeled with [U-$^{13}C_5$]glutamine. 95

Figure A- 4-8 APEs of malate and glutamate for LA+ fed cells labeled with [U-$^{13}C_5$]glutamine. 96

Figure A- 4-9 APEs of alanine, glycine, serine, aspartate, and asparagine for LA+ fed cells labeled with [U-$^{13}C_5$]glutamine. 97

Figure A- 4-10 APEs of glutamine for cells cultured in each media variant. 100% of the intracellular glutamine was labeled by day 2. 98

Figure A- 4-11 MIDs of labeled intracellular metabolites as measured (gray bars) by GC-MS and simulated (black bars) by the best-fit model for the CM condition. 99

Figure A- 4-12 Fluxes of extracellular metabolites as measured (gray bars) and simulated (black bars) by the best-fit model for the CM condition. 100

Figure A- 4-13 MIDs of labeled intracellular metabolites as measured (gray bars) by GC-MS and simulated (black bars) by the best-fit model for the LA condition. 101

Figure A- 4-14 Fluxes of extracellular metabolites as measured (gray bars) and simulated (black bars) by the best-fit model for the LA medium condition. 102

Figure A- 4-15 MIDs of labeled intracellular metabolites as measured (gray bars) by GC-MS and simulated (black bars) by the best-fit model for the LA+ condition. 103

Figure A- 4-16 Fluxes of extracellular metabolites as measured (gray bars) and simulated (black bars) by the best-fit model for the LA+ medium condition. 104

Figure 5-1 Apoptosis signaling cascade in mammalian cells. The anti-apoptotic genes studied in this paper are shown in purple ovals. Bcl-2Δ and AVEN inhibit the signaling cascade that triggers apoptosis due to DNA damage while AVEN also inhibits the apoptosome complex early in the apoptotic process as shown. XIAP inhibits the activation of caspases 3, 7, and 9 which play a critical role in the late stages of apoptosis. Bcl-2Δ and E1B-19K are homologous. 115

Figure 5-2 (A) Viable cell densities and (B) percent viabilities over time. (C) Zoomed in data from boxed region in (A). (D) Zoomed in data from boxed region of (B). Means ± SEM plotted, n=5. *indicates significance relative to control (C1013A) at $\alpha<0.05$, ** $\alpha<0.01$, *** $\alpha<0.001$, and **** $\alpha<0.0001$. 119

Figure 5-3 Specific death rate of the studied cell lines during stationary growth phase. Means ± SEM plotted, n=5. † indicates significance from the control (C1013A) at $\alpha<0.1$. 120

Figure 5-4 (A) Glucose and (B) lactate uptake rates of the three cell lines during stationary phase. Means ± SEM plotted, n=5. ** indicates significance at $\alpha<0.01$, and † $\alpha<0.1$. (Unless noted by brackets, significance relative to control (C1013A). 120

Figure 5-5 (A) Serine, (B) threonine, (C) isoleucine, and (D) leucine consumption rates. Means ± SEM plotted, n=5. * indicates significance from control (C1013A) unless indicated by brackets at $\alpha<0.05$, ** $\alpha<0.01$, and † $\alpha<0.1$. 120

Figure 5-6(A) Aspartate, (B) glutamate, (C) asparagine, and (D) glycine extracellular fluxes. Negative flux indicates net consumption. Means ± SEM plotted, n=3. *indicates significance at $\alpha<0.05$, ** $\alpha<0.01$, **** $\alpha<0.0001$, † $\alpha<0.1$. 121

Figure 5-7 Intracellular fluxes where significant differences were calculated. (A) Lactate dehydrogenase (LDH), (B) propionyl-CoA carboxylase (PCC), (C) glycine synthase (Gly syn), (D) methionine catabolism (Met cat), (E) phenylalanine hydroxylase (PAH), (F) serine hydroxymethyl transferase (SHMT), (G) isoleucine catabolism (Ile cat), (H) leucine

catabolism (Leu cat), and (I) valine catabolism (Val cat). For reaction details corresponding to each enzyme reported, see the complete flux map in Table A- 5-3. Means ± SEM plotted, n=3. * indicates significance $\alpha<0.05$ and † $\alpha<0.1$. Significance reported relative to control (C1013A) unless otherwise noted by brackets. 122

Figure 5-8 Metabolic flux maps of the apoptosis resistant clones compared to the parental. Arrow width and color corresponds to flux value. 123

Figure A- 5-1 (A) Glucose and (B) lactate profiles. 126

Figure 6-1 The Thioredoxin (Trx) system is responsible for the disulfide (DS) bond reduction mechanism that can occur in the harvested cell medium. The NADPH that initiates the Trx system is created from the first steps of glycolysis and the pentose phosphate pathway. Thioredoxin reductase (TrxR) reduces Trx using that NADPH. The reduced Trx then reduces the DS bonds of the protein. The terminal enzyme has been identified as mammalian thioredoxin 1 (TXN1). 137

Figure 6-2 Carbon rearrangement of each lactate fragment as analyzed by GC/MS if a [1,2-$^{13}C_2$]Glucose molecule is metabolized through glycolysis. Dashed lines indicate intermediate reactions not shown. 137

Figure 6-3 Carbon rearrangement of lactate fragments as analyzed by GC/MS if a [1,2-$^{13}C_2$]Glucose molecule was metabolized through the OPPP. Dashed lines indicate intermediate reactions not shown. A 1 or 2 on an arrow indicates number of molecules shunted down that reaction. 138

Figure 6-4 Predicted labeling of (A) Lac 261 and (B) Lac 233 fragments if [1,2-$^{13}C_2$] glucose is metabolized through glycolysis or OPPP to generate lactate. 142

Figure 6-5 The ratio of M1 lactate over M2 lactate for both lactate fragments. There were no statistically significant differences between the two cell lines at any time. 142

Figure 6-6 Utilization of oxidative pentose phosphate pathway (OPPP) metabolism as a percentage of overall glucose metabolism. Means +/- SEM plotted, n=2. SEM calculated by dividing reaction 3 (Table 6-1) flux's 95% confidence interval upper and lower bounds by 3.92. 144

Figure A- 6-1 Lactate MIDs of both lactate fragments for each cell line. Labeling shown is corrected for natural ^{13}C abundances. 150

Figure A- 6-2 (A) Growth, (B) percent viability, (C) culture pH, (D) glucose profile, (E) lactate profile, and (F) glutamate profile over time. *Indicates significance at $\alpha<0.05$; ** $\alpha<0.01$; † $\alpha<0.1$. 150

LIST OF ABBREVIATIONS

AMBIC: ammonium bicarbonate
APE: average percent enrichment
AST: aspartate aminotransferase
bcl2: B-cell lymphoma 2
CAC: citric acid cycle
CHO: Chinese hamster ovary
CM: control medium
EMU: elementary metabolite unit
ER: endoplasmic reticulum
ETA: extracellular time course analysis
GC/MS: gas chromatography/mass spectrometry
GDH: glutamine dehydrogenase
GS: glutamine synthetase
GUR: glucose uptake rate
HPLC: high performance liquid chromatography
IDH: isocitrate dehydrogenase
INCA: isotopomer network compartmental analysis
INST-MFA: isotopically nonstationary metabolic flux analysis
IVCD: integrated viable cell density
LA: low ammonia producing medium
LA+: low ammonia producing medium plus ammonia
LB: lower bound (95% confidence interval)
LUR: lactate uptake rate
mAb: monoclonal antibody
ME: malic enzyme
MFA: metabolic flux analysis
MID: mass isotopomer distribution
MOX: methoxamine
MSX: L-Methionine sulfoximine
OAA: oxaloacetate
OPPP: oxidative pentose phosphate pathway
OUR: oxygen uptake rate
PC: pyruvate carboxylase
PGC-1α: peroxisome proliferator-activated receptor gamma coactivator 1-alpha
PPP: pentose phosphate pathway
qP: specific productivity
QUR: glutamine uptake rate
RT-qPCR: reverse transcriptase quantitative polymerase chain reaction
SEM: standard error of the mean
SSR: sum of squares residual
TBDMS: tert-butyldimethylsilyl chloride
TCA: tricarboxylic acid
Trx: thiorexodin
UB: upper bound (95% confidence interval)

VCD: viable cell density
WB: Western blot
XIAP: X-linked inhibitor of apoptosis protein

1 INTRODUCTION

The primary theme of this dissertation is the application of ^{13}C metabolic flux analysis (MFA) to the industrial biopharmaceutical hosts, Chinese hamster ovary (CHO) cells. The current climate of health crises in this country, and globally, driving the development of strategies to increase the metabolic efficiency and productivity of biomanufacturing hosts. Biotherapeutic drugs produced by CHO cells are used in the treatment of a myriad of conditions such as cancer, infertility, rheumatoid arthritis, diabetes, and more [1]. With the aging population and increase of obesity related illnesses, the scope for antibody and other protein therapeutics is ever expanding. Therefore, there is a critical need to characterize and assess metabolic phenotypes of these host organisms such that clones can be engineered for optimal production of therapeutics in the most cost efficient method possible.

^{13}C MFA is a robust analytical tool for evaluating intracellular metabolic fluxes [2–5]. Here, we demonstrate the versatility of ^{13}C MFA in assessing CHO cell metabolic phenotypes resulting from various experimental conditions. This dissertation discusses the results of these ^{13}C MFA experiments on CHO cells in the following chapters:

Chapter 2 expounds the relevance of CHO cells in biopharmaceutical manufacturing and provides a summary of CHO cell energy metabolism as it relates to this dissertation. The ^{13}C MFA methodologies upon which this dissertation builds are highlighted in detail along with the current state of CHO cell metabolic analysis.

Chapter 3 details the development and metabolic analysis of industrial CHO cells engineered to overexpress a global regulator of oxidative metabolism, PGC-1α [6,7]. From previous work performed in this lab [8,9], high-producing CHO cells have been discovered to have a higher rate

of oxidative metabolic activity than those producing lower amounts of product protein. Upon this foundation, we set out to induce an increase in oxidative metabolic fluxes in CHO cells to increase product protein production. Stable cell lines were developed and studied in fed-batch reactions imitating industrial growth conditions. The resulting engineered clones consumed up to 2.4-fold more oxygen, exhibited an approximate 300% increase in oxidative mitochondrial metabolic fluxes, and increased mAb productivities by up to 5.2-fold over parental cultures.

Chapter 4 provides the results of ^{13}C MFA experiments on industrial CHO cells grown in a proprietary medium designed to reduce ammonia production and accumulation [10]. Ammonia is a toxic byproduct produced by industrial CHO cell cultures [11,12]. Sanofi developed a novel proprietary medium designed to prohibit the excess production and accumulation of ammonia by manipulating the amino acid profile of said medium. Cells cultured in the experimental medium were profiled in comparison to cells cultivated in a control medium. To further examine the specific effects of ammonia on cell metabolism, we also performed studies with the novel experimental medium supplemented with ammonia to the levels observed during growth on the control medium. The metabolic phenotype of CHO cells cultivated in each medium were compared and it was discovered that the proprietary low-ammonia medium did not significantly alter central carbon metabolism while significantly decreasing ammonia production.

Chapter 5 details the development of protocols and methodology for fed-batch ^{13}C MFA studies performed on CHO cells during stationary growth phase. The stationary growth phase is when the majority of product protein is manufactured and secreted by CHO cell cultures [13]. This phase occurs after the cells have transitioned out of exponential growth. In order to study intracellular metabolism during stationary phase only, the isotope tracer needs to be fed during the switch from exponential to stationary growth phase in order to avoid secondary tracer

effects—the consumption of ^{13}C labeled byproducts previously secreted by the cells during exponential growth phase. The experimental design from this experiment laid the foundation for the experiments detailed in chapter 3.

Chapter 6 summarizes a simplified metabolic study of industrial CHO cells to determine if intracellular metabolism was responsible for post-production breakdown of the product protein. Two CHO cell lines producing an identical protein product were experiencing variations in protein quality. One cell line was producing protein that was being degraded post-secretion due to disulfide bond reduction. ^{13}C MFA was performed on each cell line to determine if increased NADPH production via oxidative pentose phosphate pathway (OPPP) was to blame for the breakdown of disulfide bonds in culture. We discovered that OPPP fluxes were not significantly altered between the two cell lines; therefore, the original hypothesis of excess NADPH causing the breakdown observed in the culture was disproven.

Chapter 7 provides the conclusions from this dissertation as well as future directions for the research presented within.

1.1 References

[1] An Z. Monoclonal antibodies - a proven and rapidly expanding therapeutic modality for human diseases. Protein Cell 2010;1:319–30. doi:10.1007/s13238-010-0052-8.

[2] Young JD. 13C metabolic flux analysis of recombinant expression hosts. Curr Opin Biotechnol 2014;30:238–45. doi:10.1016/j.copbio.2014.10.004.

[3] Sauer U. Metabolic networks in motion: 13C-based flux analysis. Mol Syst Biol 2006;2:62. doi:10.1038/msb4100109.

[4] Zamboni N, Sauer U. Novel biological insights through metabolomics and 13C-flux analysis. Curr Opin Microbiol 2009;12:553–8. doi:10.1016/j.mib.2009.08.003.

[5] Wiechert W. 13C metabolic flux analysis. Metab Eng 2001;3:195–206. doi:10.1006/mben.2001.0187.

[6] Wu Z, Boss O. Targeting PGC-1 a to control energy homeostasis. Expert Opin Ther Targets 2007;11:1329–38.

[7] Shoag J, Arany Z. Regulation of hypoxia-inducible genes by PGC-1 alpha. Arterioscler Thromb Vasc Biol 2010;30:662–6. doi:10.1161/ATVBAHA.108.181636.

[8] Templeton N, Lewis A, Dorai H, Qian E a, Campbell MP, Smith KD, et al. The impact of anti-apoptotic gene Bcl-2Δ expression on CHO central metabolism. Metab Eng 2014;25:92–102. doi:10.1016/j.ymben.2014.06.010.

[9] Templeton N, Xu S, Roush DJ, Chen H. 13C metabolic flux analysis identifies limitations to increasing specific productivity in fed-batch and perfusion. Metab Eng 2017;44:126–33. doi:10.1016/j.ymben.2017.09.010.

[10] Pereira AGM, Walther JL, Hollenbach M, Young JD. 13 C flux analysis reveals that rebalancing medium amino acid composition can reduce ammonia production while

preserving central carbon metabolism of CHO cell cultures. Biotechnol J 2018;1700518. doi:10.1002/biot.201700518.

[11] Chen P, Harcum SW. Effects of elevated ammonium on glycosylation gene expression in CHO cells. Metab Eng 2006;8:123–32. doi:10.1016/j.ymben.2005.10.002.

[12] Yang M, Butler M. Effects of ammonia on CHO cell growth, erythropoietin production, and glycosylation. Biotechnol Bioeng 2000;68:370–80.

[13] Templeton N, Dean J, Reddy P, Young JD. Peak antibody production is associated with increased oxidative metabolism in an industrially relevant fed-batch CHO cell culture. Biotechnol Bioeng 2013;110:2013–24. doi:10.1002/bit.24858.

2 BACKGROUND AND SIGNIFICANCE

2.1 Chinese hamster ovary cells in biomanufacturing

Modern medicine has been revolutionized by the production of novel biotherapeutic protein drugs using recombinant DNA technology. These novel biotherapeutics are now employed to treat a myriad of human diseases including some cancers. Recently, a new generation of biopharmaceutical proteins based on monoclonal antibody (mAb) technology has emerged. These human proteins are produced in genetically modified eukaryotic host cells capable of complex post-translational modifications that are intrinsically impossible for simpler prokaryotic hosts, such as *E. coli* or yeast strains, to perform [1–3]. Mammalian cell lines such as Chinese hamster ovary (CHO) cells, human embryonic kidney (HEK) cells, baby hamster kidney (BHK) cells, and mouse myeloma cells (NS0) are typical choices for biopharmaceutical production because they are properly equipped to process these complex biotherapeutic proteins [3–5]. Historically, the most commonly utilized mammalian host cell line has been CHO cells due to their innate capabilities for high productivity of recombinant proteins, robustness, and safety track record [6]. Currently, CHO cells account for the production of approximately 60-70% of recombinant protein therapeutics on the market, including mAbs [3,4,7–9]. mAbs are structurally complex proteins that require post-translational modifications to functionally yield highly targeted therapies to treat a plethora of human diseases. Multiple large doses of mAb therapeutics are generally required to treat a single patient, sometimes as much as 1 mg/kg body weight as is the case in the anti-rejection drug Zenapax® used in organ transplant patients [10], while some mAb drugs in discovery are required at 2 mg/kg body weight [11]. These large effective doses of mAb drugs have led to a critical need for enhanced productivity in CHO cell

bioprocesses to increase overall culture titer and decrease the associated cost of development. Much work has been performed to increase bioreactor titers and viable cell density (VCD) in CHO cell cultures now regularly reaching 1-5 g/L and $20x10^6$ cells/mL, respectively [12].

CHO cells are perhaps the most prolific mammalian host cell line in the biopharmaceutical industry due more to historical precedence than biological superiority. When the protein biotherapeutic industry was still in its infancy, in the early 1980's, a dihydrofolate reductase deficient ($DHFR^-$) CHO cell line was generated where both alleles encoding for the dihydrofolate reductase (DHFR) enzyme were mutated or deleted—CHO-DUK-XB11 [13]. Expanding on this work, the CHO-DG44 cell line was created next, where both DHFR alleles were effectively eliminated [14]. These cell lines remain two of the most commonly used CHO cell lines in the biopharmaceutical industry today [14]. DHFR is an enzyme required for the biosynthesis of purine and pyrimidine nucleotides; therefore, cells cannot survive unless DHFR is recombinantly co-expressed with the mAb protein construct of interest. For this reason, $DHFR^-$ CHO cell lines make excellent selection systems that do not require the addition of antibiotics. Antibiotic addition is avoided in biotherapeutic production because the removal of any antibiotics during downstream purification would result in increased processing costs. Another such selection system widely used in industry today is the glutamine synthetase (GS) system. GS is the enzyme required for the synthesis of glutamine from glutamate, and GS deficiency is a characteristic of most CHO cell lines, making it an excellent selection system (**Error! Reference source not found.**). When the GS selection vector is used, exogenous glutamine is not fed to the CHO cell cultures as is generally required for CHO cell growth. Any cells that have not incorporated the GS vector into their genome will be unable to grow in glutamine-free medium. The GS system additionally offers the benefit of decreased ammonia

buildup in culture. Ammonia is produced via the spontaneous breakdown of glutamine in the culture; therefore, when glutamine is not added for growth of GS-expressing CHO cell lines, the toxicity from ammonia is all but eliminated from the cultures. Effective clones can be generated utilizing the GS system in roughly half the time required for $DHFR^-$ selection. Both CHO cell selection methods continue to be utilized by the biopharmaceutical industry. Additionally, both selection systems require chemical inhibitors to suppress any endogenous DHFR or GS activity that may be present in host cells.

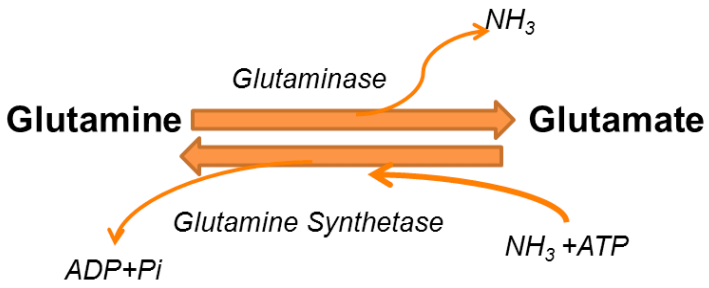

Figure 2-1 The role of glutamine synthetase (GS). GS allows for the synthesis of glutamine from glutamate and is not expressed at high endogenous levels in CHO cells.

Due to the demand for high VCDs, titers, and specific productivities, the industry has seen increased accumulation of toxic metabolites, specifically lactate and ammonia, which are byproducts of inefficient central carbon metabolism. Accumulation of lactate and ammonia have been linked to drastic declines in VCD and volumetric titers as a result of apoptotic cell death [15–17]. Due to these undesirable traits of high-density CHO cell cultures, much of the recent research in the field has focused on limiting said byproduct accumulation [7,9,15,18,19], anti-apoptotic engineering [15], and media manipulations [20] to combat these commonly occurring problems plaguing the industry.

As was previously mentioned, the GS selection system effectively eliminates excess ammonia accumulation in cultures [21–23]. Media manipulations have been successfully employed to combat ammonia accumulation in cultures where the GS system is not utilized [20].

However, much research in the field has been devoted to lactate reduction. Specifically, genetic engineering has been applied to combat excess lactate production, for example, by knockdown of the lactate dehydrogenase-A (LDH-A) enzyme responsible for the conversion of pyruvate into lactate [9,18,24]. LDH-A down-regulation in combination with other genetic engineering or alone, has resulted in 21-90% and 45-79% decreases in lactate production, respectively [9,18,24]. However, many industrial CHO cell lines (and other mammalian cell lines [25]) cease lactate production at the end of exponential growth phase and switch to lactate consumption during stationary phase [26]. This metabolic switch results in lower culture concentrations of lactate, longer culture durations, and higher product protein titers [25]. All studies presented in this dissertation involve CHO cell clones that undergo this metabolic shift.

2.2 Energy metabolism and protein production

CHO cell energy metabolism is of utmost importance in pharmaceutical bioprocessing. Protein synthesis and secretion place high energetic demands on the host cells. This energy sink is in addition to the energy demands of cell growth. ATP is the energy currency of cells required to fuel cell biosynthesis and protein production. Each peptide bond in proteins, like mAbs, require four ATP equivalents to fuel the formation of each peptide bond [23,27]. This energy is manufactured by central carbon metabolism, specifically glycolysis combined with mitochondrial citric acid cycle (CAC) and oxidative phosphorylation (OXPHOS) [23,28]. As was previously mentioned, CHO cells are generally characterized by high conversion rates of lactate from glucose, referred to as the Warburg effect [26]. This state of aerobic glycolysis can generate ATP independently of mitochondrial metabolism; however, prior studies have elucidated that high lactate production is generally closely associated with low titers of recombinant proteins [23,29–31]. Glycolysis terminating in lactate produces two net moles of

ATP per mole of glucose consumed. However, if glycolytic flux is instead diverted into the mitochondria for CAC metabolism and OXPHOS instead of lactate production, a net 36 moles of ATP are produced per mole of glucose [23,28], a much more efficient energy production pathway.

Several studies have confirmed that CHO cell lines with high rates of recombinant protein production also have highly active CAC metabolism [23,32]. A high rate of CAC activity is further associated with high oxygen uptake rate (OUR) [26], and OUR has been further demonstrated to be directly correlated with high recombinant mAb production in CHO cell cultures [23,33]. This relationship between highly productive CHO cell clones and increased utilization of the more efficient mitochondrial mechanism for ATP production is potentially explained by the significant increase in energetic demands for mAb synthesis. Additionally, clones with high rates of lactate production, a hallmark of inefficient carbon metabolism, have been reported to have decreased mitochondrial oxidative capacity, further cementing the correlation between high lactate production and decreased mAb productivity phenotype previously mentioned [26].

This relationship between efficient metabolic phenotypes and high productivity is further observed in CHO cell hosts engineered to express anti-apoptotic genes [9,15,23]. The anti-apoptotic gene Bcl-2 is known to regulate mitochondrial permeability, control calcium dynamics [23,34], and prohibit the cascade of cytochrome c into the cytosol which triggers apoptotic cell death [23,35]. This sequence of events enabled by Bcl-2 expression not only prolongs culture longevity, but it may additionally activate OXPHOS by maintaining high levels of cytochrome c and calcium in the mitochondria. While the expression of Bcl-2Δ, a truncated form of Bcl-2, has reportedly increased glucose uptake rates (GURs) in CHO cell clones, that extra glucose was

efficiently transported into the mitochondria for CAC metabolism instead of toward wasteful lactate accumulation [23].

Some CHO cell lines experience a natural metabolic switch at the transition from exponential growth phase to stationary growth phase. At this junction in culture progression, cells drastically slow their duplication rate and enter peak recombinant protein production [32]. This switch in cell metabolism from biomass to mAb synthesis is often accompanied by the metabolic switch from lactate production to consumption. As was previously mentioned, this metabolic shift in lactate metabolism has been correlated with increased mAb productivities [36]. Additionally, this shift to lactate uptake has been proposed to be related to altered oxidative capacity of the cells [26,30]. While the exact mechanism responsible for the shift in lactate metabolism remains unknown, it is clear that there exists a fundamental connection between efficient metabolism of carbon, increased oxidative metabolic activity, and high recombinant protein biosynthesis.

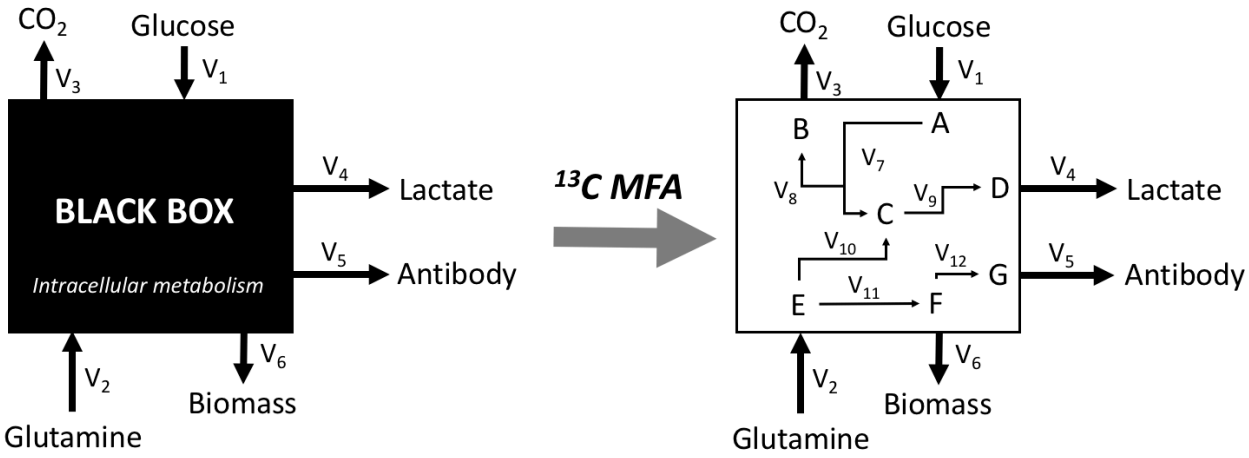

Figure 2-2 ^{13}C metabolic flux analysis (MFA) allows researchers to peek inside the black box to elucidate metabolic phenotype beyond that described by extracellular analysis alone. On the left, inputs and outputs can be quantified; however, it is impossible to define intracellular metabolic fluxes without further information due to the large number of unknown fluxes. ^{13}C MFA applies ^{13}C tracers to provide such information. V_i indicates an individual flux value; A-G represent generic intracellular metabolites.

2.3 ^{13}C metabolic flux analysis allows for the quantification of energy metabolism

The production of commodity chemicals, specialty chemicals, small-molecule drugs, therapeutic proteins, and other biomolecules of commercial value are produced via bacterial, yeast, plant, and mammalian cells [37]. Of particular interest to this dissertation is the industrial production of therapeutic proteins such as mAbs. As previously detailed, this production process typically requires mammalian host cells as biocatalysts, most commonly CHO cells. These CHO cell cultures are often restricted by toxic byproduct accumulation and low specific productivities. To investigate these issues, genome-scale modeling, cell-wide 'omics' platforms, and high-throughput screening methods have been developed to combat these challenges by identifying target genes for engineering improved host cell performance. However, a more direct approach for the quantification and elucidation of *in vivo* metabolic pathway activities exists—^{13}C metabolic flux analysis (MFA) [38–40]. Isotope labeling experiments allow strain and process engineers to look inside the black box of cellular metabolism by tracking the progression and, therefore, rearrangement of ^{13}C labeled substrate molecules as they are metabolized via the host cells' metabolic pathways as shown in Figure 2-2 [41–43]. ^{13}C labeled glucose and ^{13}C labeled glutamine are the most commonly utilized for the study of CHO cell metabolism via ^{13}C MFA. MFA stands apart from other flux modeling approaches in that it is able to integrate numerous independent measurements into a single, comprehensive flux map while simultaneously elucidating inconsistent data that would not be obviously identified through localized analysis of specific metabolic nodes. Additionally, the flux maps produced from ^{13}C MFA have direct biological relevance and can be compared across independent experiments. Metabolic quantifications obtained from ^{13}C MFA experiments have been successfully employed to (1) characterize new host cells, (2) identify wasteful metabolic pathways responsible for diverting

carbon away from product formation, and (3) identify metabolic bottlenecks that restrict carbon flow from successful conversion into product. By quantifying the fluxes at individual nodes of the host metabolic network, and by determining how carbon is re-routed in response to targeted engineering or environmental perturbations, fundamental insights into metabolic network regulation can be discovered to rationally guide subsequent iterations of metabolic engineering.

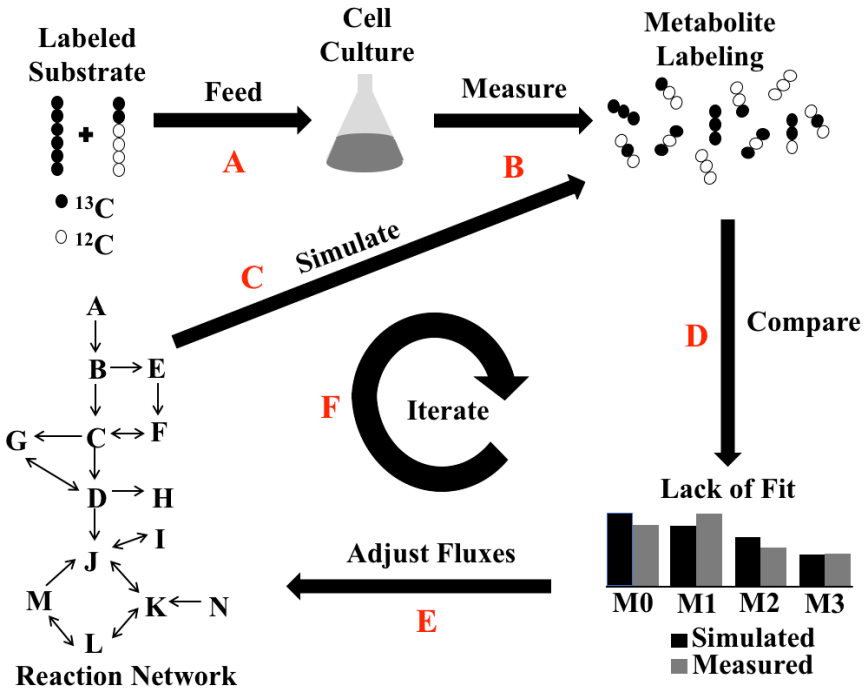

Figure 2-3 ^{13}C metabolic flux analysis workflow. (A) Stably labeled ^{13}C isotopic substrate (e.g., glucose) is fed to cell cultures. (B) Intracellular metabolites are analyzed for ^{13}C incorporation. (C) Intracellular metabolite ^{13}C labeling is simulated from an established network of metabolic reactions. (D) These simulated labeling data are compared to the experimentally measured labeling data. (E) From the lack of fit between the simulated and measured isotopic data, the fluxes of the reaction network are adjusted, and (F) the process detailed in steps (C)-(E) are repeated until the lack of fit is minimized to a statistically acceptable level.

^{13}C MFA studies are performed by feeding cells stable ^{13}C isotope tracers as a primary substrate source and subsequently measuring isotope incorporation in downstream metabolites and secreted products as depicted in Figure 2-3 [38,43]. These measurements of isotope isomers, or isotopomers, obtained via gas chromatography in tandem with mass spectrometry (GC/MS) are combined with rates of cell growth and uptake/secretion of amino acids measured via high

performance liquid chromatography (HPLC) [8,44]. These data sets are then computationally analyzed to construct comprehensive, quantitative flux maps describing intracellular metabolism. A vital assumption of traditional ^{13}C MFA is that the culture in question is in metabolic and isotopic steady state. Metabolic steady state is defined as the state when constant metabolic fluxes and intracellular pool sizes are achieved over the course of the labeling experiment. Since testing for this is not readily practicable, we assume that if growth and extracellular exchange rates are constant, then intracellular metabolism is also at steady state. Isotopic steady state is achieved when the relative abundances of different isotopomers reaches a constant distribution. When metabolic steady state is reached but isotopic steady state is not achieved or is not experimentally possible, isotopically nonstationary MFA (INST-MFA) can be employed to compute fluxes based on transient isotope labeling measurements over time (Figure 2-4) [45]. INST-MFA generally reduces the duration of isotope labeling experiments while providing increased flux resolution. However, it is computationally more demanding. INST-MFA can be employed for the analysis of autotrophic or methylotrophic organisms since they only consume single-carbon substrates [45–49]. Stationary ^{13}C MFA is inadequate for analysis of such systems due to the fact that every carbon atom in the system is derived from a single source and therefore all intermediate metabolites will become uniformly labeled at isotopic steady state regardless of the fluxes of the organism. The transient labeling patterns that emerge from a change in substrate from ^{12}C to ^{13}C, however, can be analyzed by INST-MFA to precisely measure the resulting intracellular fluxes [45].

Additionally, and of more relevance to the work detailed in this dissertation, INST-MFA can be utilized for systems where metabolic steady state cannot be held for a long enough period to also reach isotopic steady state [45]. This scenario can arise in cell culture when a later growth

phase is studied, resulting in a fed-batch experiment where ^{13}C tracers are spiked in after the experiment is underway [15,23,50]. Additionally, this scenario is relevant when metabolic phenotypes are not maintained for significant periods of time relative to the rate of carbon distribution throughout cell metabolism. Slow incorporation of ^{13}C into downstream metabolites can occur due to the presence of pathway bottlenecks or large intracellular pools of intermediate metabolites [51].

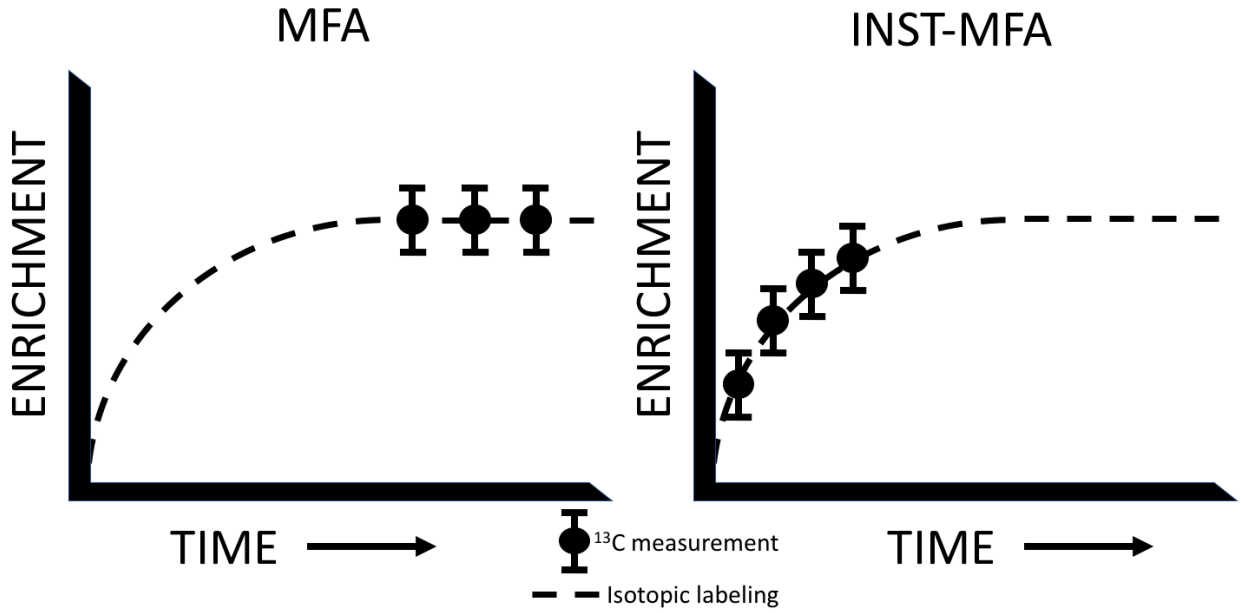

Figure 2-4 Comparison of stationary metabolic flux analysis (MFA) and isotopically nonstationary (INST)-MFA. The left panel shows conventional MFA while the right panel shows INST-MFA based on the analysis of samples collected prior to isotopic steady state.

When designing a ^{13}C MFA study, the choice of ^{13}C tracer is paramount to the successful phenotyping of host cell metabolism. A good stable isotope tracer is consumed in large quantities by the organism in question and permeates the major pathways of the metabolic network. In mammalian cells, such as CHO cells, the primary substrate consumed is glucose followed by glutamine. For this reason, ^{13}C-glucose isotopomers are the most common tracer choice. Uniformly labeled glucose, [U-$^{13}C_6$] glucose penetrates the metabolic network most thoroughly and rapidly. It also is the best glucose tracer choice for defining CAC metabolism since there are

six carbon atoms per ^{13}C-glucose molecule and more ^{13}C atoms reach the mitochondria than would if less enriched ^{13}C glucose tracers were used. To gain insight into oxidative pentose phosphate pathway (OPPP) activity, [1,2-$^{13}C_2$] glucose is the most commonly utilized tracer. Doubly labeled glucose on the first two carbons adequately defines fluxes though both glycolysis and OPPP (Figure 2-5). However, since only two labeled atoms per glucose molecule consumed enter the metabolic network, only half of the pyruvate molecules entering the mitochondria are enriched with ^{13}C. Additionally, if the [1,2-$^{13}C_2$] glucose molecule is metabolized via OPPP, the first ^{13}C atom is lost to CO_2 in the first reaction of the OPPP catalyzed by glucose-6-phosphate dehydrogenase (G6PDH)—therefore, the pyruvate molecules resulting from OPPP activity could potentially only have one ^{13}C atom, further diluting the enrichment of ^{13}C entering the mitochondria for CAC metabolism. Therefore, if [1,2-$^{13}C_2$] glucose is used in ^{13}C MFA for elucidation of OPPP fluxes, it is generally combined with [U-$^{13}C_6$] glucose in order to adequately enrich the mitochondrial metabolism with ^{13}C for precise calculation of CAC fluxes. This combination of ^{13}C-glucose tracers has been frequently used to study CHO cell metabolism.

Perhaps the most efficient ^{13}C tracer combination for comprehensive quantification of CHO cell metabolism is [1,2-$^{13}C_6$-glucose] in combination with [U-$^{13}C_5$] glutamine. The [1,2-$^{13}C_6$] glucose provides mass isotopomer distribution (MID) data to quantify the split ratio of glycolysis:OPPP activity while the [U-$^{13}C_5$] glutamine is directly metabolized into the CAC at the alpha-ketoglutarate node. Glutamine is generally consumed by CHO cells at rates such that isotopic enrichment of the CAC is achieved relatively quickly. This combinatorial labeling strategy is generally executed via parallel labeling experiments. This approach provides the quickest method for labeling all the main pathways of the metabolic network. However, glutamine is not typically fed to GS-CHO cell clones. In cases such as this, ^{13}C-glucose must be

used at high enough concentrations to successfully penetrate and enrich mitochondrial metabolism with ^{13}C. As was previously mentioned, [1,2-$^{13}C_6$] glucose will not enrich the CAC adequately in a timely fashion; therefore, if mitochondrial metabolism is of experimental interest, [U-$^{13}C_6$] glucose is the best option for stable isotope labeling of GS-CHO cell lines.

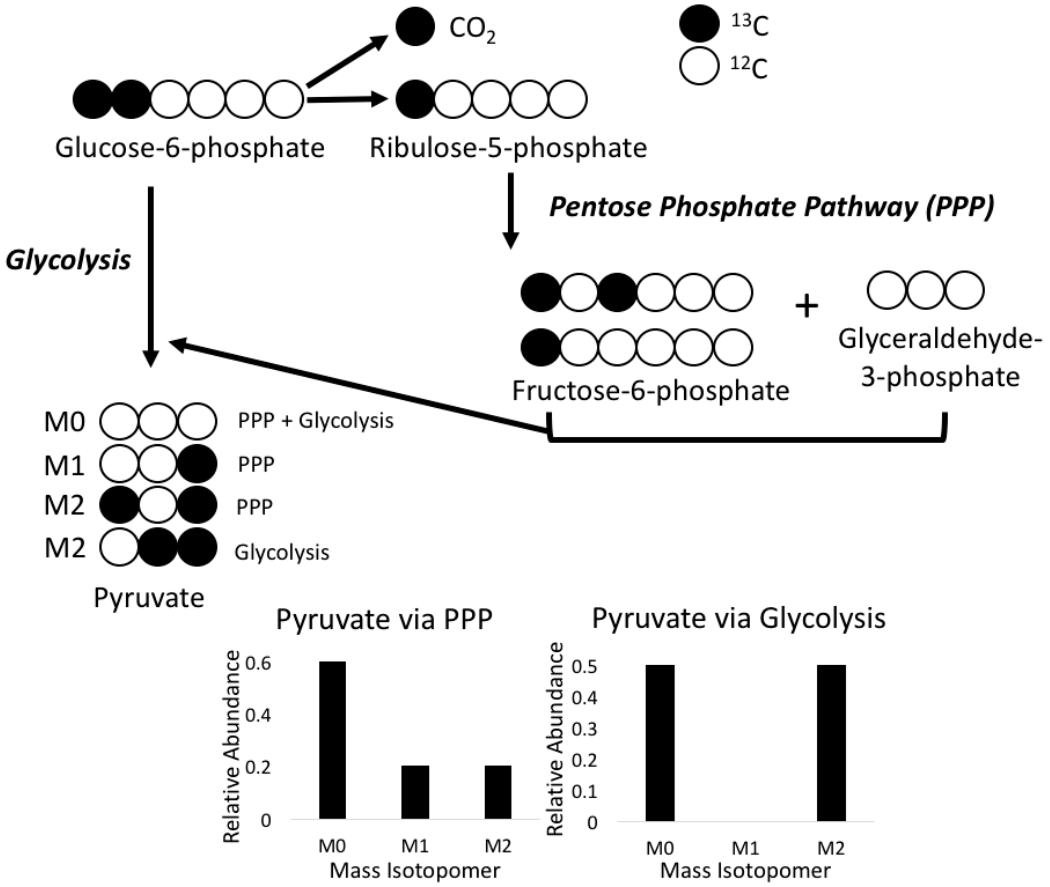

Figure 2-5 Discerning the split of glycolysis and pentose phosphate pathway metabolic activity. The mass isotopomer distribution of pyruvate if generated purely through glycolysis or the PPP is shown. Any linear combination of the two can exist as cells generally utilize both pathways simultaneously. Linear regression can be used to determine the actual split ratio of glycolysis/PPP by fitting the experimental data to a mathematical model that accounts for the stoichiometry and atom rearrangements caused by the metabolic network.

^{13}C MFA can also be performed with the utilization of parallel labeling studies. Parallel studies are desirable when two substrates are consumed by cells and incorporated into separate metabolic pathways—such as glucose and glutamine in mammalian host cells [52,53]. Parallel labeling studies are performed in separate cultures and the data are combined for computational

analysis. In the case of ^{13}C glucose and ^{13}C glutamine parallel experiments, the glucose cultures are analyzed for glycolytic intermediates to assess glycolysis and OPPP metabolic fluxes whereas the glutamine cultures are analyzed for mitochondrial metabolism, i.e., CAC-associated reactions. Both experiments are analyzed for extracellular amino acid fluxes, growth rates, GURs, and recombinant protein production rates. The two sets of intracellular metabolite MID measurements are analyzed in combination with the extracellular measurements. This method also increases the enrichment of ^{13}C labeling in downstream metabolites by feeding tracers that enter the metabolic network proximal to the target analytes. However, as was previously mentioned, the GS selection system is extremely popular in the development of industrial CHO cell lines, and, therefore, ^{13}C glutamine is not a viable tracer option since these cell lines do not consume exogenous glutamine. In this scenario, ^{13}C tracers must be chosen such that infiltration into mitochondrial metabolism at sufficient levels for detection is possible. Glucose is slow to incorporate into the mitochondria. If exponential growth phase is the desired phase of study, this may not pose a serious problem; however, if stationary growth phase is the metabolic phase in question, slow incorporation could result in the impossibility of reaching isotopic steady state. In this case, INST-MFA can be utilized for metabolic mapping.

Since peak mAb productivity occurs during stationary growth, this phase of culture is of great experimental interest in the biopharmaceutical industry. However, since the metabolic phenotype is significantly altered when cultures make the shift from exponential to stationary phase, ^{13}C MFA experiments with an initial bolus of ^{13}C tracers do not adequately characterize stationary phase. When the culture switches from lactate production to consumption, the accumulated lactate serves as a secondary source of ^{13}C, which significantly complicates subsequent flux analysis. To avoid the introduction of secondary isotope tracers, ^{13}C substrates

must be introduced at the onset of the growth phase of interest. Such fed-batch experiments are already rather common in biopharmaceutical protein production. The introduction of fed-batch cultures has increased maximum cell densities in CHO cell cultures by several fold thus increasing possible volumetric mAb titers [25]. Furthermore, feeding substrate(s) throughout the duration of cultivation provides opportunities for introducing ^{13}C tracers at multiple points in culture growth. Continuous monitoring of lactate concentrations in CHO cell cultures provides real-time insight into the exact timing of the metabolic shift from exponential to stationary growth phase. This method requires the clone in question to undergo the metabolic shift from lactate production to lactate consumption. However, as has already been explained, high-producing clones do often experience said shift. Introducing the ^{13}C tracer at this juncture in cell metabolism means that any ^{13}C incorporated into downstream metabolites reflects stationary phase metabolism. This technique allows for the rigorous characterization of stationary phase metabolism, thus providing relevant information for further rational engineering of mAb production and the potential to elucidate energetic/carbon sinks that could be inhibited to enhance overall protein productivity.

2.4 References

[1] Wlaschin KF, Hu W-S. Engineering cell metabolism for high-density cell culture via manipulation of sugar transport. J Biotechnol 2007;131:168–76. doi:10.1016/j.jbiotec.2007.06.006.

[2] Nolan RP, Lee K. Dynamic model of CHO cell metabolism. Metab Eng 2011;13:108–24. doi:10.1016/j.ymben.2010.09.003.

[3] Butler M. Animal cell cultures: recent achievements and perspectives in the production of biopharmaceuticals. Appl Microbiol Biotechnol 2005;68:283–91. doi:10.1007/s00253-005-1980-8.

[4] Hossler P, Khattak SF, Li ZJ. Optimal and consistent protein glycosylation in mammalian cell culture. Glycobiology 2009;19:936–49. doi:10.1093/glycob/cwp079.

[5] Butler M. Optimisation of the Cellular Metabolism of Glycosylation for Recombinant Proteins Produced by Mammalian Cell Systems. Cytotechnology 2006;50:57–76. doi:10.1007/s10616-005-4537-x.

[6] Meleady P, Doolan P, Henry M, Barron N, Keenan J, O'Sullivan F, et al. Sustained productivity in recombinant Chinese hamster ovary (CHO) cell lines: proteome analysis of the molecular basis for a process-related phenotype. BMC Biotechnol 2011;11:78. doi:10.1186/1472-6750-11-78.

[7] McAtee AG, Templeton N, Young JD. Role of Chinese hamster ovary central carbon metabolism in controlling the quality of secreted biotherapeutic proteins. Pharm Bioprocess 2014;2:63–74.

[8] Ahn WS, Antoniewicz MR. Towards dynamic metabolic flux analysis in CHO cell cultures. Biotechnol J 2012;7:61–74. doi:10.1002/biot.201100052.

[9] Jeon MK, Yu DY, Lee GM. Combinatorial engineering of ldh-a and bcl-2 for reducing lactate production and improving cell growth in dihydrofolate reductase-deficient Chinese hamster ovary cells. Appl Microbiol Biotechnol 2011;92:779–90. doi:10.1007/s00253-011-3475-0.

[10] González-Roncero FM, Gentil-Govantes MÁ, González-Molina M, Rivero M, Cantarell C, Alarcón A, et al. Late evolution of kidney transplants in elderly donors and recipients receiving initial immunosuppressant treatment with daclizumab, mycophenolate mofetil, and delayed introduction of tacrolimus. Nefrol Publicaci{ó}n Of La Soc Espa{ñ}ola Nefrol 2012;32:446–54. doi:10.3265/Nefrologia.pre2012.Mar.11024.

[11] Sautto G, Mancini N, Gorini G, Clementi M, Burioni R. Possible future monoclonal antibody (mAb)-Based Therapy against arbovirus infections. Biomed Res Int 2013;2013:838491. doi:10.1155/2013/838491.

[12] Jayapal KP, Wlaschin KF, Yap MGS. Recombinant Protein Therapeutics from CHO Cells — 20 Years and Counting. CHO Consort 2007:40–7.

[13] Urlaub G, Chasin L a. Isolation of Chinese hamster cell mutants deficient in dihydrofolate reductase activity. Proc Natl Acad Sci U S A 1980;77:4216–20.

[14] Urlaub G, Käs E, Carothers AM, Chasin LA. Deletion of the diploid dihydrofolate reductase locus from cultured mammalian cells. Cell 1983;33:405–12. doi:10.1016/0092-8674(83)90422-1.

[15] Templeton N, Lewis A, Dorai H, Qian E a, Campbell MP, Smith KD, et al. The impact of anti-apoptotic gene Bcl-2Δ expression on CHO central metabolism. Metab Eng 2014;25:92–102. doi:10.1016/j.ymben.2014.06.010.

[16] Dorai H, Kyung YS, Ellis D, Kinney C, Lin C, Jan D, et al. Expression of anti-apoptosis

genes alters lactate metabolism of Chinese Hamster Ovary cells in culture. Biotechnol Bioeng 2009;103:592–608. doi:10.1002/bit.22269.

[17] Lao MS, Toth D. Effects of ammonium and lactate on growth and metabolism of a recombinant Chinese hamster ovary cell culture. Biotechnol Prog 1997;13:688–91. doi:10.1021/bp9602360.

[18] Zhou M, Crawford Y, Ng D, Tung J, Pynn AFJ, Meier A, et al. Decreasing lactate level and increasing antibody production in Chinese Hamster Ovary cells (CHO) by reducing the expression of lactate dehydrogenase and pyruvate dehydrogenase kinases. J Biotechnol 2011;153:27–34. doi:10.1016/j.jbiotec.2011.03.003.

[19] Kim DY, Chaudhry MA, Kennard ML, Jardon MA, Braasch K, Dionne B, et al. Fed-batch CHO cell t-PA production and feed glutamine replacement to reduce ammonia production. Biotechnol Prog 2013;29:165–75. doi:10.1002/btpr.1658.

[20] Pereira AGM, Walther JL, Hollenbach M, Young JD. 13 C flux analysis reveals that rebalancing medium amino acid composition can reduce ammonia production while preserving central carbon metabolism of CHO cell cultures. Biotechnol J 2018;1700518. doi:10.1002/biot.201700518.

[21] Duarte TM, Carinhas N, Barreiro LC, Carrondo MJT, Alves PM, Teixeira AP. Metabolic responses of CHO cells to limitation of key amino acids. Biotechnol Bioeng 2014;111:2095–106. doi:10.1002/bit.25266.

[22] Dorai H, Corisdeo S, Ellis D, Kinney C, Chomo M, Hawley-Nelson P, et al. Early prediction of instability of Chinese hamster ovary cell lines expressing recombinant antibodies and antibody-fusion proteins. Biotechnol Bioeng 2012;109:1016–30. doi:10.1002/bit.24367.

[23] Templeton N, Smith KD, McAtee-Pereira AG, Dorai H, Betenbaugh MJ, Lang SE, et al. Application of13C flux analysis to identify high-productivity CHO metabolic phenotypes. Metab Eng 2017;43:218–25. doi:10.1016/j.ymben.2017.01.008.

[24] Kim SH, Lee GM. Down-regulation of lactate dehydrogenase-A by siRNAs for reduced lactic acid formation of Chinese hamster ovary cells producing thrombopoietin. Appl Microbiol Biotechnol 2007;74:152–9. doi:10.1007/s00253-006-0654-5.

[25] Mulukutla BC, Gramer M, Hu W-SS. On metabolic shift to lactate consumption in fed-batch culture of mammalian cells. Metab Eng 2012;14:138–49. doi:10.1016/j.ymben.2011.12.006.

[26] Zagari F, Jordan M, Stettler M, Broly H, Wurm FM. Lactate metabolism shift in CHO cell culture: the role of mitochondrial oxidative activity. N Biotechnol 2012;00. doi:10.1016/j.nbt.2012.05.021.

[27] Seth G, Hossler P, Chong J, Hu YW. Engineering Cells for Cell Culture Bioprocessing – Physiological Fundamentals. Adv Biochem Engin/Biotechnol 2006;101:119–64. doi:10.1007/10_017.

[28] Vander Heiden MG, Cantley LC, Thompson CB. Understanding the Warburg effect: the metabolic requirements of cell proliferation. Science 2009;324:1029–33. doi:10.1126/science.1160809.

[29] Le H, Kabbur S, Pollastrini L, Sun Z, Mills K, Johnson K, et al. Multivariate analysis of cell culture bioprocess data--lactate consumption as process indicator. J Biotechnol 2012;162:210–23. doi:10.1016/j.jbiotec.2012.08.021.

[30] Luo J, Vijayasankaran N, Autsen J, Santuray R, Hudson T, Amanullah A, et al. Comparative metabolite analysis to understand lactate metabolism shift in Chinese

hamster ovary cell culture process. Biotechnol Bioeng 2012;109:146–56. doi:10.1002/bit.23291.

[31] Wilkens C a, Gerdtzen ZP. Engineering CHO cells for improved central carbon and energy metabolism. BMC Proc 2011;5 Suppl 8:P120. doi:10.1186/1753-6561-5-S8-P120.

[32] Templeton N, Dean J, Reddy P, Young JD. Peak antibody production is associated with increased oxidative metabolism in an industrially relevant fed-batch CHO cell culture. Biotechnol Bioeng 2013;110:2013–24. doi:10.1002/bit.24858.

[33] Huang Y-M, Hu W, Rustandi E, Chang K, Yusuf-makagiansar H, Ryll T. Maximizing productivity of CHO cell-based fed-batch culture using chemically defined media conditions and typical manufacturing equipment. Biotechnol Prog 2010;26:1400–10. doi:10.1002/btpr.436.

[34] Williams A, Hayashi T, Wolozny D, Yin B, Su TC, Betenbaugh MJ, et al. The non-apoptotic action of Bcl-xL: regulating Ca2+signaling and bioenergetics at the ER-mitochondrion interface. J Bioenerg Biomembr 2016;48:211–25. doi:10.1007/s10863-016-9664-x.

[35] Tait SWG, Green DR. Mitochondria and cell death: outer membrane permeabilization and beyond. Nat Rev Mol Cell Biol 2010;11:621–32. doi:10.1038/nrm2952.

[36] Templeton N, Smith KD, McAtee-Pereira AG, Dorai H, Betenbaugh MJ, Lang SE, et al. Application of 13C flux analysis to identify high-productivity CHO metabolic phenotypes. Metab Eng 2017;29:53–62. doi:10.1016/j.ymben.2017.01.008.

[37] Jullesson D, David F, Pfleger B, Nielsen J. Impact of synthetic biology and metabolic engineering on industrial production of fine chemicals. Biotechnol Adv 2015;33:1395–402. doi:10.1016/j.biotechadv.2015.02.011.

[38] Wiechert W. 13C metabolic flux analysis. Metab Eng 2001;3:195–206. doi:10.1006/mben.2001.0187.

[39] Sauer U. Metabolic networks in motion: 13C-based flux analysis. Mol Syst Biol 2006;2:62. doi:10.1038/msb4100109.

[40] Varman AM, He L, You L, Hollinshead W, Tang YJ. Elucidation of intrinsic biosynthesis yields using 13C-based metabolism analysis. Microb Cell Fact 2014;13:42. doi:10.1186/1475-2859-13-42.

[41] Jung J-Y, Oh M-K. Isotope labeling pattern study of central carbon metabolites using GC/MS. J Chromatogr B 2015;974:101–8. doi:10.1016/j.jchromb.2014.10.033.

[42] Crown SB, Ahn WS, Antoniewicz MR. Rational design of 13C-labeling experiments for metabolic flux analysis in mammalian cells. BMC Syst Biol 2012;6:43. doi:10.1186/1752-0509-6-43.

[43] Antoniewicz MR. (13)C metabolic flux analysis: optimal design of isotopic labeling experiments. Curr Opin Biotechnol 2013;24:1–6. doi:10.1016/j.copbio.2013.02.003.

[44] Metallo CM, Walther JL, Stephanopoulos G. Evaluation of 13C isotopic tracers for metabolic flux analysis in mammalian cells. J Biotechnol 2009;144:167–74. doi:10.1016/j.jbiotec.2009.07.010.

[45] Jazmin LJ, Young JD. Isotopically Nonstationary 13C Metabolic Flux Analysis. In: Alper HS, editor. Syst. Metab. Eng. Metthods Protoc. Methods Mol. Biol., vol. 985, Springer Science + Business Media; 2013, p. 367–90. doi:10.1007/978-94-007-4534-6.

[46] Jazmin LJ, O'Grady JP, Ma F, Allen DK, Morgan JA, Young JD. Isotopically nonstationary MFA (INST-MFA) of autotrophic metabolism. Methods Mol Biol 2014;1090:181–210. doi:10.1007/978-1-62703-688-7-12.

[47] Cheah YE, Young JD. Isotopically nonstationary metabolic flux analysis (INST-MFA): putting theory into practice. Curr Opin Biotechnol 2018;54:80–7. doi:10.1016/j.copbio.2018.02.013.

[48] Shastri AA, Morgan JA. A transient isotopic labeling methodology for 13C metabolic flux analysis of photoautotrophic microorganisms. Phytochemistry 2007;68:2302–12. doi:10.1016/j.phytochem.2007.03.042.

[49] Young JD, Shastri AA, Stephanopoulous G, Morgan JA. Mapping photoautotrophic metabolism with isotopically nonstationary 13C flux analysis. Metab Eng 2011;13:656–65. doi:10.1016/j.biotechadv.2011.08.021.Secreted.

[50] Templeton N, Smith KD, McAtee-Pereira AG, Dorai H, Betenbaugh MJ, Lang SE, et al. Application of 13C flux analysis to identify high-productivity CHO metabolic phenotypes. Metab Eng 2015;29:53–62. doi:10.1016/j.ymben.2017.01.008.

[51] Zhao Z, Kuijvenhoven K, Ras C, van Gulik WM, Heijnen JJ, Verheijen PJT, et al. Isotopic non-stationary 13C gluconate tracer method for accurate determination of the pentose phosphate pathway split-ratio in Penicillium chrysogenum. Metab Eng 2008;10:178–86. doi:10.1016/j.ymben.2008.04.003.

[52] Crown SB, Antoniewicz MR. Parallel labeling experiments and metabolic flux analysis: Past, present and future methodologies. Metab Eng 2013;16:21–32. doi:10.1016/j.ymben.2012.11.010.

[53] Ahn WS, Antoniewicz MR. Parallel labeling experiments with [1,2-^{13}C] glucose and [U-^{13}C] glutamine provide new insights into CHO cell metabolism. Metab Eng 2013; 15:34-47. doi: 10.1016/j.ymben.2012.10.001.

3 ^{13}C MFA of industrial CHO cells overexpressing the global metabolic regulator PGC-1α

3.1 Summary

Monoclonal antibody (mAb) protein therapeutics are used to treat a myriad of human diseases. Most commonly, Chinese hamster ovary (CHO) cells are used as mammalian host cells for biomanufacturing mAb drugs due to their innate abilities to synthesize, fold, glycosylate, and secrete complex proteins. Large effective doses, sometimes as high as 2 mg/kg patient body weight, are frequently required; therefore, CHO host cells capable of achieving high viable cell density (VCD) and cell specific productivity (qP) are needed to meet demands for mAb production. Highly productive CHO cell lines typically exhibit an oxidative metabolic phenotype, especially during the stationary growth phase when peak mAb production occurs. The major oxidative pathway of CHO cell metabolism is the mitochondrial citric acid cycle (CAC). We hypothesized that by engineering CHO cells to have higher CAC fluxes, we could increase qP. To accomplish this, we engineered CHO cells to constitutively overexpress peroxisome proliferator-activated receptor gamma coactivator 1-alpha (PGC-1α), a global regulator of mitochondrial biogenesis. The PGC-1α overexpressing lines exhibited 2.6- to 5.2-fold increases in qP and consumed up to 2.4-fold more oxygen than the parental control. ^{13}C metabolic flux analysis (MFA) was employed to quantify intracellular metabolic fluxes and elucidated approximately 3-fold increases in CAC fluxes in the PGC-1α lines over the control. These findings support the hypothesis that high oxidative metabolic activity is correlated with, and can be potentially engineered to obtain, high qP in industrial CHO cell cultures.

3.2 Introduction

Monoclonal antibody (mAb) based therapeutics represent a ground-breaking class of biotherapeutic drugs used to treat cancer, acute organ rejection, rheumatoid arthritis, and many other diseases [1,2]. MAb drugs have shown favorable safety profiles, high efficiency at interfering with protein/protein interactions, and high target specificity and affinity, thus making them excellent therapeutics [3]. These favorable attributes, however, cause difficulty in biomanufacturing due to the complex post-translational modifications such as folding patterns and glycosylation profiles required for efficacy. Additionally, high effective doses of up to 2 mg/kg body weight are often required for treatment of patients [4]. Due to this need for large quantities of drug product and the associated high costs of their production and downstream purification, it is of utmost importance to maximize the cell specific productivity (qP) of host cultures.

Chinese hamster ovary (CHO) cells are historically the most utilized mammalian host cells for industrial production of mAb-based therapeutics [5,6]. Approximately 60 to 70% of recombinant biotherapeutics are produced by CHO cells due to their superior abilities to synthesize, fold, glycosylate, and secrete complex proteins (e.g., mAbs) in large-scale suspension cultures [7–9]. High viable cell densities (VCDs) resulting in high volumetric titers are routinely accomplished in industrial biomanufacturing; therefore, a focal point of ongoing research is on increasing qP of host cell lines to further increase mAb productivities and decrease associated costs.

Peak mAb qP has been previously observed during CHO cell stationary growth phase [10,11]. Cells transition from a cell proliferation metabolic phenotype during exponential growth to a protein production phenotype during stationary growth [12]. Furthermore, a switch from

lactate production to consumption at the onset of stationary phase has also been associated with high producing CHO cell lines [13,14]. This metabolic switch provides an alternate carbon source to directly fuel mitochondrial metabolism. Furthermore, host cultures with high qP values have been observed to express increased flux through oxidative metabolism. Specifically, increased flux through the mitochondrial citric acid cycle (CAC) has been associated with highly productive CHO cell cultures [11,15].

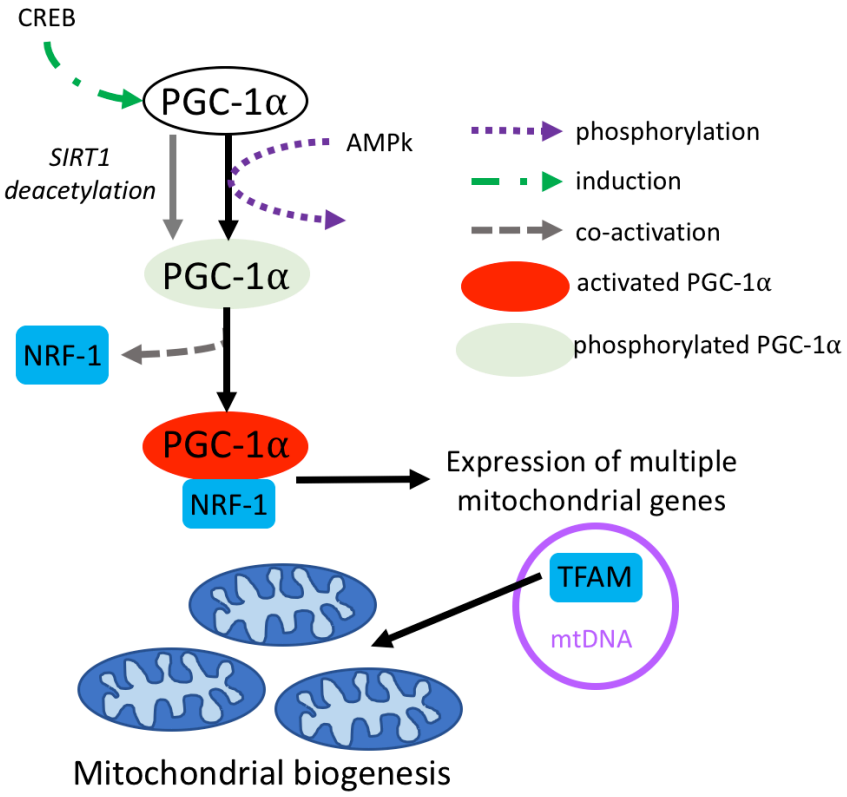

Figure 3-1 Role of PGC-1α as a master regulator of mitochondrial biogenesis. PGC-1α can be induced by CREB and activated by a variety of post-translational modifications including SIRT1 deacetylation and AMP kinase dependent phosphorylation. Active PGC-1α is a transcriptional co-activator which allows transcription factors such as NRF-1 to promote the nuclear expression of numerous mitochondrial genes including TFAM—a mitochondrial transcription factor that initiates expression of the mitochondrial genome resulting in mitochondrial biogenesis.

To induce a highly oxidative metabolic phenotype in CHO cells, we engineered an industrial host line to overexpress PGC-1α, a transcriptional coactivator widely reported to regulate mitochondrial biogenesis as shown in Figure 3-1 [16–19]. PGC-1α expression is

enriched in many highly oxidative tissues such as skeletal muscle, heart, fasted liver, and has been repeatedly shown to become upregulated in conditions such as exercise where oxidative metabolism is elevated [20]. PGC-1α has been shown to increase the number of mitochondria in cells, thereby increasing their oxidative capacity as demonstrated by increased oxygen uptake rates (OURs) [21]. Additionally, PGC-1α overexpression has led to lower reactive oxygen species (ROS) production by mitochondria in muscle tissue and an upregulation of mitochondrial protein expression directly involved in oxidative phosphorylation, indicating PGC-1α expression directly affects mitochondrial metabolism [22]. Although PGC-1α activity and signaling vary by tissue and environmental stimuli, a clear pattern of regulation has emerged through the literature that PGC-1α ultimately is a master regulator of mitochondrial metabolism [23]. Here, we hypothesized that increasing the oxidative capacity of CHO cells through PGC-1α overexpression would increase mitochondrial metabolism, thus increasing CAC flux and driving qP upward.

^{13}C metabolic flux analysis (MFA) is a robust tool for elucidating intracellular metabolic phenotypes of cells. Previous ^{13}C MFA studies identified an increased oxidative metabolic phenotype as a target for rational engineering of CHO cell metabolism for higher qP [15,24] and was therefore utilized in this study to elucidate the effectiveness of our metabolic engineering strategy. ^{13}C MFA enables the quantification of intracellular metabolism through the administration of ^{13}C-labeled substrates followed by measurement of isotope enrichment patterns in metabolic intermediates formed from those substrates. Since the ^{13}C atoms are rearranged via metabolic pathways in predictable patterns, the intracellular labeling configurations of intermediates allows for the calculation of fluxes based on the observed dynamics of ^{13}C

incorporation. This technique allows for a comprehensive assessment of metabolic phenotype resulting from experimental perturbations such as metabolic engineering of host cells.

^{13}C MFA provided confirmation that increased CAC flux and mitochondrial activity were conferred to some CHO cells through transfection of a PGC-1α expression vector followed by antibiotic selection to enrich cell populations for PGC-1α overexpressing clones. ^{13}C-labeled glucose was spiked into fed-batch cultures to characterize their stationary phase metabolism, since that is when peak mAb production typically occurs. Due to the short duration of stationary phase, isotopic steady state was not achieved before culture death rates began to affect cellular metabolism. Therefore, isotopically nonstationary (INST)-MFA was used to quantify metabolic fluxes over the course of the limited stationary growth phase. INST-MFA is more computationally demanding than stationary MFA, but it provides increased accuracy of flux estimation and can be applied to experiments where isotopic steady state is not achieved.

This study reinforced the hypothesis postulated by previous studies that high CAC fluxes is associated with enhanced qP [11,12]. PGC-1α overexpressing CHO cells consumed up to 2.4-fold more oxygen, exhibited an approximately 3-fold increase in carbon flux through the CAC, and experienced up to a 5.2-fold increase in qP.

3.3 Materials and methods

3.3.1 Generation of cell lines

The industrial mAb producing CHO cell line, C2869A (Janssen), was used for this study. The line expresses a model IgG antibody targeting respiratory syncytial virus (B21M). Two days preceding transfection with PGC-1α DNA (pcDNA4 myc PGC-1α was a gift from Toren Finkel, Addgene plasmid #10974) [25], C2869A cells were seeded at 2x10^5 cells/mL in 50 mL fresh

MACH-1 (SAFC) medium in 125 mL shake flasks at 37°C, 5% CO_2, and shaking at 135 RPM. Since the recombinant mAb was expressed in the parental line using the glutamine synthetase (GS) expression system, methionine sulfoximine (MSX) was added to the MACH-1 medium to inhibit endogenous GS activity. On the day of transfection, cells were seeded in T-25 flasks containing $1x10^7$ live cells in 1 mL fresh medium + MSX. Then, 15 µg purified PGC-1α DNA was incubated in 1.8 mL MSX-containing MACH-1 medium, while 37.5 µL polyethylenimine (PEI) was separately incubated in 1.8 mL MSX-containing MACH-1 medium. Next, the PEI incubation was combined with the PGC-1α DNA-containing aliquot and mixed thoroughly. The DNA/PEI mixture was incubated for 15 minutes at room temperature and then added to the T-25 flask containing C2869A cells. The cultures were incubated for 48 hours, then harvested, centrifuged at 1000 RPM for five minutes, and the transfection medium was aspirated. The transiently transfected cells were re-suspended in fresh MACH-1 + MSX, phenol red, and 300 µg/mL zeocin (Invitrogen) at a density of $1.6x10^4$ cells/200 µL. Phenol red (Sigma) was added for visual assessment of cell growth, while zeocin was added for antibiotic selection to inhibit the growth of any cells not containing the PGC-1α DNA construct as previously described [8]. The cell suspension was aliquoted into 96-well plates (200 uL/well) for mini-pool selection to obtain stable lines.

Roughly half of the medium in each well was removed via aspiration every three to four days and replaced with fresh growth medium. When the medium color change indicated rapid cell growth, the cells in those wells were expanded into 24-well plates, then to 12- and 6-well plates before finally expanding to T-25 and then T-75 flasks. Once the expanded mini-pools reached sufficiently high cell densities, they were seeded at $3x10^5$ cells/mL in 30 mL medium in

125 mL shake flasks as stable populations. The expanded stable C2869A+PGC-1α cell lines were next characterized to verify successful transfection of PGC-1α.

3.3.2 Characterization of stable PGC-1α overexpressing lines

A total of 20 C2869A+PGC-1α stable cell lines were generated from the antibiotic-resistant mini-pools. These lines were analyzed for recombinant PGC-1α mRNA expression, mAb titer and qP, lactate and glucose extracellular fluxes, growth rates, and viability profiles. Eight of the transfected lines exhibited a loss of mAb production and were not studied further. Additionally, three stable lines did not demonstrate PGC-1α mRNA overexpression as measured by RT-qPCR and were not studied further. The remaining nine cell lines were further analyzed to identify lines exhibiting high mAb productivity, moderate levels of PGC-1α mRNA overexpression, and a range of growth rates. Four PGC-1α overexpressing C2869A lines were selected for ^{13}C MFA experiments. Lines B5, C3, and D4 exhibited the highest qP levels of the twenty C2869A+PGC-1α lines and mid-range mRNA overexpression of PGC-1α. Line C1 also had moderate levels of mRNA expression and increased qP, though not as substantially increased as the other three lines. However, C1 exhibited increased growth rate and final volumetric titer compared to the other three stable lines and was chosen for further analysis due to its altered growth phenotype.

3.3.3 Generation and characterization of stable empty vector (EV) overexpressing lines

To control for the effects of the selection process, C2869A parental cells were transfected with an empty vector (EV) using the same transfection and selection method previously described for PGC-1α overexpressing lines. The EV utilized was pcDNA3-EGFP gifted by Doug Golenbock (Addgene plasmid #13031). A total of 13 stable cell lines were generated and

analyzed by the same metrics as the PGC-1α lines—mAb titer, qP, lactate and glucose extracellular fluxes, growth rates, and viability profiles.

3.3.4 Total RNA isolation and quantitative real-time PCR

Total RNA was isolated from cells using the RNeasy Mini Kit (Qiagen, Germantown, MD) according to the manufacturer's protocol and then reverse transcribed using a cDNA reverse transcriptase kit (BioRad, Hercules, CA). Quantitative real-time PCR (RT qPCR) was performed using iQ SYBR Green Supermix (BioRad, Hercules, CA) and BioRad CFX96 Cycler (BioRad, Hercules, CA). The sequences of the primers were as follows: PGC-1α sense (5'- GTC ACC ACC CAA ATC CTT AT -3') and antisense (5'- ATC TAC TGC CTG GAG ACC TT -3'), HPRT sense (5'- TGC TCG AGA TGT CAT GAA GGA G -3') and antisense (5'- TTT AAT GTA ATC CAG CAG GTC AGC -3'). Target gene expression was normalized to the expression of the housekeeping gene hypoxanthine guanine phosphoribosyltransferase (HPRT).

3.3.5 Cell culture and isotope labeling experiment

Parental C2869A and the C2869A+PGC-1α lines B5, C1, C3, and D4 were grown in 125 mL shake flasks at 37°C and 5% CO_2 while shaking at 135 RPM. Four replicate flasks of each line were expanded from a single culture and grown in parallel. The cells were cultivated in the proprietary cell culture medium, MACH-1 (Janssen) with MSX and 300 ug/mL zeocin (Invitrogen) and fed proprietary feeds (Janssen) of amino acids and other nutrients according to Table 3-1.

Table 3-1 Experimental timeline of ^{13}C labeling experiments. Days 5-8 are shaded to indicate presence of^{13}C glucose in the cell culture medium. The ^{13}C glucose bolus fed on day 5 initiated the labeling experiment (time = 0 hours), and samples were withdrawn and cold quenched at multiple time points to measure ^{13}C enrichments of intermediate metabolites.

Day	0	1	2	3	4	5	6	7		8	
Event	Inoculate			Feed		Feed ^{13}C 0h		RT qPCR		OUR	
								Cold Quenches			
								40h	48h	60h	72h

A bolus of 100% [U-$^{13}C_6$] glucose was fed to two replicate flasks of each line at the start of stationary growth phase (day five). The onset of stationary growth phase was designated as the point when lactate metabolism switched from production to consumption. Two additional replicate flasks were fed natural (unlabeled) glucose at this time. The size of the glucose bolus was chosen to be 70% of the total glucose in the culture after the feed. The unlabeled cultures were sampled daily to assess growth and extracellular exchange rates. After two days of ^{13}C glucose exposure, cell pellets were collected from the labeled cultures roughly every 12 hours and were immediately cold-quenched as previously described [10].

3.3.6 Determination of growth and extracellular exchange rates

Culture VCDs and percent viabilities were measured using a trypan blue exclusion method with a Cedex XS automated counter (Roche, Basel, Switzerland). Medium amino acid concentrations were analyzed using an Agilent 1200 series high performance liquid chromatograph (HPLC) as described previously [10]. Medium glucose and lactate concentrations were measured using a YSI 2300 biochemical analyzer (YSI, Yellow Springs, OH), and mAb titers were measured by a ForteBio Octet RED96 (Pall, Menlo Park, CA). Net growth rates, death rates, and extracellular fluxes were calculated by the ETA software package [26] as previously described [10].

3.3.7 Oxygen consumption measurements

OURs were measured using an Oroboros Oxygraph-2k instrument, which contains two chambers with separate oxygen probes to monitor on-line changes in oxygen concentration over time. The instrument was set to 37ºC and cells were harvested from each culture and re-suspended in growth medium at a density of $2x10^6$ cells/mL. For each C2869A+PGC-1α line, two million cells were injected into one chamber of the instrument while two million cells of the C2869A parental control line were injected into the opposite chamber. The parental line was included in each experiment to control for chamber effects. The rates of oxygen consumption were allowed to reach equilibrium for a minimum of five minutes before OUR was measured.

3.3.8 Gas chromatography-mass spectrometry (GC-MS) measurements

Intracellular metabolites were extracted from the cold-quenched cell pellets, derivatized, and analyzed by gas chromatography-mass spectrometry (GC-MS) as described previously [12]. GC-MS analysis of medium glucose was performed by di-*O*-isopropylidene derivatization to accurately identify the enrichment of ^{13}C-glucose in each labeled flask as previously described [27].

3.3.9 ^{13}C isotopically non-stationary metabolic flux analysis (INST-MFA)

An isotopomer model was constructed based on a previously described CHO cell metabolic network in order to simulate the ^{13}C labeling profile of intracellular metabolites [10,11]. The model comprised 80 metabolic reactions, 22 extracellular metabolite exchange rates, and two macromolecular products (mAb and biomass) as detailed in Table A-3-3. Isotopomer models were regressed by the INCA software package [28] to fit the experimental data sets as previously described [10]. All model fits were overdetermined and calculated from a

random starting point with a minimum of 50 random restarts to ensure the identification of a global minimum. Due to the absence of isotopic steady state, isotopically non-stationary metabolic flux analysis (INST-MFA) was used to regress flux maps of the studied lines over days six through eight of the experiment. Goodness-of-fit metrics for the models are given in Table A-3-1. The Cytoscape software package was used to visualize the resulting flux maps [29].

3.3.10 Statistical analysis

Significant differences between fluxes of the different cell lines were analyzed via two-way ANOVA ($\alpha = 0.05$) with Tukey-Kramer post-hoc testing. Standard errors of the mean (SEM) for each flux were calculated from the 95% confidence intervals generated in INCA by dividing the difference between the upper and lower bounds by 3.92.

3.4 Results

3.4.1 Stable PGC-1α lines exhibit higher PGC-1α mRNA levels than parental control line

All four of the C2869A+PGC-1α CHO cell lines had increased PGC-1α mRNA levels as shown in **Error! Reference source not found.**. Line B5 exhibited the highest level of PGC-1α mRNA expression followed by C1, C3, and D4. These results confirm that the PGC-1α expression vector was successfully integrated into the DNA of these stable cell lines, and that they exhibited increased transcriptional activity of the recombinant PGC-1α gene.

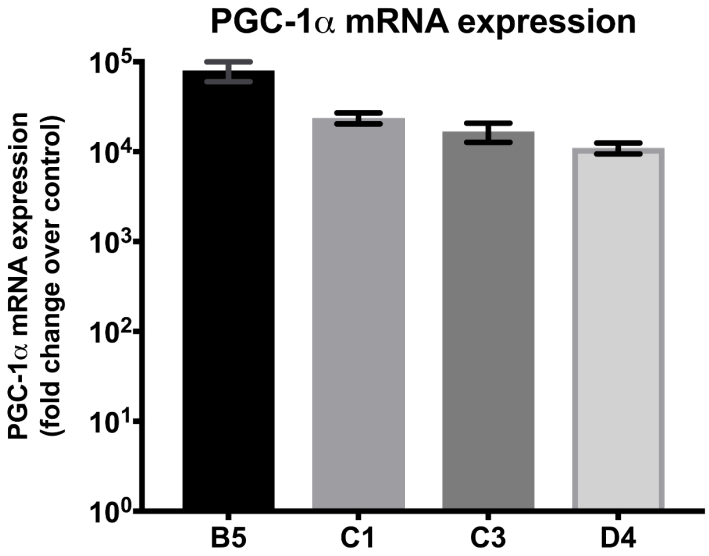

Figure 3-2 Recombinant PGC-1α mRNA levels reported as fold changes over control expression. Expression levels were normalized to expression of the housekeeping gene, HPRT, on day seven of the fed-batch experiment as indicated in **Error! Reference source not found.**. Means +/- SEM plotted, n=2.

3.4.2 PGC-1α lines consume more oxygen than the control

Oxygen uptake rates (OURs) were measured for each C2869A+PGC-1α line in comparison to the parental control on the final day of the fed-batch experiment as indicated by the experimental timeline described in Table 3-1. All C2869A+PGC-1α lines exhibited significantly increased OURs with the exception of line C1, which consumed oxygen at the same cell-specific rate as the parental control (Figure 3-3). These results indicate that three out of the four PGC-1α overexpressing lines exhibited substantial enhancements in oxidative metabolism during stationary phase. The only PGC-1α line that did not follow this trend (C1) also exhibited a different growth phenotype during stationary phase in comparison to the other PGC-1α lines.

3.4.3 Net growth rates of all PGC-1α lines except C1 are similar to the parental control

Net growth rates were calculated from the VCD time course, and death rates were calculated from the estimated dead cell densities over time where dead cell density is total cell density minus VCD. The net growth rates along with specific death rates are reported in Figure

3-3B and C. The net growth rate is equal to the gross growth rate minus the death rate and is measured from the growth curves shown in Figure 3-3A. The gross growth rate, which accounts for cell growth and cell death, was used for ^{13}C MFA and is shown in Figure A-3-1**.** The net growth rates were similar across all lines with the exception of C1, which experienced a roughly 2.5-fold higher rate of growth than the other cell lines during stationary phase.

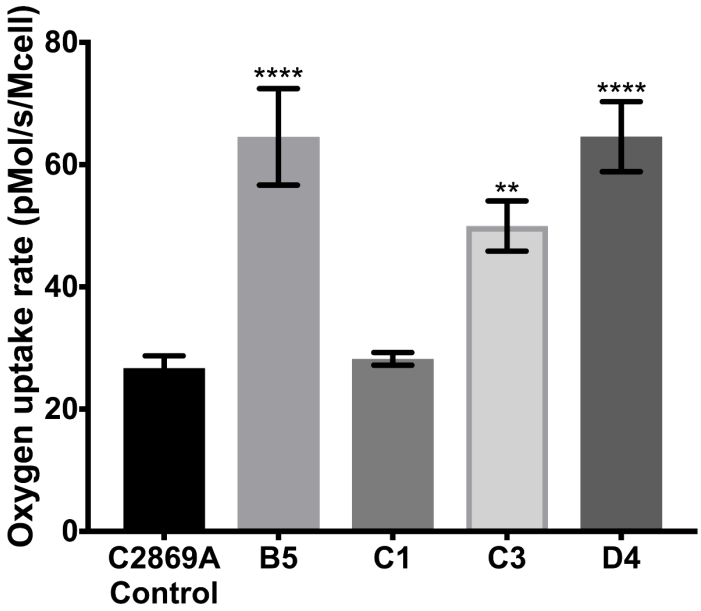

Figure 3-3 Oxygen uptake rates (OURs) of the four PGC-1α CHO cell lines compared to the C2869Acontrol line. Means +/- SEM reported, n=2; **** indicates significant difference from the control, α <0.0001; ** α<0.01.

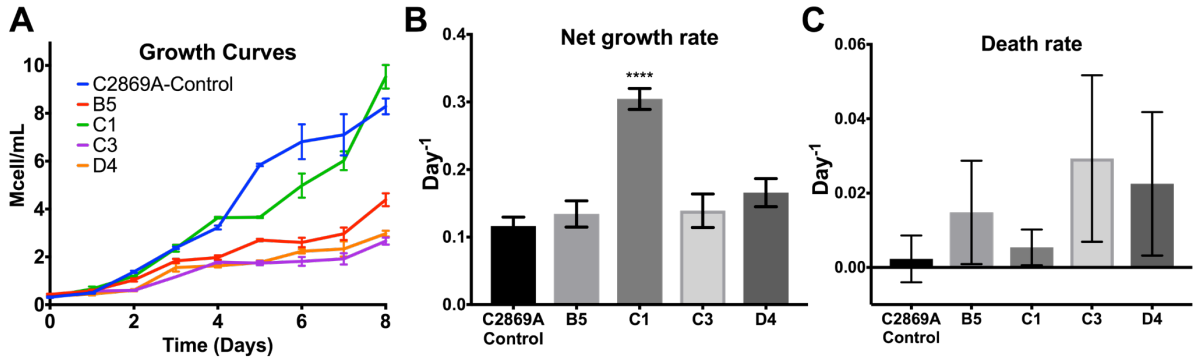

Figure 3-4 (A) Growth curves over the full duration of the experiment. (B) Net growth rates calculated during stationary growth phase (days 5-8). (C) Death rates of each line during stationary growth phase. The gross growth rate reported in **Figure A-3-1** was calculated by adding the death rates in (C) to the net growth rates in (B). Means +/- SEM reported, n=4; **** indicates significant difference from control, α<0.0001.

3.4.4 PGC-1α lines exhibit higher volumetric titers and qP than the control

All four PGC-1α lines exhibited significantly higher mAb qP than the parental control (Figure 3-5). Line B5 had both the highest final volumetric titer of 641 µg/mL as well as the highest qP of any line at 37.3 µg/Mcell/day, approximately four times the rate of the parental control. C1 had the second highest final volumetric mAb titer at 550 µg/mL but the lowest qP of the PGC-1α lines, which was still 2.7-fold higher than the parental control. This divergence is explained by the elevated growth and VCD of the C1 line, as a result of the trade-off between growth and product biosynthesis.

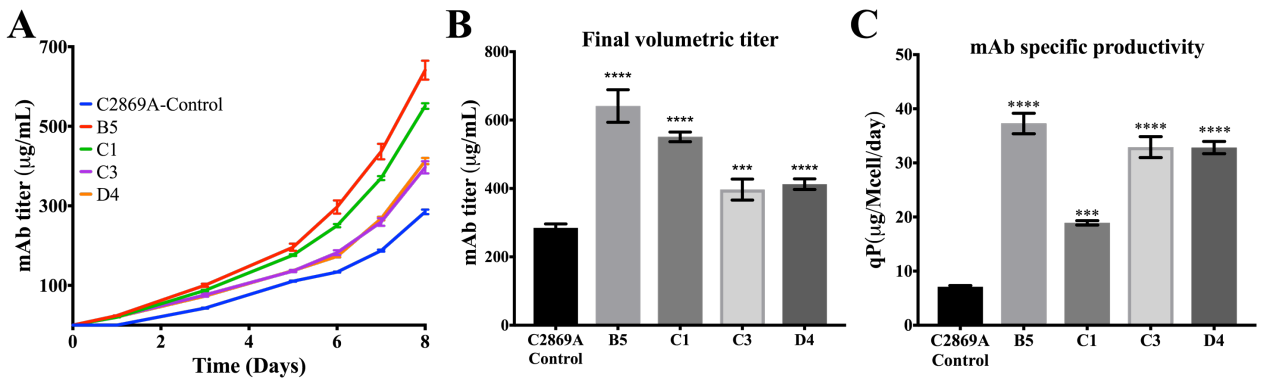

Figure 3-5 (A) mAb titer profiles, (B) final volumetric mAb titer measured on day eight of the experiment, and (C) cell specific productivity (qP) of each line. Means +/- SEM shown, n=4; *** indicates significant difference from control, α <0.001, **** α <0.0001.

3.4.5 PGC-1α lines consume both glucose and lactate at higher rates than the control

Glucose uptake rates (GURs) were significantly higher in PGC-1α lines than in the parental control with the exception of C1 (Figure 3-6A). Similarly, the lactate uptake rates (LURs) of all four PGC-1α lines were significantly increased over the parental control line during stationary phase (Figure 3-6B). The LUR of C1 was the lowest of the PGC-1α lines at ~0.17 µmol/Mcell/day, but was still significantly increased over the control line (0.06 µmol/Mcell/day).

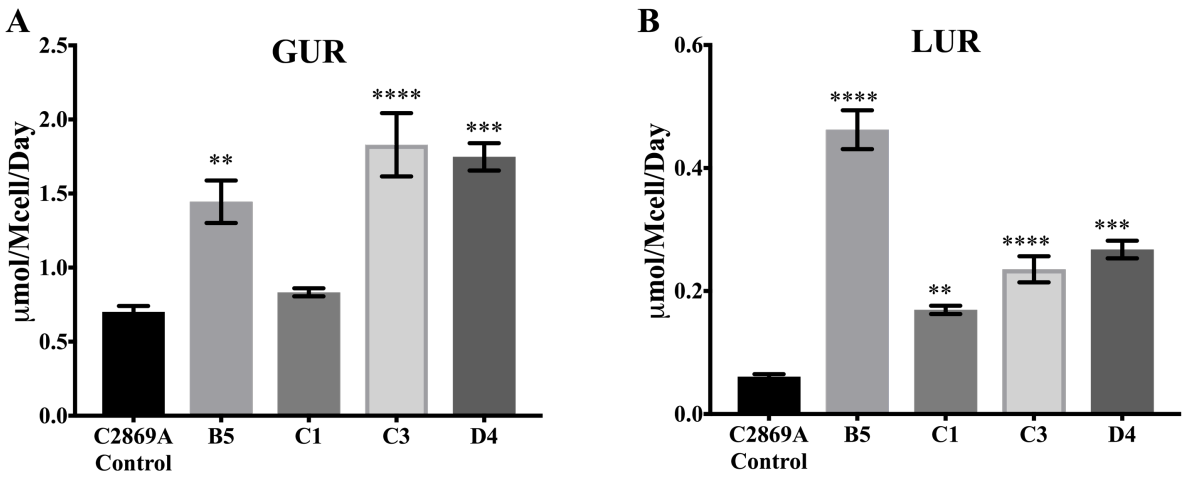

Figure 3-6 (A) Glucose uptake rate (GUR) and (B) lactate uptake rate (LUR) of each cell line. Means +/- SEM shown, n=4; ** indicates significant difference from control, α <0.01, *** α <0.001, **** α <0.0001.

3.4.6 PGC-1α lines have higher oxidative metabolic fluxes than control

Three PGC-1α lines (B5, C3, and D4) exhibited higher rates of CAC metabolism (up to three-fold increases in some cases) than that of the C2869A control and PGC-1α line C1 (Figure 3-7). Furthermore, lines B5, C3, and D4 had elevated overall central carbon metabolism as compared to the control and C1 lines, consistent with the increased substrate uptake rates shown in Figure 3-6. The higher consumption of carbon from glucose was not mirrored by increased rates of growth for the three PGC-1α lines (B5, C3, and D4) but the excess carbon was funneled into mAb production (Figure 3-5) by all four lines showing increased GURs and/or LURs.

3.4.7 EV overexpressing cell lines

The 13 PGC-1α overexpressing lines (still producing mAb) and the 13 EV overexpressing cell lines were compared for mAb volumetric titer (Figure A-3-11), qP (Figure A-3-10), growth, viability, LUR and GUR (Figure A-3-12). The population spread of qP and the other metrics were all similar with no stark differences in trends between the EV and the PGC-1α

overexpressing cell lines. This data suggested that the zeocin antibiotic selection process seemingly selected for more robust cells with increased rates of growth and overall metabolism.

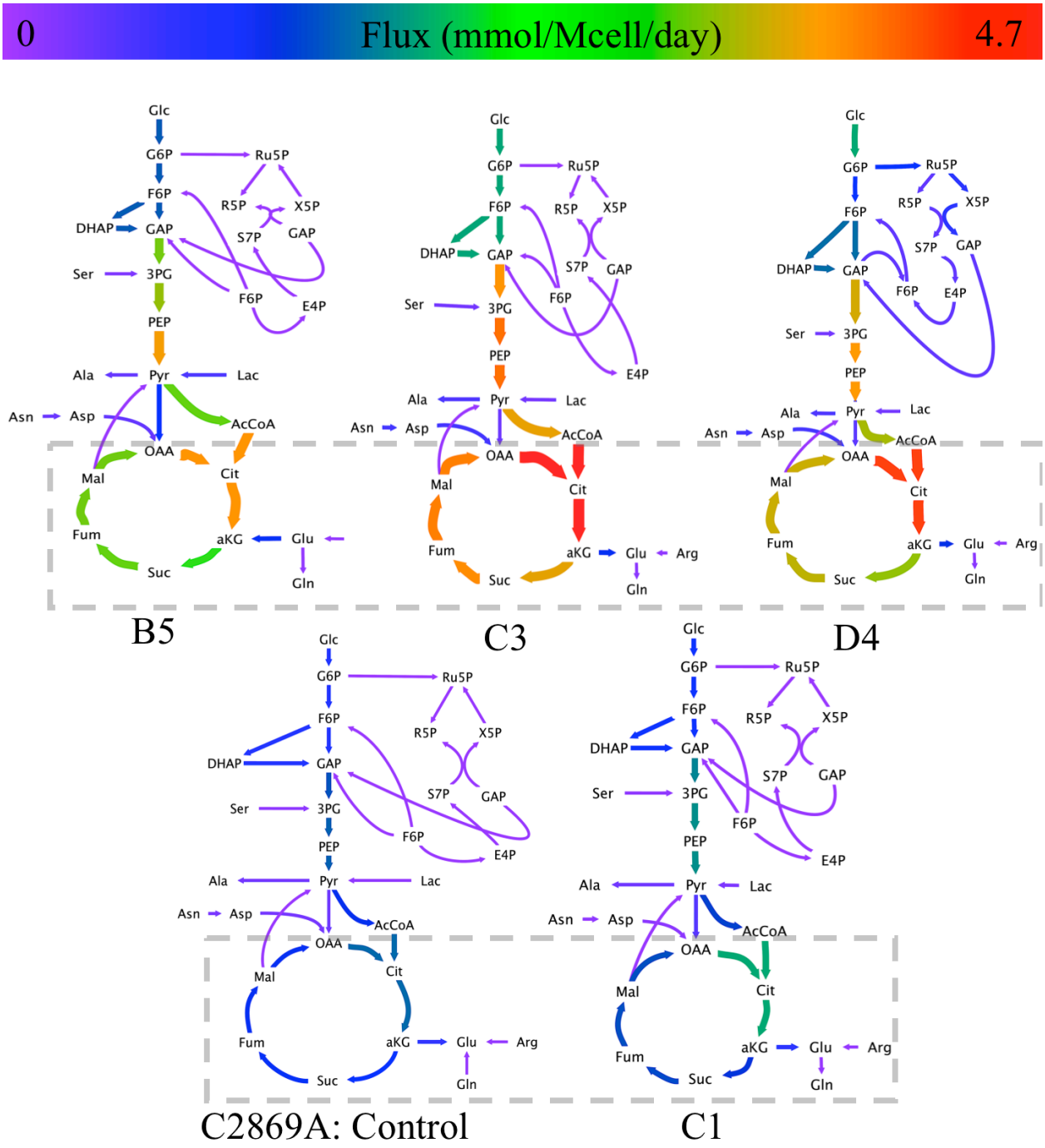

Figure 3-7 Metabolic flux maps during stationary growth phase. The magnitude of each reported net carbon flux corresponds with the color and the width of the corresponding arrow. The mitochondrial oxidative citric acid cycle fluxes are boxed for emphasis.

3.5 Discussion

This study sought to assess the correlation between elevated oxidative metabolism and qP in industrial CHO cell lines. Previous studies have uncovered an association between high mAb producing CHO cell clones and elevated CAC metabolism [10,11]. Here, we sought to engineer mAb producing industrial CHO cells with elevated oxidative metabolic activity through the introduction of PGC-1α. PGC-1α is a global regulator of mitochondrial metabolism extensively shown in the literature to increase mitochondrial number and, therefore, cellular oxidation [16–18,30–34]. Since the highly oxidative CAC is located in the mitochondria, we hypothesized that increasing mitochondrial capacity of industrial CHO cells via PGC-1α overexpression would lead to increased qP.

The B5, C3, and D4 lines exhibited an increase in both glucose and lactate consumption, the main sources of carbon for stationary-phase CHO cell cultures. High lactate consumption rates during stationary growth phase have been correlated to high productivities in CHO cell lines, a finding mirrored in this study [11]. Higher LURs also prolong culture longevity by removing toxic lactate buildup from the extracellular environment and provide a more direct source of carbon to mitochondrial metabolism. In order to fuel mitochondrial oxidative metabolism, carbon from lactate only needs one enzymatic step to be converted to pyruvate, whereas carbon from glucose must traverse all of glycolysis in order to successfully enter the mitochondria.

The PGC-1α lines selected for this study all exhibited some level of upregulated CAC metabolic activity, with C1 more closely resembling the parental control. In previous work performed in cultured cardiac myocytes overexpressing PGC-1α, mitochondrial genes

responsible for energy production pathways (e.g., CAC enzymes) exhibited increased expression along with increased mitochondrial numbers [35]. We hypothesize that the increase in CAC flux was directly related to the increase in oxygen consumption of the PGC-1α lines as shown in previous work [35]. The OURs (Figure 3-3) indicated an increase in mitochondrial activity in three of the four PGC-1α lines, which was reflected by the increase in CAC fluxes regressed by ^{13}C INST-MFA. The OURs independently confirm the MFA results, as the OURs were not used to constrain the ^{13}C MFA model. Functional PGC-1α overexpression has been repeatedly shown to increase mitochondrial number in mammalian cells, therefore increasing oxidative metabolic capacity as reflected in higher rates of oxygen consumption [21]. This evidence of higher rates of mitochondrial metabolism, both in measured metabolic fluxes and cellular OURs, suggests that PGC-1α was functionally overexpressed in the B5, C3, and D4 cell lines.

All PGC-1α lines exhibited significantly enhanced qP over the parental control, with C1 trending more closely with the parental control than the other three engineered lines (Figure 3-5). This data supports the hypothesis that an increased oxidative capacity leads to an increase in qP and further established that high producing lines require a highly active CAC to support increased qP. There appears to be a trade-off between mAb production and growth, which can lead to higher final volumetric titers in rapidly growing cells as demonstrated by line C1. This was the only cell line studied with increased growth rate compared to the control (Figure 3-4), and it had the second highest final volumetric titer but the lowest qP of all the PGC-1α lines studied (Figure 3-5). Further contributing to the final volumetric titer differences were the significantly slower growth rates exhibited by PGC-1α lines during exponential growth phase (Figure A-3-2). These slower growth rates resulted in fewer viable cells during the peak mAb production phase (Figure 3-4A).

In most the data presented here, line C1 trended with the parental control cell line. From preliminary Western Blot (WB) analysis, we have evidence that line C1 expressed an alternate isoform of PGC-1α, the NT-PGC-1α splice variant (Figure A-3-4). NT-PGC-1α results from alternate 3' splicing and results in a short, truncated version of the PGC-1α protein [36,37]. The truncated PGC-1α variant likely has different regulatory properties compared to the full-length protein [37]. Further, PGC-1α4 has similar alternate 3' splicing as NT-PGC-1α and has been shown to control muscle hypertrophy without co-activation of known PGC-1α targets involved in mitochondrial biogenesis [20,37]. NT- PGC-1α is reported to have a molecular weight of 37 kDa, whereas PGC-1α4 is predicted to be 29.1 kDa [20]. Other splice variants of PGC-1α are reported to have similar predicted molecular weights [20], making them difficult to decipher via WB. Another possible explanation for the divergent metabolic phenotype of the C1 line is that the mini-pool selection process could have allowed cells with superior growth and productivity attributes to outcompete and overtake the polyclonal population. This conclusion would lead to the hypothesis that some of the differences in phenotype between PGC-1α lines may in fact be due to the selection process and not due to the overexpression of PGC-1α. Further supporting this alternate hypothesis are the data collected from the EV lines. These data show a similar spread in qP and other metrics used to initially characterize the PGC-1α lines. Further testing, specifically OUR measurements of the EV lines, will be required in order to determine if oxidative metabolism is significantly altered during the selection process.

Taken together, these data provide evidence that increased carbon flux through mitochondrial oxidative metabolism drives CHO cell qP upward. Overall, this study concluded that PGC-1α overexpression was associated with high oxidative metabolism and qP in industrial CHO cell cultures.

3.6 Future Directions

In order to confirm our hypothesis that PGC-1α leads to the highly oxidative metabolic phenotype seen in three of the four PGC-1α lines, we propose performing siRNA knockdowns of PGC-1α in the PGC-1α overexpressing stable lines studied here. Therefore, if the metabolic phenotype shifts from highly oxidative to trend more with the control cell line, it can be reasonably concluded that PGC-1α gene expression is responsible for the shift in metabolism seen in the PGC-1α lines generated in this study. Furthermore, OURs of the EV lines will be required to determine if the spread in the data is due to the selection of antibiotic resistant lines.

Through the rational design of RT-qPCR primers, it should be possible for future experiments to elucidate which PGC-1α variants we have present in each C2869A+PGC-1α cell line studied here. If, in fact, line C1 does express the PGC-1α4 or NT- PGC-1α splice variants, that could explain some of the differences in metabolic phenotype between the engineered cell lines.

Since peak mAb productivity in CHO cells occurs during stationary phase naturally, inducing PGC-1α overexpression during the onset of stationary phase could further increase effectiveness of the enhanced oxidative metabolic phenotype. This method could allow cells to reach higher VCDs by not sacrificing growth during early exponential phase (see Figure A-3-2), which would lead to increased volumetric titers at later stages of culture. The gene could be placed on a variety of different inducible expression systems. One possibility would be a chemically induced expression system like the reverse cumate gene-switch that induces gene expression upon the addition of cumate to the culture [38,39]. Another option would be gene expression on a self-regulating promoter such as *Txnip* [40,41]. The *Txnip* expression system has previously been used in CHO cells to express genes as culture growth slows, with one study

showing increased gene expression over time with certain cultures getting activated at the onset of stationary phase [40]. Ultimately, further experiments to optimize the timing and intensity of PGC-1α expression should be carried out to maximize qP and titer.

3.7 Appendix

Table A-3-1 Model goodness-of-fit assessment metrics as determined by INCA software and the best-fit model for each cell line.

	SSR best fit	SSR expected range	DOF
C2869A	146.5	104.7 - 169.1	135
B5	127.5	85.5 - 144.3	113
C1	134	89.8 - 150.0	118
C3	89.8	103.8 - 167.9	134
D4	118.5	95.9 - 157.8	125

Table A-3-2 Precursor requirements for growth.

Metabolite	Coefficient (µmol/Mcells/day)
Alanine	1.776×10^{-4}
Arginine	1.116×10^{-4}
Asparagine	1.396×10^{-4}
Aspartate	8.529×10^{-5}
Cysteine	4.292×10^{-5}
Glutamine	9.528×10^{-5}
Glutamate	1.143×10^{-4}
Glycine	1.948×10^{-4}
Histidine	4.229×10^{-5}
Isoleucine	9.591×10^{-5}
Leucine	1.67×10^{-4}
Lysine	1.687×10^{-4}
Methionine	4.085×10^{-5}
Phenylalanine	6.487×10^{-5}
Proline	9.267×10^{-5}
Serine	1.305×10^{-4}
Threonine	1.143×10^{-4}
Tryptophan	1.305×10^{-5}
Tyrosine	5.389×10^{-5}
Valine	1.232×10^{-4}
G6P	8.538×10^{-5}
R5P	6.892×10^{-5}
C_1	7.458×10^{-5}
DHAP	3.599×10^{-5}
AcCoA.c	7.326×10^{-4}

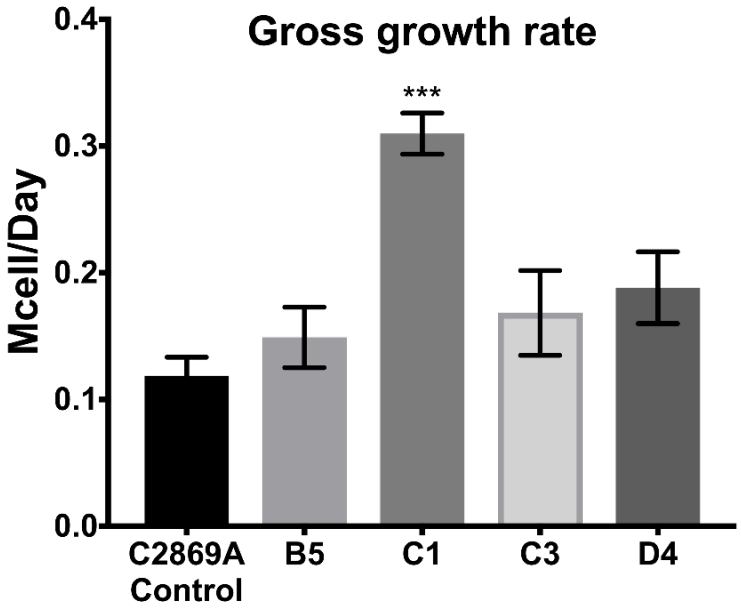

Figure A-3-1 Gross growth rates during stationary growth phase. Gross growth was used in the ^{13}C MFA experimental analysis as it accounts for total biomass generation. Means +/- SEM plotted, n=4; *** indicates significant difference from control, $\alpha < 0.001$.

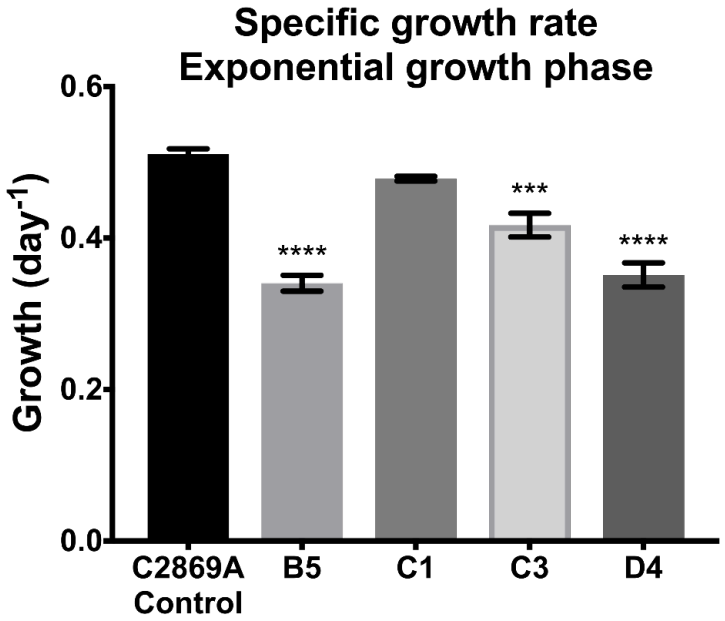

Figure A-3-2 Specific growth rates during exponential growth phase. The control line (C2869A) and line C1 trend together while the remaining PGC-1α lines experience significantly decreased rates of growth during exponential phase, days zero through five of the experiment. Means +/- SEM plotted, n=4; *** indicates significant difference from control, $\alpha < 0.001$, **** $\alpha < 0.0001$.

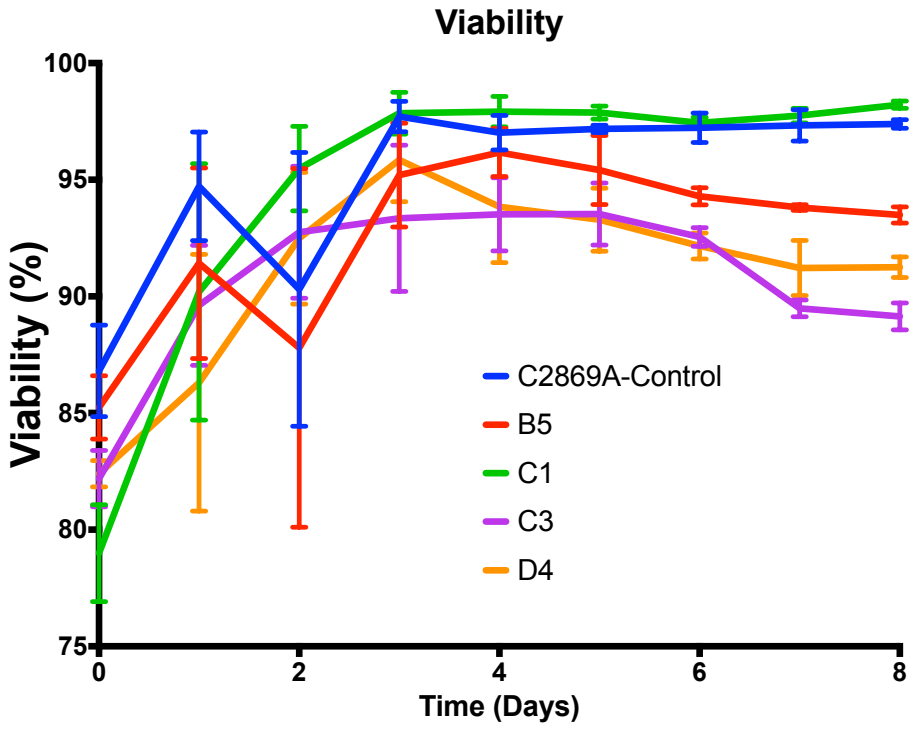

Figure A-3-3 Viability profiles of the cultures. Mean +/- SEM reported; n=4.

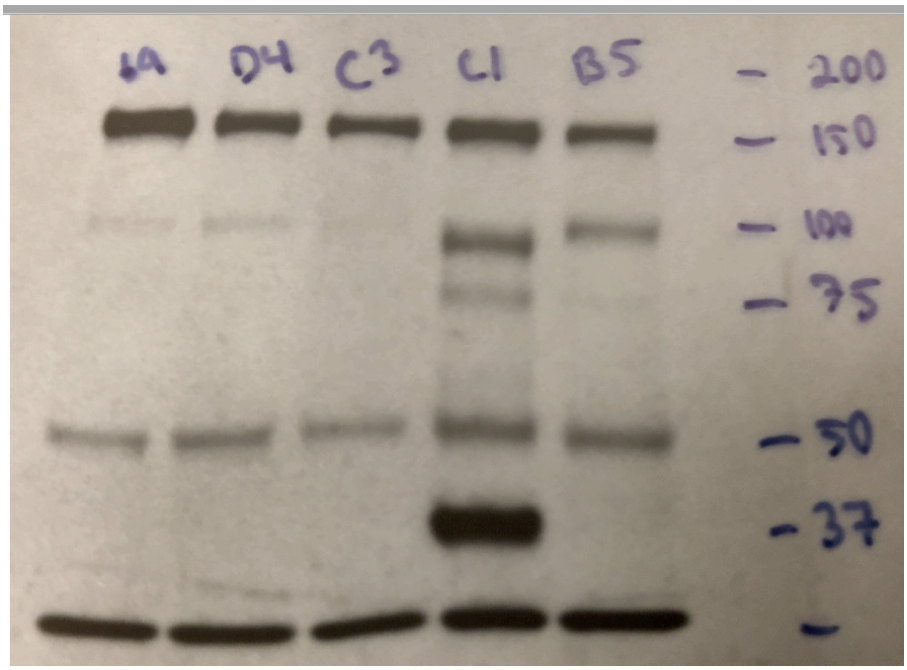

Figure A-3-4 Anti- PGC-1α Western Blot (WB) of the selected PGC-1α lines and parental line (leftmost lane). C1 appeared to express a different PGC-1α isoform than the other lines. Anti-PGC-1α antibody should detect both recombinant and endogenous PGC-1α. Intact PGC-1α should be detected at 113 kDa, NT- PGC-1α at 37 kDa, and PGC-1α4 at 29.1 kDa.

Table A-3-3 Flux maps with 95% confidence intervals indicated by lower bound (LB) and upper bound (UB).

		C2869A: control			B5			C1			C3			D4		
		Flux	LB	UB	Flux	LB	UB	Flux	LB	UB	Flux	LB	UB	Flux	LB	UB
1	Glc.e → Glc	0.7262	0.6428	0.8021	1.504	1.274	1.77	0.8564	0.8055	0.9075	1.8924	1.5143	2.2958	1.9172	1.5765	2.2874
2	Glc.l ↔ Glc.e	0.4979	0.4405	0.551	1.3274	1.1207	1.579	0.5838	0.5485	0.6191	1.6308	1.2983	2.0189	1.2967	1.0657	1.5483
3	Glc.u → Glc.e	0.2283	0.2007	0.2572	0.1766	0.0984	0.3425	0.2726	0.2537	0.2919	0.2616	0.1482	0.3902	0.6205	0.5064	0.7431
4	Glc → G6P	0.7262	0.6428	0.8021	1.504	1.274	1.77	0.8564	0.8055	0.9075	1.8924	1.5143	2.2958	1.9172	1.5765	2.2874
5	G6P ↔ F6P	0.7262	0.4461	0.8115	1.504	1.2357	1.7705	0.8564	0.6583	0.9068	1.8924	1.481	2.296	0.9378	-1.1575	2.1512
6	F6P → DHAP + GAP	0.7261	0.624	0.8052	1.504	1.266	1.7716	0.8564	0.7806	0.9059	1.8924	1.5146	2.2961	1.5907	0.9328	2.1585
7	DHAP ↔ GAP	0.7261	0.6431	0.8114	1.504	1.2732	1.77	0.8564	0.781	0.9074	1.8924	1.515	2.296	1.5907	0.9482	2.16
8	GAP ↔ 3PG	1.4523	1.2847	1.6225	3.0079	2.5515	3.5404	1.7128	1.6106	1.8141	3.7848	3.029	4.592	3.5078	2.8252	4.1837
9	3PG ↔ PEP	1.5183	1.3513	1.6741	3.1754	2.7169	3.7066	1.7777	1.6705	1.879	4.0197	3.2634	4.8273	3.7426	3.0469	4.4207
10	Ser ↔ 3PG	0.066	0.0545	0.0774	0.1674	0.1425	0.1925	0.0649	0.0584	0.0714	0.2349	0.199	0.2708	0.2348	0.199	0.2707
11	OAA + AcCoA.m → Cit	1.567	1.333	1.766	3.7765	3.1821	4.4324	1.9091	1.7266	2.066	4.6814	3.8862	5.7254	4.3221	3.6673	5.1137
12	Cit ↔ aKG + CO2	1.5669	1.3333	1.7658	3.7764	3.1845	4.4316	1.9089	1.7247	2.0656	4.6813	3.8854	5.7251	4.322	3.6662	5.1025
13	aKG → Suc + CO2	0.9412	0.7242	2.0368	2.7049	2.1888	4.4577	1.243	1.0147	1.9145	3.6004	2.77	5.2248	3.1616	2.5548	4.2017
14	Suc ↔ Fum	1.0589	0.8411	2.1585	2.9274	2.4127	4.5071	1.3788	1.1492	2.054	3.8135	2.9826	5.4368	3.3747	2.7584	4.4074
15	Fum ↔ Mal	1.0913	0.8729	2.2568	2.9918	2.479	4.7651	1.4169	1.1874	2.0925	3.9004	3.0691	5.5243	3.4614	2.8486	4.5041
16	Mal ↔ OAA	1.0913	0.6948	1.4328	2.9918	2.0471	3.9882	1.4169	1.0747	1.6705	3.9004	3.0685	5.5235	3.4614	2.8442	4.4946
17	G6P → Ru5P + CO2	1.00E-07	0	0.2176	1.00E-07	0	0.2468	1.00E-07	0	0.1674	1.00E-07	0	0.2708	0.9793	0	3.2324
18	Ru5P ↔ X5P	-5.39E-06	-7.01E-06	0.1891	-6.78E-06	-8.93E-06	0.1647	-1.42E-05	-1.56E-05	0.1326	-7.67E-06	-1.07E-05	0.1744	0.6529	-1.82E-06	2.1668
19	Ru5P ↔ R5P	5.49E-06	4.17E-06	0.0745	6.88E-06	4.73E-06	0.0824	1.43E-05	1.28E-05	0.0574	7.77E-06	4.76E-06	0.1114	0.3264	6.80E-06	1.0764
20	Mal → Pyr + CO2	1.00E-07	0	1.2647	1.00E-07	0	1.9915	1.00E-07	0	0.8224	1.00E-07	0	0.4661	1.00E-07	0	0.0872
21	Cit → AcCoA.c + OAA	8.70E-05	6.60E-05	1.08E-04	1.09E-04	7.48E-05	1.44E-04	2.27E-04	2.04E-04	2.50E-04	1.23E-04	7.53E-05	1.71E-04	1.38E-04	9.71E-05	1.79E-04
22	OAA ↔ PEP + CO2	2.64E-04	-0.1169	0.1476	0.5191	-0.6086	0.9984	2.22E-16	-0.1194	0.0584	0	-0.4355	0.7391	0	-0.405	0.3878
23	Asp ↔ Asn	-0.2003	-0.2176	-0.1849	-0.2771	-0.2932	-0.261	-0.0678	-0.073	-0.0627	-0.5026	-0.554	-0.4512	-0.5027	-0.554	-0.4513
24	ProCoA + CO2 → Suc	0.1177	0.1065	0.1284	0.2225	0.2014	0.2436	0.1358	0.13	0.1416	0.2131	0.1824	0.2439	0.213	0.1824	0.2439
25	Gln ↔ Glu	-0.0117	-0.0127	-0.0105	-0.0459	-0.052	-0.0399	-0.0242	-0.0285	-0.0199	-0.0904	-0.1028	-0.0781	-0.0904	-0.1028	-0.0781
26	Glu ↔ Pro	0.7275	-0.4286	0.8349	1.1997	-0.5975	1.4844	0.753	0.011	0.8589	1.213	0.5253	1.4333	1.2922	0.9229	1.4107
27	CO2 + C1 ↔ Gly	0.0212	0.0179	0.0247	0.0616	0.056	0.0671	0.0246	0.0218	0.0274	0.0845	0.0733	0.0956	0.0844	0.0732	0.0956
28	His → C1 + Glu	0.0136	0.0081	0.0196	0.0271	0.0211	0.0332	0.0151	0.0122	0.018	0.0661	0.0487	0.0836	0.066	0.0486	0.0835
29	Phe → Tyr	0.0187	0.0168	0.0205	0.0356	0.031	0.0403	0.0207	0.0192	0.0221	0.0449	0.0367	0.0531	0.0449	0.0366	0.0531
30	Ser ↔ Gly + C1	-0.0072	-0.0108	-0.0036	0.0163	0.0108	0.0219	-6.32E-04	-0.0034	0.0022	0.0018	-0.0094	0.0129	0.0018	-0.0094	0.013
31	Trp → CO2 + CO2 + Ala + aKetoadi	0.0055	0.0043	0.0068	0.0073	0.0054	0.0091	0.0043	0.0028	0.0059	0.0075	0.0047	0.0102	0.0075	0.0047	0.0102
32	aKetoadi → CO2 + CO2 + 2xAcCoA.m	0.0454	0.0324	0.0572	0.0936	0.0737	0.1135	0.0736	0.0661	0.0811	0.1744	0.1304	0.2186	0.1736	0.13	0.2178
33	aKG ↔ Glu	0.6256	-0.4584	0.7317	1.0715	-0.7182	1.3549	0.6659	-0.0656	0.7824	1.0809	0.3939	1.2959	1.1604	0.7961	1.2729
34	Ile → AcCoA.m + CO2 + ProCoA	0.0615	0.0512	0.071	0.1195	0.1013	0.1377	0.0785	0.0736	0.0834	0.1114	0.0846	0.1383	0.1113	0.0845	0.1382
35	Leu + CO2 → CO2 + 3xAcCoA.m	0.077	0.0686	0.0855	0.1421	0.1207	0.1636	0.093	0.086	0.1001	0.1428	0.1201	0.1655	0.1424	0.1199	0.1651
36	Tyr → CO2 + Fum + 2xAcCoA.m	0.0324	0.0285	0.0368	0.0643	0.0565	0.0722	0.0381	0.0346	0.0416	0.0868	0.0688	0.1049	0.0867	0.0687	0.1047
37	Val → CO2 + CO2 + ProCoA	0.0415	0.0378	0.0453	0.0849	0.0747	0.0951	0.0471	0.0444	0.0499	0.0851	0.0708	0.0995	0.0852	0.0708	0.0995
38	Lys → aKetoadi	0.04	0.0269	0.0522	0.0863	0.0665	0.1062	0.0693	0.062	0.0766	0.167	0.123	0.211	0.1662	0.1228	0.2098
39	OAA ↔ Asp	-0.2202	-0.2357	-0.2048	-0.3132	-0.3312	-0.2952	-0.0778	-0.0843	-0.0713	-0.5039	-0.5586	-0.4491	-0.504	-0.5587	-0.4492
40	Arg → Glu + Urea	0.0231	0.0172	0.029	0.0336	0.0243	0.0428	0.0284	0.0233	0.0335	0.0587	0.0422	0.0751	0.0586	0.0422	0.0751
41	Lys.e → Lys	0.04	0.0284	0.0532	0.0864	0.0667	0.1062	0.0693	0.0621	0.0766	0.167	0.123	0.2111	0.1662	0.1227	0.2099
42	Thr.e → Thr	0.0235	0.0181	0.0295	0.0716	0.0628	0.0804	0.043	0.0377	0.0482	0.0987	0.0713	0.1262	0.1	0.0728	0.1274
43	Phe.e → Phe	0.0187	0.017	0.0206	0.0357	0.031	0.0404	0.0207	0.0192	0.0221	0.0449	0.0367	0.0532	0.0449	0.0367	0.0531
44	Tyr.e → Tyr	0.0137	0.0102	0.0177	0.0287	0.0224	0.035	0.0175	0.0143	0.0206	0.042	0.0259	0.058	0.0419	0.0258	0.0579
45	Val.e → Val	0.0415	0.0378	0.0457	0.085	0.0748	0.0952	0.0472	0.0445	0.05	0.0852	0.0709	0.0995	0.0852	0.0709	0.0995
46	Leu.e → Leu	0.077	0.0686	0.0855	0.1422	0.1208	0.1637	0.0931	0.0861	0.1002	0.1428	0.1201	0.1656	0.1425	0.12	0.1651
47	Ile.e → Ile	0.0615	0.0524	0.0717	0.1195	0.1013	0.1378	0.0786	0.0737	0.0835	0.1114	0.0846	0.1383	0.1113	0.0845	0.1383
48	Trp.e → Trp	0.0055	0.0041	0.0068	0.0073	0.0055	0.0092	0.0044	0.0028	0.0059	0.0075	0.0047	0.0102	0.0075	0.0047	0.0102
49	His.e → His	0.0136	0.0076	0.0196	0.0272	0.0211	0.0332	0.0151	0.0122	0.0181	0.0661	0.0487	0.0836	0.066	0.0485	0.0835
50	Met.e → Met	0.0148	0.0129	0.0167	0.0181	0.0152	0.021	0.0102	0.0088	0.0115	0.0166	0.0125	0.0207	0.0166	0.0125	0.0207
51	Ser.e ↔ Ser	0.0736	0.0627	0.0844	0.2019	0.1776	0.2264	0.0745	0.0686	0.0804	0.2533	0.2192	0.2874	0.2533	0.2192	0.2874
52	Ala ↔ Ala.e	0.2332	0.2132	0.2509	0.3261	0.301	0.3512	0.2482	0.235	0.2614	0.4645	0.4047	0.5243	0.4644	0.4048	0.5242
53	Arg.e ↔ Arg	0.0231	0.0172	0.0298	0.0336	0.0244	0.0428	0.0284	0.0233	0.0335	0.0587	0.0422	0.0751	0.0587	0.0422	0.0751
54	Asp ↔ Asp.e	-0.02	-0.0222	-0.0178	-0.0362	-0.0443	-0.0279	-0.01	-0.0139	-0.0061	-0.0013	-0.0203	0.0177	-0.0013	-0.0204	0.0177
55	Cys.e ↔ Cys	0.0192	0.0188	0.0196	0.0011	-0.0192	0.023	0.0246	0.0142	0.035	0.025	-0.0189	0.0781	0.0252	-0.0189	0.0785
56	Glu ↔ Glu.e	-0.0769	-0.0861	-0.0677	-0.1135	-0.1283	-0.0987	-0.0679	-0.073	-0.0628	-0.0977	-0.1264	-0.0691	-0.0977	-0.1263	-0.0691
57	Gln.e ↔ Gln	-0.0117	-0.0127	-0.0107	-0.0459	-0.052	-0.0398	-0.0242	-0.0285	-0.0199	-0.0904	-0.1027	-0.0781	-0.0904	-0.1027	-0.078
58	Gly.e ↔ Gly	-0.0139	-0.0169	-0.0106	-0.0778	-0.0867	-0.0691	-0.0239	-0.0284	-0.0194	-0.0862	-0.0995	-0.0728	-0.0861	-0.0995	-0.0728
59	Pro.e ↔ Pro	-0.7275	-0.835	0.497	-1.1997	-1.4842	0.5951	-0.753	-0.8688	-0.0149	-1.2129	-1.4328	-0.5249	-1.2922	-1.4115	-0.9257
60	Asn.e ↔ Asn	0.2003	0.185	0.2177	0.2771	0.2611	0.2931	0.0679	0.0628	0.073	0.5026	0.4513	0.554	0.5027	0.4514	0.5542
61	Lac ↔ Lac.e	-0.06	-0.0691	-0.0508	-0.4581	-0.519	-0.3973	-0.1657	-0.1787	-0.1527	-0.235	-0.2766	-0.1934	-0.2339	-0.2753	-0.1923
62	→ Biomass	0.1187	0.0901	0.1473	0.149	0.1021	0.1959	0.3098	0.278	0.3417	0.1683	0.1028	0.2338	0.1882	0.1326	0.2438
63	Cys → Pyr	0.034	0.0322	0.0359	0.0192	0	0.0414	0.0347	0.0242	0.0453	0.0415	0	0.095	0.0417	0	0.0952
64	X5P ↔ EC2 + GAP	-5.39E-06	-7.01E-06	0.1891	-6.78E-06	-8.93E-06	0.1647	-1.42E-05	-1.56E-05	0.1326	-7.67E-06	-1.07E-05	0.1744	0.6529	-1.82E-06	2.1668
65	F6P ↔ EC2 + E4P	2.69E-06	-0.0946	3.50E-06	3.39E-06	-0.0823	4.47E-06	7.08E-06	-0.0663	7.81E-06	3.83E-06	-0.0872	5.34E-06	-0.3264	-1.0834	9.11E-07
66	S7P ↔ EC2 + R5P	2.69E-06	-0.0946	3.50E-06	3.39E-06	-0.0823	4.47E-06	7.08E-06	-0.0663	7.81E-06	3.83E-06	-0.0872	5.34E-06	-0.3264	-1.0834	9.11E-07
67	F6P ↔ EC3 + GAP	2.69E-06	-0.0946	3.50E-06	3.39E-06	-0.0823	4.47E-06	7.08E-06	-0.0663	7.81E-06	3.83E-06	-0.0872	5.34E-06	-0.3264	-1.0834	9.11E-07
68	S7P ↔ EC3 + E4P	-2.69E-06	-3.50E-06	0.0946	-3.39E-06	-4.47E-06	0.0823	-7.08E-06	-7.81E-06	0.0663	-3.83E-06	-5.34E-06	0.0872	0.3264	-9.11E-07	1.0834
69	Met + Ser → C1 + Cys + ProCoA + CO2	0.0148	0.0129	0.0167	0.0181	0.0152	0.021	0.0101	0.0088	0.0115	0.0166	0.0125	0.0207	0.0166	0.0125	0.0207
70	Amino Acids → Antibody	1.00E-07	0	0	5.08E-07	4.57E-07	5.58E-07	2.58E-07	2.47E-07	2.68E-07	4.48E-07	3.97E-07	4.98E-07	4.47E-07	4.17E-07	4.78E-07
71	PEP → Pyr.c	1.5185	1.3371	1.77	3.6944	2.6302	4.4406	1.7777	1.6381	1.885	4.0197	3.0593	5.1426	3.7426	2.8625	4.437
72	Lac ↔ Pyr.c	0.06	0.0508	0.0691	0.4581	0.3973	0.519	0.1657	0.1527	0.1787	0.235	0.1934	0.2766	0.2339	0.1923	0.2753
73	Ala ↔ Pyr.c	-0.2277	-0.2481	-0.2076	-0.3188	-0.344	-0.2937	-0.2439	-0.2572	-0.2306	-0.4571	-0.5169	-0.3972	-0.457	-0.5168	-0.3972
74	Pyr.m → AcCoA.m + CO2	1.1188	0.8903	1.2727	2.9148	2.3263	3.5643	1.3281	1.1457	1.4833	3.6192	2.8345	4.654	3.2629	2.6224	4.0331
75	Pyr.m + CO2 → OAA	0.2556	0.1131	0.4592	0.9905	0	1.435	0.4142	0.2145	0.5843	0.2771	0	0.538	0.3566	0	0.4829
76	Pyr.c ↔ Pyr.m	1.3508	1.1675	1.6025	3.8337	2.7437	4.5862	1.6994	1.5579	1.8096	3.7976	2.8333	4.9202	3.5196	2.6265	4.3673
77	Thr → Pyr.m + CO2	0.0235	0.0175	0.0295	0.0716	0.0628	0.0803	0.0429	0.0376	0.0482	0.0987	0.0713	0.1261	0.0999	0.0728	0.1272
78	0*Pyr.c → Pyr	69.2612	0	94.3591	1.00E-07	0	95.9324	95.9109	48.0225	99.9694	1.00E-07	0	NaN	1.00E-07	0	94.5068
79	0*Pyr.m → Pyr	30.7048	4.8689	97.7113	99.9808	13.728	100	4.0544	0	52.4824	99.9585	0	100	99.9583	0	NaN
80	Pyr → sink	100	100	100	100	100	100	100	100	100	100	100	100	100	100	100

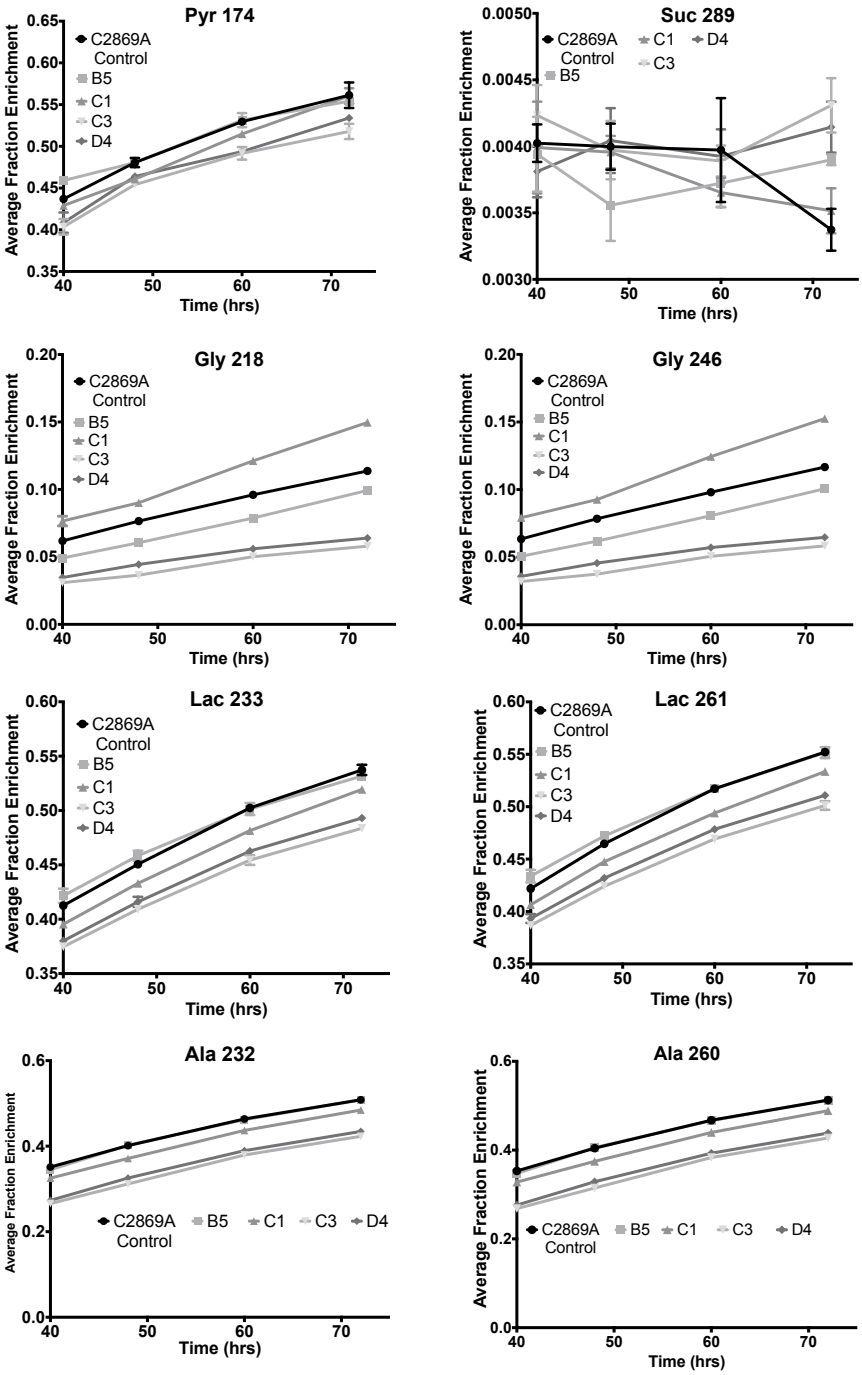

Figure A-3-5 Average percent enrichments (APEs) of intracellular metabolites over the course of the experiment. Isotopic steady state is reached when the fractional enrichment does not change over time. These data prompted the conclusion that isotopic steady state was not obtained. Therefore, INST-MFA was used to regress fluxes in the stationary phase CHO cell cultures studied here.

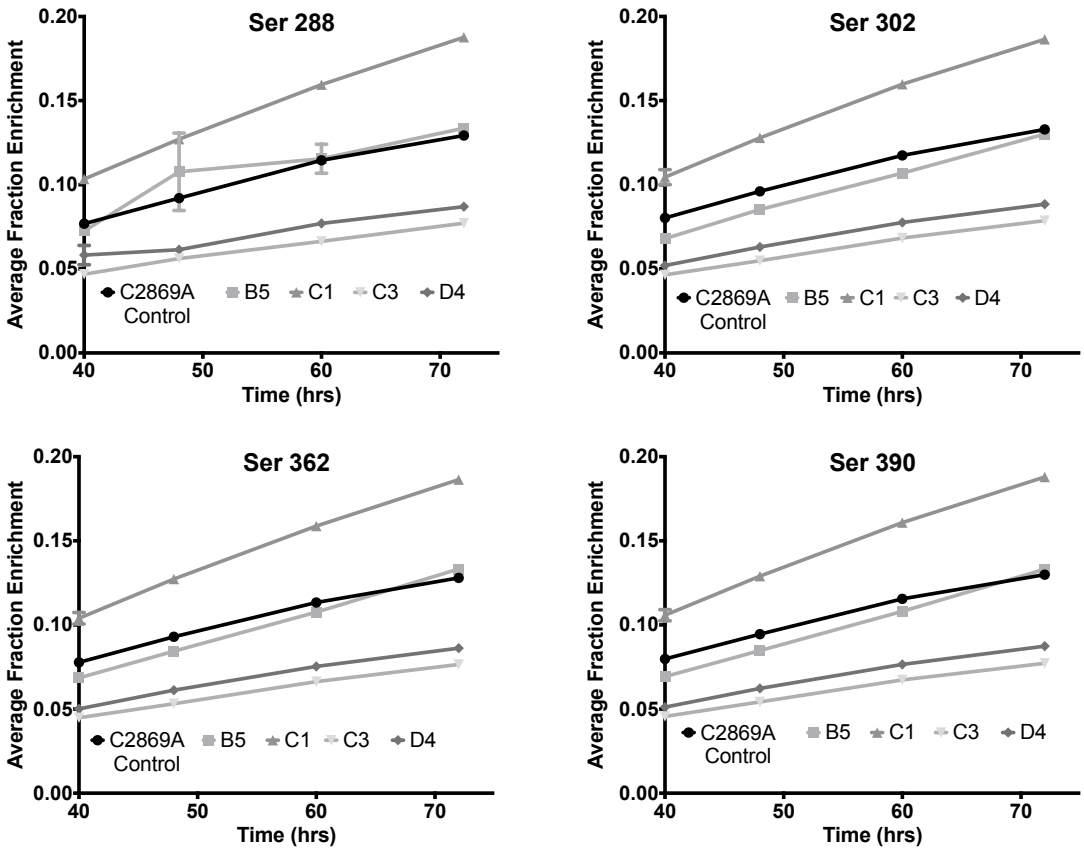

Figure A-3-6 Average percent enrichments (APEs) of intracellular metabolites over the course of the experiment (continued). Isotopic steady state is reached when the fractional enrichment does not change over time. These data prompted the conclusion that isotopic steady state was not obtained. Therefore, INST-MFA was used to regress fluxes over time in the CHO cell cultures studied here.

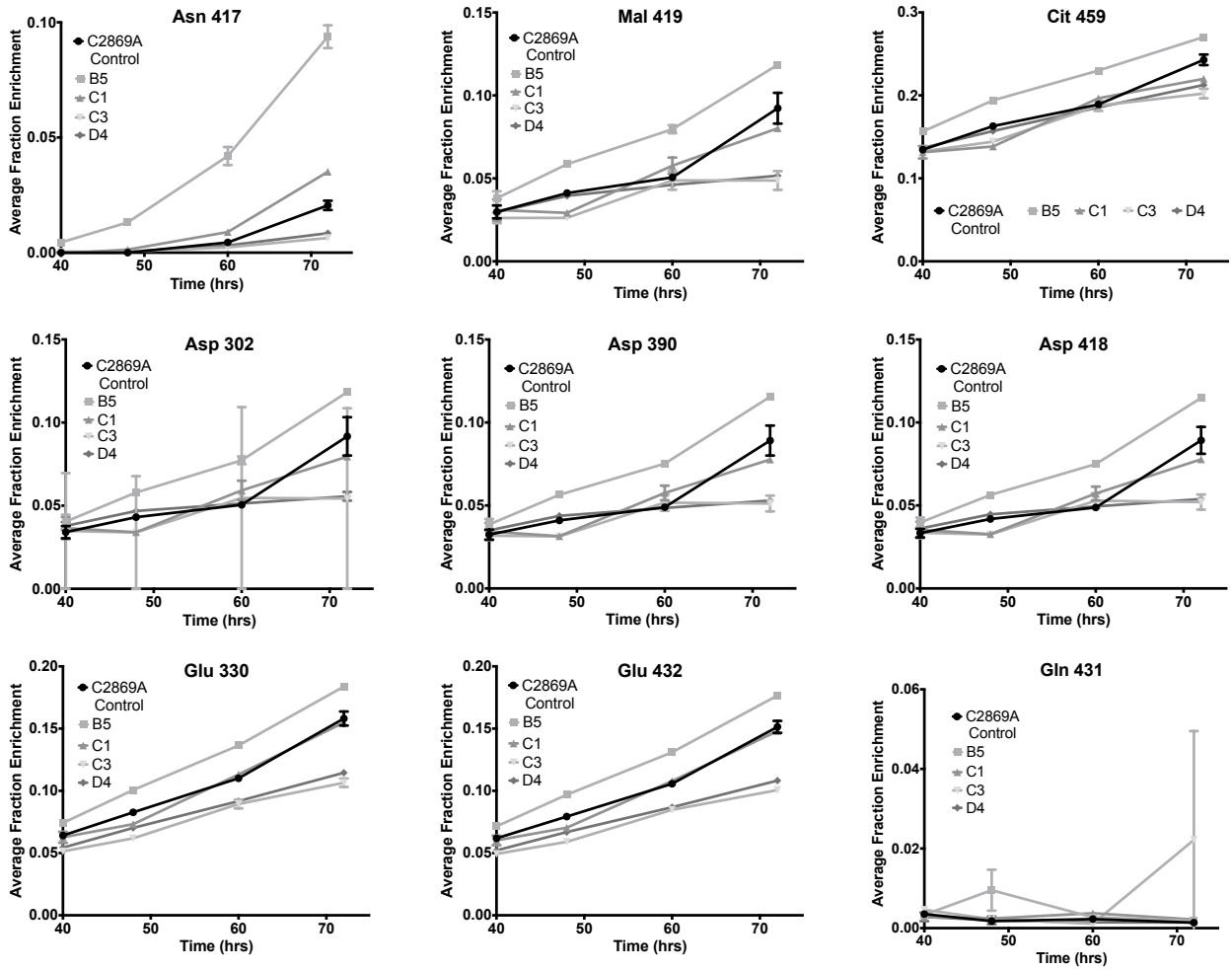

Figure A-3-7 Average percent enrichments (APEs) of intracellular metabolites over the course of the experiment (continued). Isotopic steady state is reached when the fractional enrichment does not change over time. These data prompted the conclusion that isotopic steady state was not obtained. Therefore, INST-MFA was used to regress fluxes over time in the CHO cell cultures studied here.

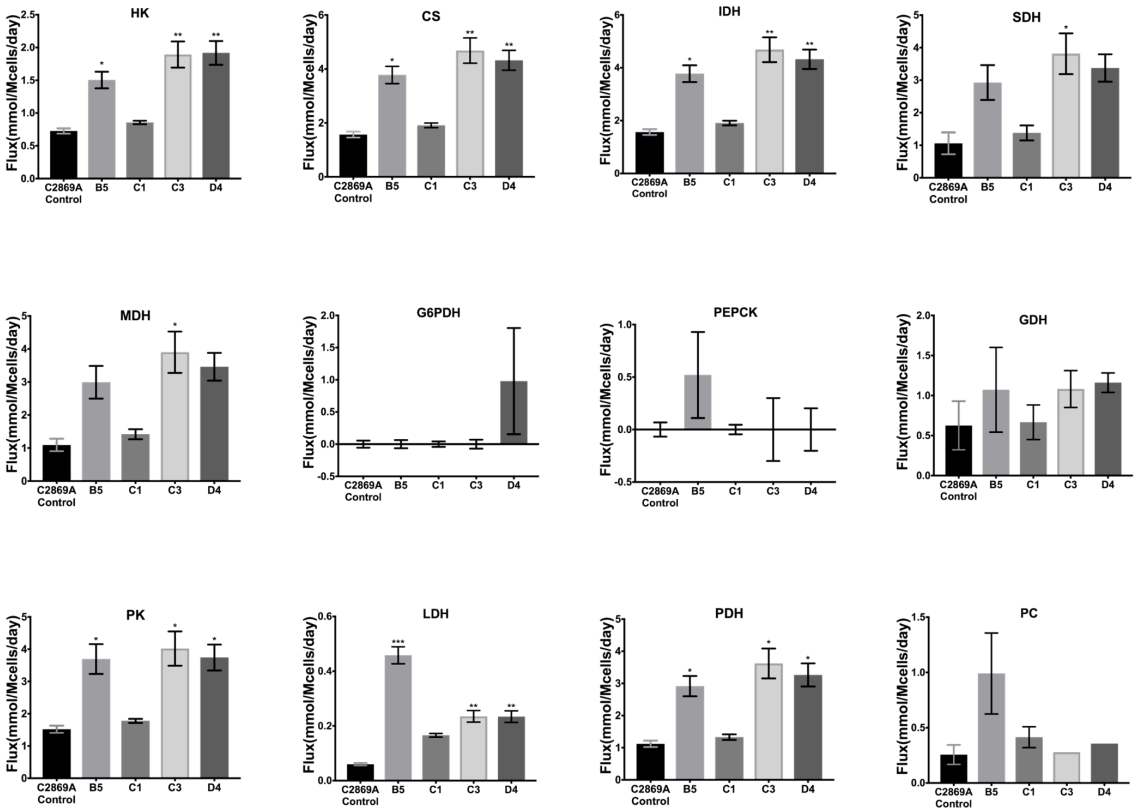

Figure A-3-8 Flux results of selected intracellular fluxes. Means +/- SEM reported, n=2.

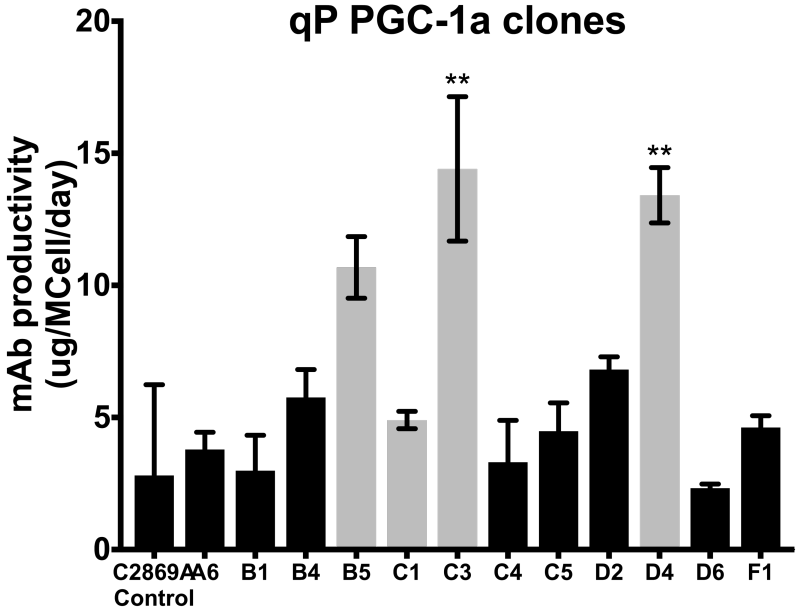

Figure A-3-9 Characterization of twelve of the twenty PGC-1a stable lines generated from mini-pool selection. The other eight lines were not measured due to their lack of PGC-1a mRNA expression (measured via RT qPCR), and three with no mAb expression are not included here. The gray bars are the lines chosen for the ^{13}C MFA study described in this chapter. Mean +/- SEM, n=2; grown in batch and measured during stationary growth phase.

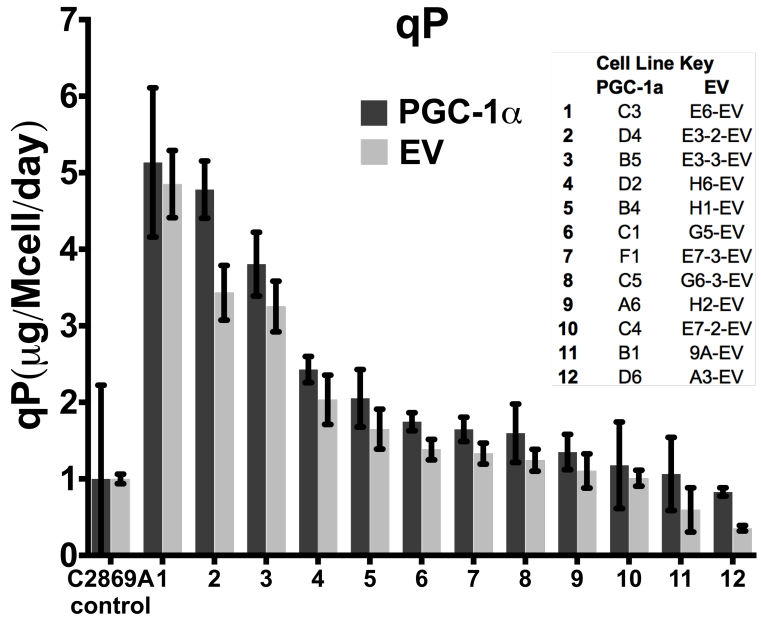

Figure A-3-10 Comparison of EV- and PGC-1α stable lines specific productivities (qP) in descending order normalized to the C2869A control line. Other lines are denoted as indicated by the accompanying table. These experiments were performed in batch growth and measurements were taken over stationary phase. N=2.

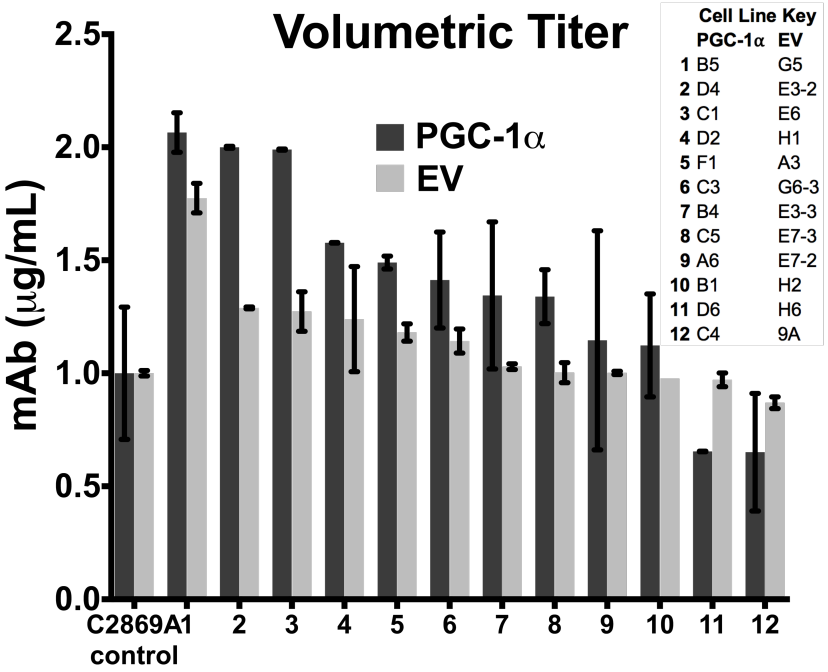

Figure A- 3-11 Comparison of EV- and PGC-1α stable lines mAb volumetric titers in descending order. All values are normalized to the respective control, C2869A. All lines are displayed as indicated in the accompanying table.

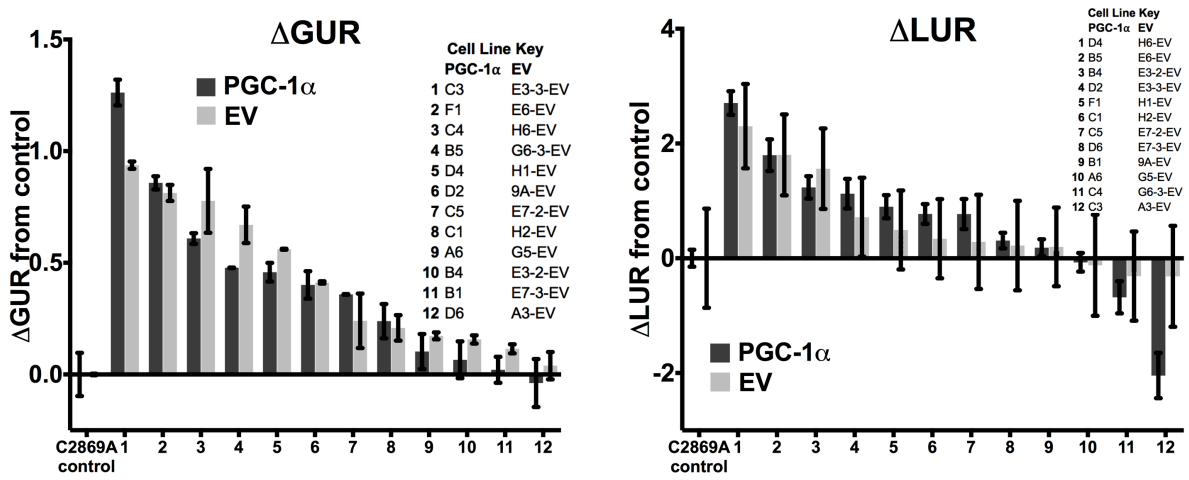

Figure A- 3-12 ΔGUR and ΔLUR of EV and PGC-1a lines plotted in descending order. The ΔGUR and ΔLUR values were calculated by subtracting the GUR and LUR of the respective control. Cultures were grown in batch culture and measurements taken during stationary growth phase.

3.8 References

[1] González-Roncero FM, Gentil-Govantes MÁ, González-Molina M, Rivero M, Cantarell C, Alarcón A, et al. Late evolution of kidney transplants in elderly donors and recipients receiving initial immunosuppressant treatment with daclizumab, mycophenolate mofetil, and delayed introduction of tacrolimus. Nefrol Publicaci{ó}n Of La Soc Espa{ñ}ola Nefrol 2012;32:446–54. doi:10.3265/Nefrologia.pre2012.Mar.11024.

[2] Saylor C, Dadachova E, Casadevall A. Monoclonal antibody-based therapies for microbial diseases. Vaccine 2009;27:38–46. doi:10.1016/j.vaccine.2009.09.105.

[3] An Z. Monoclonal antibodies - a proven and rapidly expanding therapeutic modality for human diseases. Protein Cell 2010;1:319–30. doi:10.1007/s13238-010-0052-8.

[4] Sautto G, Mancini N, Gorini G, Clementi M, Burioni R. Possible future monoclonal antibody (mAb)-Based Therapy against arbovirus infections. Biomed Res Int 2013;2013:838491. doi:10.1155/2013/838491.

[5] Omasa T, Onitsuka M, Kim W-D. Cell engineering and cultivation of chinese hamster ovary (CHO) cells. Curr Pharm Biotechnol 2010;11:233–40.

[6] Birch JR, Racher AJ. Antibody production. Adv Drug Deliv Rev 2006;58:671–85. doi:10.1016/j.addr.2005.12.006.

[7] Ahn WS, Antoniewicz MR. Towards dynamic metabolic flux analysis in CHO cell cultures. Biotechnol J 2012;7:61–74. doi:10.1002/biot.201100052.

[8] Jeon MK, Yu DY, Lee GM. Combinatorial engineering of ldh-a and bcl-2 for reducing lactate production and improving cell growth in dihydrofolate reductase-deficient Chinese hamster ovary cells. Appl Microbiol Biotechnol 2011;92:779–90. doi:10.1007/s00253-011-3475-0.

[9] Son Y-D, Jeong YT, Park S-Y, Kim JH. Enhanced sialylation of recombinant human erythropoietin in Chinese hamster ovary cells by combinatorial engineering of selected genes. Glycobiology 2011;21:1019–28. doi:10.1093/glycob/cwr034.

[10] Templeton N, Lewis A, Dorai H, Qian E a, Campbell MP, Smith KD, et al. The impact of anti-apoptotic gene Bcl-2Δ expression on CHO central metabolism. Metab Eng 2014;25:92–102. doi:10.1016/j.ymben.2014.06.010.

[11] Templeton N, Smith KD, McAtee-Pereira AG, Dorai H, Betenbaugh MJ, Lang SE, et al. Application of 13C flux analysis to identify high-productivity CHO metabolic phenotypes. Metab Eng 2017;29:53–62. doi:10.1016/j.ymben.2017.01.008.

[12] Templeton N, Dean J, Reddy P, Young JD. Peak antibody production is associated with increased oxidative metabolism in an industrially relevant fed-batch CHO cell culture. Biotechnol Bioeng 2013;110:2013–24. doi:10.1002/bit.24858.

[13] Zagari F, Jordan M, Stettler M, Broly H, Wurm FM. Lactate metabolism shift in CHO cell culture: the role of mitochondrial oxidative activity. N Biotechnol 2012;00. doi:10.1016/j.nbt.2012.05.021.

[14] Luo J, Vijayasankaran N, Autsen J, Santuray R, Hudson T, Amanullah A, et al. Comparative metabolite analysis to understand lactate metabolism shift in Chinese hamster ovary cell culture process. Biotechnol Bioeng 2012;109:146–56. doi:10.1002/bit.23291.

[15] Templeton N, Dean J, Reddy P, Young JD. Peak Antibody Production is Associated With Increased Oxidative Metabolism in an Industrially Relevant Fed-Batch CHO Cell Culture 2013;xxx:1–13. doi:10.1002/bit.24858.

[16] Wu Z, Boss O. Targeting PGC-1 a to control energy homeostasis. Expert Opin Ther

Targets 2007;11:1329–38.

[17] Rodgers JT, Lerin C, Gerhart-Hines Z, Puigserver P. Metabolic adaptations through the PGC-1 alpha and SIRT1 pathways. FEBS Lett 2008;582:46–53. doi:10.1016/j.febslet.2007.11.034.

[18] Shoag J, Arany Z. Regulation of hypoxia-inducible genes by PGC-1 alpha. Arterioscler Thromb Vasc Biol 2010;30:662–6. doi:10.1161/ATVBAHA.108.181636.

[19] Puigserver P, Spiegelman BM. Peroxisome proliferator-activated receptor-gamma coactivator 1 alpha (PGC-1 alpha): transcriptional coactivator and metabolic regulator. Endocr Rev 2003;24:78–90. doi:10.1210/er.2002-0012.

[20] Ruas JL, White JP, Rao RR, Kleiner S, Brannan KT, Harrison BC, et al. A PGC-1α isoform induced by resistance training regulates skeletal muscle hypertrophy. Cell 2012;151:1319–31. doi:10.1016/j.cell.2012.10.050.

[21] Wu Z, Puigserver P, Andersson U, Zhang C, Adelmant G, Mootha V, et al. Mechanisms controlling mitochondrial biogenesis and respiration through the thermogenic coactivator PGC-1. Cell 1999;98:115–24. doi:10.1016/S0092-8674(00)80611-X.

[22] Liang H, Balas B, Tantiwong P, Dube J, Goodpaster BH, O'Doherty RM, et al. Whole body overexpression of PGC-1alpha has opposite effects on hepatic and muscle insulin sensitivity. Am J Physiol Endocrinol Metab 2009;296:E945-54. doi:10.1152/ajpendo.90292.2008.

[23] Fernandez-Marcos P, Auwerx J. Regulation of PGC-1a , a nodal regulator of mitochondrial biogenesis. Am J Clin … 2011;93:884–90. doi:10.3945/ajcn.110.001917.884S.

[24] Templeton N, Smith KD, McAtee-Pereira AG, Dorai H, Betenbaugh MJ, Lang SE, et al.

Application of13C flux analysis to identify high-productivity CHO metabolic phenotypes. Metab Eng 2017;43:218–25. doi:10.1016/j.ymben.2017.01.008.

[25] Ichida M, Nemoto S, Finkel T. Identification of a specific molecular repressor of the peroxisome proliferator-activated receptor γ coactivator-1 α (PGC-1α). J Biol Chem 2002;277:50991–5. doi:10.1074/jbc.M210262200.

[26] Murphy TA, Young JD. ETA: robust software for determination of cell specific rates from extracellular time courses. Biotechnol Bioeng 2013;110:1748–58. doi:10.1002/bit.24836.

[27] Wall ML, Pound LD, Trenary I, O'Brien RM, Young JD. Novel stable isotope analyses demonstrate significant rates of glucose cycling in mouse pancreatic islets. Diabetes 2015;64:2129–37. doi:10.2337/db14-0745.

[28] Young JD. INCA: a computational platform for isotopically non-stationary metabolic flux analysis. Bioinformatics 2014;30:1333–5. doi:10.1093/bioinformatics/btu015.

[29] Smoot ME, Ono K, Ruscheinski J, Wang P-L, Ideker T. Cytoscape 2.8: new features for data integration and network visualization. Bioinformatics 2011;27:431–2. doi:10.1093/bioinformatics/btq675.

[30] Puigserver P, Spiegelman BM. Peroxisome proliferator-activated receptor-γ coactivator 1α (PGC-1α): Transcriptional coactivator and metabolic regulator. Endocr Rev 2003;24:78–90. doi:10.1210/er.2002-0012.

[31] Benton CR, Nickerson JG, Lally J, Han X-XX, Holloway GP, Glatz JFC, et al. Modest PGC-1alpha overexpression in muscle in vivo is sufficient to increase insulin sensitivity and palmitate oxidation in subsarcolemmal, not intermyofibrillar, mitochondria. J Biol Chem 2008;283:4228–40. doi:10.1074/jbc.M704332200.

[32] Liang H, Balas B, Tantiwong P, Dube J, Goodpaster BH, O'Doherty RM, et al. Whole

body overexpression of PGC-1alpha has opposite effects on hepatic and muscle insulin sensitivity. Am J Physiol Endocrinol Metab 2009;296:E945--54. doi:10.1152/ajpendo.90292.2008.

[33] Lehman JJ, Kelly DP. Experimental Biology 2001 Symposium Mitochondria and Energy Metabolism in Heart Failure , Hypertrophy and Remodeling TRANSCRIPTIONAL ACTIVATION OF ENERGY METABOLIC SWITCHES IN THE DEVELOPING AND HYPERTROPHIED HEART. Clin Exp Pharmacol Physiol 2002;29:339–45.

[34] Clark J, Silvaggi JM, Kiselak T, Zheng K, Clore EL, Dai Y, et al. Pgc-1α overexpression downregulates Pitx3 and increases susceptibility to MPTP toxicity associated with decreased Bdnf. PLoS One 2012;7:e48925. doi:10.1371/journal.pone.0048925.

[35] Lehman JJ, Barger PM, Kovacs A, Saffitz JE, Medeiros DM, Kelly DP. Peroxisome proliferator – activated receptor γ coactivator-1 promotes cardiac mitochondrial biogenesis. J Clin Invest 2000;106:847–56. doi:10.1172/JCI10268.al.

[36] Zhang Y, Huypens P, Adamson AW, Chang JS, Henagan TM, Boudreau A, et al. Alternative mRNA splicing produces a novel biologically active short isoform of PGC-1α. J Biol Chem 2009;284:32813–26. doi:10.1074/jbc.M109.037556.

[37] Ydfors M, Fischer H, Mascher H, Blomstrand E, Norrbom J, Gustafsson T. The truncated splice variants, NT-PGC-1α and PGC-1α4, increase with both endurance and resistance exercise in human skeletal muscle. Physiol Rep 2013;1:1–9. doi:10.1002/phy2.140.

[38] Mullick A, Xu Y, Warren R, Koutroumanis M, Guilbault C, Broussau S, et al. The cumate gene-switch: a system for regulated expression in mammalian cells. BMC Biotechnol 2006;6:43. doi:10.1186/1472-6750-6-43.

[39] Gaillet B, Gilbert R, Broussau S, Pilotte A, Malenfant F, Mullick A, et al. High-level

recombinant protein production in CHO cells using lentiviral vectors and the cumate gene-switch. Biotechnol Bioeng 2010;106:203–15. doi:10.1002/bit.22698.

[40] Le H, Vishwanathan N, Kantardjieff A, Doo I, Srienc M, Zheng X, et al. Dynamic gene expression for metabolic engineering of mammalian cells in culture. Metab Eng 2013;20:212–20. doi:10.1016/j.ymben.2013.09.004.

[41] Mulukutla BC, Gramer M, Hu W-SS. On metabolic shift to lactate consumption in fed-batch culture of mammalian cells. Metab Eng 2012;14:138–49. doi:10.1016/j.ymben.2011.12.006.

4 ^{13}C FLUX ANALYSIS REVEALS THAT REBALANCING MEDIUM AMINO ACID COMPOSITION CAN REDUCE AMMONIA PRODUCTION WHILE PRESERVING CENTRAL CARBON METABOLISM OF CHO CELL CULTURES

Biotechnology Journal 13 (2018):1700518.

4.1 Summary

^{13}C metabolic flux analysis (MFA) provides a rigorous approach to quantify intracellular metabolism of industrial cell lines. In this study, ^{13}C MFA was used to characterize the metabolic response of Chinese hamster ovary (CHO) cells to a novel medium variant designed to reduce ammonia production. Ammonia inhibits growth and viability of CHO cell cultures, alters glycosylation of recombinant proteins, and enhances product degradation. Ammonia production was reduced by manipulating the amino acid composition of the culture medium; specifically, glutamine, glutamate, asparagine, aspartate, and serine levels were adjusted. Parallel ^{13}C flux analysis experiments determined that, while ammonia production decreased by roughly 40%, CHO cell metabolic phenotype, growth, viability, and monoclonal antibody (mAb) titer were not significantly altered by the changes in media composition. This study illustrates how ^{13}C flux analysis can be applied to assess the metabolic effects of media manipulations on mammalian cell cultures. The analysis revealed that adjusting the amino acid composition of CHO cell culture media can effectively reduce ammonia production while preserving fluxes throughout central carbon metabolism.

4.2 Introduction

Chinese hamster ovary (CHO) cells are the most frequently utilized host organism for industrial production of biotherapeutic drugs, such as monoclonal antibodies (mAbs) used for treatment of immunological disorders and cancer [1]. CHO cells characteristically consume large

amounts of glucose and glutamine as carbon and nitrogen sources, leading to excretion of lactate and ammonia byproducts [2]. Both lactate and ammonia can become toxic to CHO cells when accumulated to high levels. Lactate toxicity can be self-corrected by some CHO cells by switching to lactate consumption at the onset of stationary phase [3–5], which can be further enhanced through genetic engineering [4–6] or closed-loop feeding strategies [7,8]. However, decreasing ammonia build up is conventionally accomplished by media manipulations [9–12].

Ammonia production is mainly a byproduct of glutaminolysis—an important pathway for energy generation, biosynthesis, and nitrogen supply to mammalian cells [13,14]. While glutamine-independent growth has been reported in CHO cells [15–17], some studies have shown that glutamine deficiency can lead to depletion of required precursors for product glycosylation [15,18]. Therefore, researchers at Sanofi formulated a novel chemically defined proprietary growth medium for decreased ammonia accumulation in CHO cell cultures by reducing the concentrations of several amino acids (glutamine, asparagine, and serine) that are metabolized to ammonia when present in excess. In order to maintain balanced flux of amino acids entering central carbon metabolism, the concentrations of downstream amino acids (glutamate and aspartate) formed from glutamine and asparagine were increased to offset the decreased availability of their upstream precursors. Although glutamate and aspartate typically accumulate in the control medium as waste products, it was hypothesized that supplementing these amino acids would inhibit ammonia-producing metabolic reactions while maintaining a consistent supply of anaplerotic substrates to support the citric acid cycle (CAC). These five amino acids were identified from literature as having potential significant impacts on ammonia production and regulation [10,11,13,19,20].

A multivariate experiment [21–23] was previously performed to identify an optimal

combination of the five selected amino acids that reduced ammonia production in culture without significantly affecting cell growth or productivity. However, it was unclear whether the new medium formulation might have unanticipated impacts on central carbon metabolism of CHO cells. Standard assays generally utilized for media optimization studies include viable cell density (VCD), growth rate, percent viability, culture longevity, product titer, and specific productivity. While these metrics generate practical data about cellular responses to media alterations, they do not provide quantitative readouts of the intracellular metabolic response to media manipulations. ^{13}C metabolic flux analysis (MFA) bridges the gap between extracellular manipulations and intracellular metabolic pathway perturbations, providing a rigorous analytical approach to quantify changing metabolic phenotypes across different experimental conditions [24–27].

In this study, we applied parallel ^{13}C MFA to assess a newly developed proprietary medium that reduced ammonia production by industrial CHO cells by roughly 40% without negatively affecting culture growth or mAb specific productivity. The low-ammonia (LA) medium variant was formulated with decreased glutamine, asparagine, and serine compensated by increased availability of their downstream glutamate and aspartate products. ^{13}C MFA revealed that intracellular metabolic fluxes were not significantly altered by the media manipulations, although there was a trend toward altered anaplerotic carbon sources for CAC metabolism in cells cultured in the LA medium. This study shows that it is possible to manipulate amino acid metabolism in CHO cell cultures while maintaining consistent fluxes through central carbon metabolism, if reductions in certain amino acids are offset by addition of other complementary nutrients.

4.3 Materials and methods

4.3.1 Media

Three media formulations were studied. The control medium (CM) was Sanofi's in-house chemically defined CHO cell growth medium. A low-ammonia (LA) variant was developed and formulated according to Table 0-2. A third medium condition was tested to ensure that any changes in CHO cell metabolism were due to the LA medium alterations and not due to the presence or absence of ammonia itself. The LA+ variant designates the LA medium supplemented with 4 mM ammonia. This value was determined by averaging the final ammonia concentrations at the conclusion of several CHO batch cultures grown in CM (data not shown).

Table 0-2 Relative amino acid composition of Low Ammonia (LA) medium. Values indicate fold-changes relative to CM.

Amino acid	Gln	Glu	Asn	Asp	Ser
Fold change	0.5X	6X	0.7X	3X	0.6X

4.3.2 Cell Culture

One vial of mAb-producing CHO cells was expanded in a 250 mL shake flask with a working volume of 60 mL of control medium. Cells were passaged into each of the three media variants once the VCD surpassed 2 Mcell/mL, with passaging occurring roughly every 3 days (Figure 4-8). Working volumes were increased to 75 mL (P2) and 250 mL in 1L shake flasks (P3) to accumulate enough cells for seeding P4 flasks. Cell doubling time was measured to be approximately 35 hours (data not shown). The parallel ^{13}C labeling studies for MFA were performed during passage four (P4) in 250 mL shake flasks with initial working volumes of 75 mL. Samples were collected after 24, 48, 60, and 72 hours during P4 for amino acid analysis and

^{13}C labeling measurements. All flasks were incubated at 37°C, 5% CO_2, 125 RPM shaking, and 80% humidity. Inoculation of stages P1-P3 targeted 0.5 Mcell/mL. The inoculation density in the ^{13}C-labeled media for P4 was 1 Mcell/mL.

4.3.3 Parallel ^{13}C Labeling Studies

[1,2-$^{13}C_2$]Glucose was added to glucose-free media for duplicate flasks of each experimental condition during P4. A second set of duplicate flasks was inoculated with [U-$^{13}C_5$]glutamine labeled media (Figure 4-8). The duplicate flasks containing ^{13}C-glucose were analyzed for labeling in glycolytic and pentose phosphate pathway (PPP) intermediates, while the ^{13}C-glutamine labeled flasks provided data on CAC and anaplerotic pathways [28]. Unlabeled samples were harvested from flasks in P3 to use as negative controls during the measurement of ^{13}C labeling.

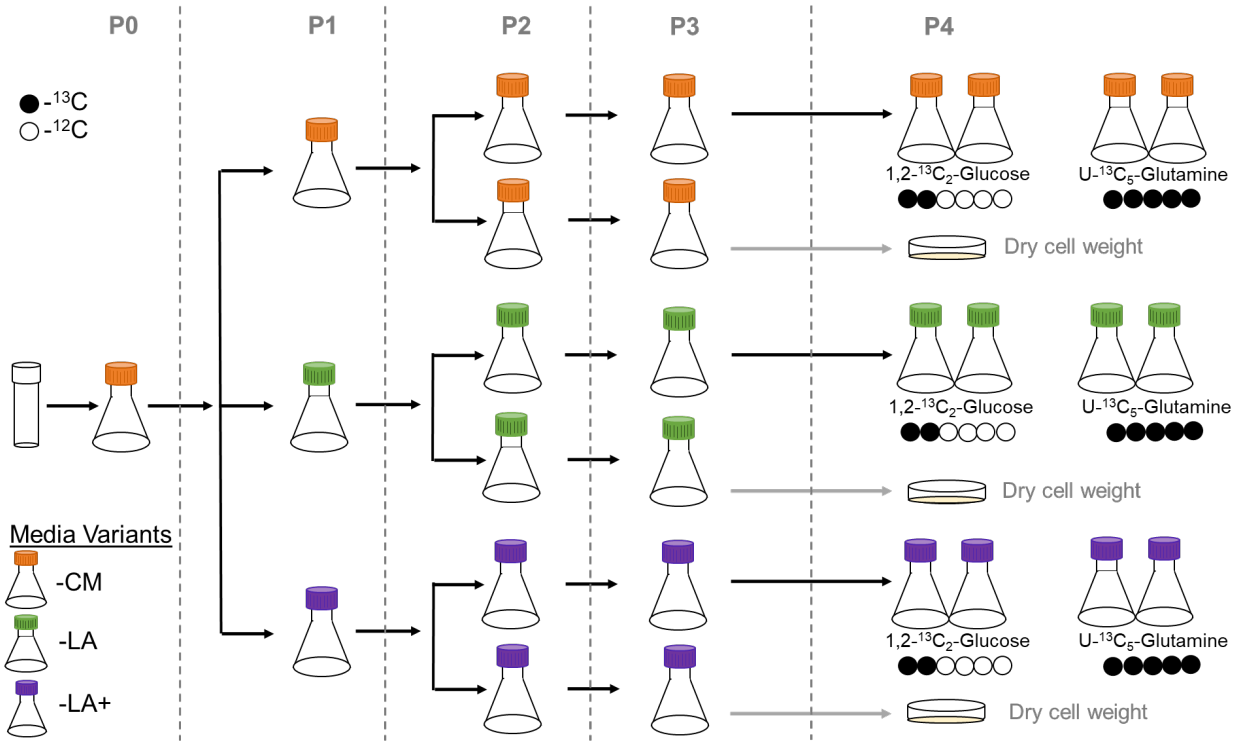

Figure 4-8 Experimental design. Cells were passaged approximately every three days. Parallel labeling experiments with [1,2-$^{13}C_2$]glucose and [U-$^{13}C_5$]glutamine took place during passage 4 (P4). Culture samples collected from P3 flasks were used to determine dry cell weight.

4.3.4 Analytical Techniques

Cell and supernatant samples were collected at 24, 48, 60, and 72 hours during P4 and analyzed for VCD, viability, glucose, lactate, pH, pCO2, pO2, osmolarity, and amino acid concentrations. Amino acid concentrations were measured via HPLC as previously described [29]. VCDs and percent viability measurements were obtained at each time point using Trypan blue exclusion with a Vi-CELL XR (Beckman Coulter). Glucose and lactate were measured with a Cedex Bio HT (Roche). pH, pCO2 and pO2 were measured with a RapidLab 1240 blood-gas analyzer (Siemens). At each time point, culture aliquots were collected containing approximately 10 million viable cells and immediately cold-quenched with a 60/40 (v/v) solution of methanol and ammonium bicarbonate (AMBIC) pre-cooled to -40°C [30]. The samples were centrifuged and the supernatant was immediately removed, thus diluting and then removing extracellular

components and minimizing the likelihood of extracellular contamination in the intracellular metabolite fractions. Following the cold-quench, intracellular metabolites were extracted via the Folch method [31]. Once extracted, intracellular metabolites were derivatized via methoxamine (MOX) and tert-butyldimethylsilyl chloride (TBDMS) reagents for analysis via gas chromatography-mass spectrometry (GC/MS) [29]. One duplicate flask of each media variant was harvested at the conclusion of P3 for dry cell mass measurements by drying a known number of cells in a non-humidified incubator at 70°C and measuring the resulting mass. The composition of the cell mass was determined based on previous work in hybridoma cells [29,32].

4.3.5 Metabolic Flux Analysis

The ^{13}C isotope labeling data generated by GC/MS analysis were analyzed using the MATLAB-based software package isotopomer network compartmental analysis (INCA) (publicly available at http://mfa.vueinnovations.com) [9]. Mass and isotopomer balances were simulated for CHO cell central carbon metabolism using an elementary metabolite unit (EMU) decomposition of the reaction network to simulate changes in isotope labeling induced by changes in metabolic fluxes [33,34]. We verified that P4 cultures achieved metabolic steady state by observing constant rates of change in extracellular metabolite concentrations. Isotopic steady state was verified by measuring equilibration of mass isotopomer distributions (MIDs), or average percent enrichments (APEs, SI Equation 1), at the time points analyzed (Figure A- 4-13–10) [35]. The APE represents the average enrichment of tracer atoms in the measured fragment ion. Isotopic steady state is reached when the change in isotopic enrichment over time falls within range of the measurement uncertainty. Extracellular fluxes were calculated using the MATLAB-based software package extracellular time course analysis (ETA) to regress the

extracellular metabolite concentration changes over time [36]. Stationary ^{13}C MFA was applied to calculate intracellular fluxes at the 60 hr time point. Experimentally measured MIDs and extracellular fluxes were regressed using a Levenberg-Marquardt optimization algorithm [5]. Parallel datasets from [1,2-$^{13}C_2$]glucose and [U-$^{13}C_5$]glutamine labeling studies were regressed simultaneously to yield one complete metabolic flux map for each medium formulation. Fluxes were calculated using a minimum of 100 unique restarts from random initial values to ensure a global minimum was found. Flux results were subjected to a chi-square statistical test to assess goodness-of-fit, and 95% confidence intervals were calculated for each estimated flux value [37]. A summary of the best-fit solutions, flux uncertainties, and goodness-of-fit metrics can be found in Table A- 4-4 1–4 and Figure A- 4-23–16. INCA model files are available upon request.

4.3.6 Statistical Analysis

The CM, LA, and LA+ cell culture fluxes were compared using one-way ANOVA. When significance was found at α=0.05, a Tukey-Kramer test was applied.

4.4 Results

4.4.1 Ammonia production was reduced in LA medium without altering growth, viability, or mAb specific productivity

Growth rate and cell viability were not significantly different across the three media variants as shown in Figure 4-9. Ammonia production was significantly decreased in the LA and LA+ media variants (Figure 4-10A) while mAb specific productivity remained unchanged across all media variants (Figure 4-10B). The media alterations resulted in a 40% reduction in ammonia production by CHO cells grown in the LA medium. The LA+ medium elicited an even more dramatic 70% reduction in ammonia production compared to the CM. This effect was perhaps

from feedback inhibition of ammonia-producing metabolic pathways by maintaining high ammonia levels in the medium throughout the experiment.

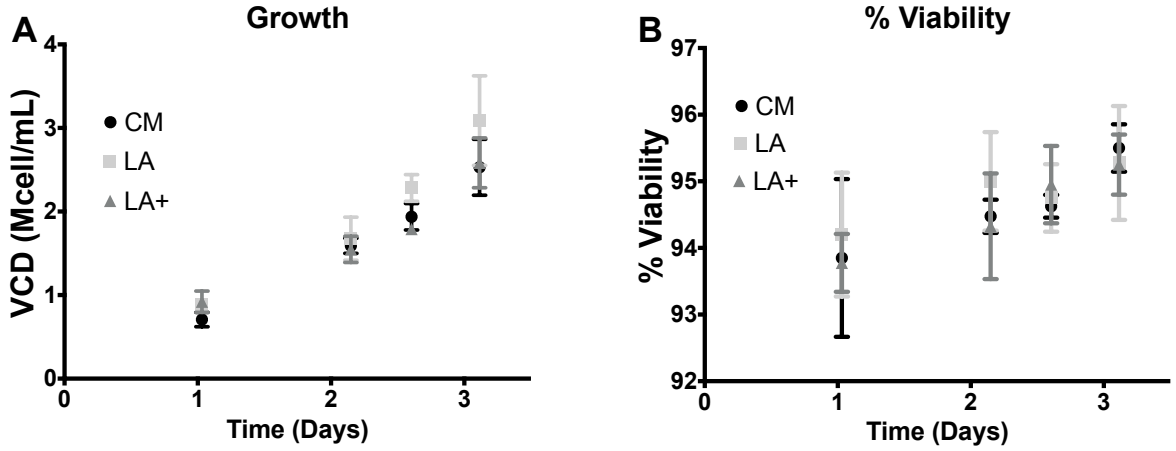

Figure 4-9 (A) Growth curve and (B) Percent viability of CHO cells cultured in the three media variants. Data indicate mean values +/- SEM, n=4.

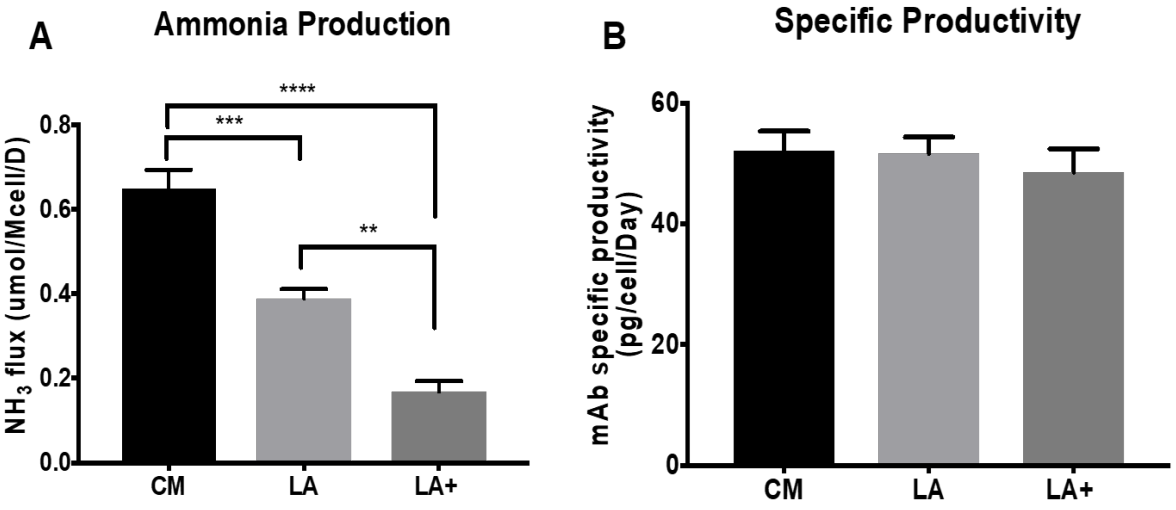

Figure 4-10 (A) Ammonia production rate and (B) mAb specific productivity of cultures in the experimental media conditions. Data indicate mean fluxes +/- SEM, n=4. ****α<0.0001; ***α<0.001; **α<0.01.

4.4.2 Glutamine, but not glucose, uptake was reduced in LA medium

Glutamine consumption rate (QUR) was significantly reduced in the LA and LA+ media variants while glucose uptake rate (GUR) was not significantly different across the three conditions (Figure 4-11A). These results indicate that the GUR did not fully compensate for reduced carbon entering through glutamine uptake. There was net production of glutamate by CHO cells grown in all three media formulations, with a trend toward lower net production in the LA and LA+ media variants as shown in Figure 4-4B. Excretion of glutamate has been previously shown to be positively correlated with glutamine consumption by CHO cells [38]. Glycine production was also reduced in the LA and LA+ media (Figure 4-11B). Glycine is utilized in CHO cells for mAb and biomass synthesis and is intracellularly produced from serine. Since serine concentrations were limited in the LA and LA+ media, less excess serine was available for conversion to glycine, leading to reduced glycine excretion as a waste product (Table A- 4-4). Alanine, aspartate, glutamate, and glycine were excreted by cells grown under CM conditions; however, their rates of excretion trended downward in the LA medium as shown in Figure 4-11B. This indicates that amino acid consumption and metabolism under the LA growth conditions were better matched to biosynthetic demands for protein synthesis, cell growth, and anaplerosis.

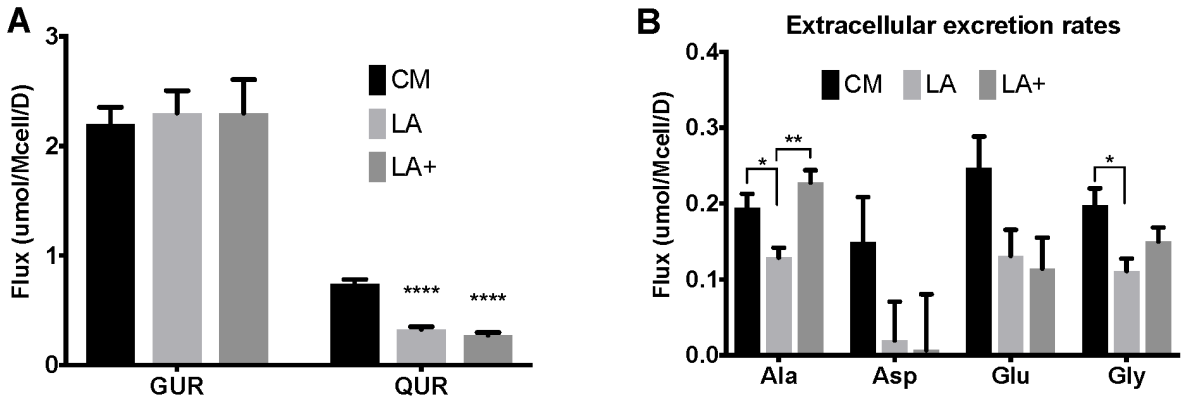

Figure 4-11 (A) Glucose uptake rate (GUR) and glutamine uptake rate (QUR). (B) Excretion rates of alanine, aspartate, glutamate, and glycine. Data indicate mean fluxes +/- SEM, n=4. ****α<0.0001; *α<0.05.

4.4.3 Alanine production is associated with ammonia accumulation

Alanine production was significantly decreased in the LA medium compared to CM (Figure 4-11B). Alanine is second only to ammonia as the major byproduct of glutaminolysis; therefore, decreased alanine excretion was expected to correlate with decreased glutamine consumption. Notably, the alanine production in the LA+ medium was at least as high as that in CM. This was the only flux that varied significantly (at $p<0.05$) between the LA and LA+ media formulations. Increased alanine excretion has been reported to compensate for ammonia stress in CHO cells since it acts as an alternative nitrogen sink [38]. Our results confirm that elevation of culture ammonia alone can drive increased alanine production. This finding was further supported by model-estimated changes in flux through alanine transaminase (ALT) (Table A- 4-4).

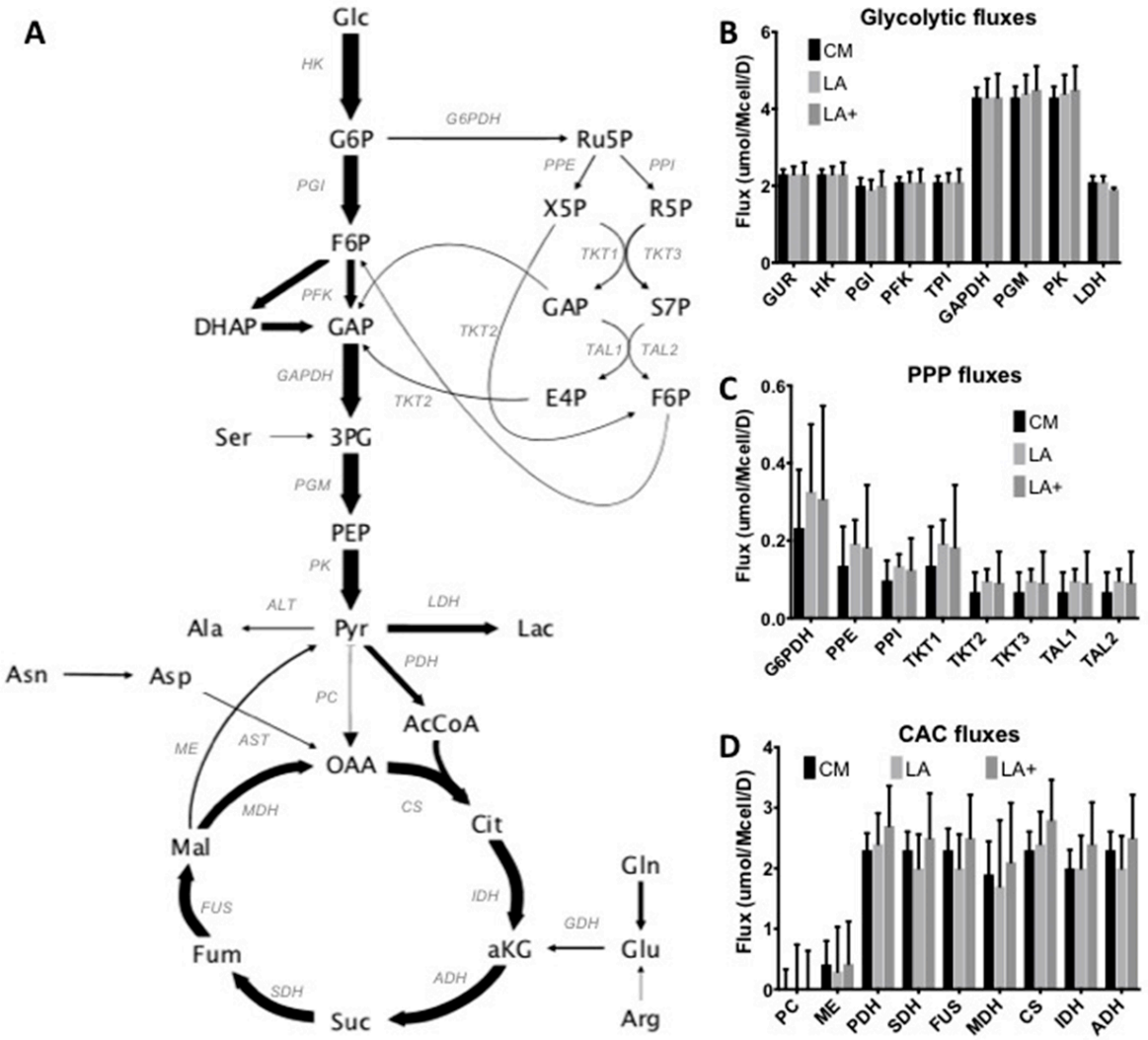

Figure 4-12 (A) Central carbon metabolic map with enzymes of interest labeled. Arrow width represents flux in carbon moles for the CM condition. (B) Glycolytic fluxes, (C) pentose phosphate pathway (PPP) fluxes, and (D) citric acid cycle (CAC) fluxes during P4. Data indicate mean fluxes +/- SEM, n=4.

4.4.4 Glycolysis and PPP fluxes were not significantly altered in LA medium

A decrease in glycolysis with decreased glutamine availability has been previously reported [15]; however, ^{13}C flux analysis showed no significant changes in glycolytic fluxes across the three media variants in our study (Figure 4-5B). Furthermore, PPP fluxes (Figure 4-5C) were not significantly affected by the altered amino acid profile of the LA and LA+ media.

Overall, PPP flux accounted for 10% of glucose consumption in CM and ~14% in LA and LA+ media (Figure 4-5A).

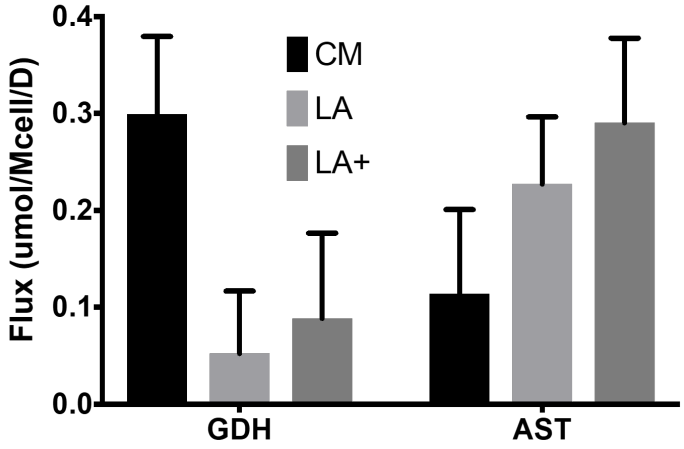

Figure 4-13 Anaplerotic fluxes through glutamate dehydrogenase (GDH) and aspartate transaminase (AST). In our flux model, GDH flux represents total anaplerosis from glutamate to alpha-ketoglutarate, while AST represents total anaplerosis from aspartate to oxaloacetate. Data indicate mean fluxes +/- SEM, n=4.

4.4.5 CAC fluxes were not significantly altered in LA medium, despite variations in anaplerotic contributions from certain amino acids

CAC fluxes were largely unchanged across the three media variants (Figure 4-5D), however, anaplerotic carbon contributions into the CAC were partially redistributed in the LA and LA+ conditions. Aspartate aminotransferase (AST) flux trended upward in LA and LA+ cultures (Figure 4-13). An increased contribution from aspartate to supply carbon into the CAC at the oxaloacetate (OAA) node appears to compensate for reduced anaplerotic flux through glutamine dehydrogenase (GDH) to supply alpha-ketoglutarate (Figure 4-13). Therefore, redistribution of anaplerotic fluxes entering the CAC could result directly from alterations to asparagine/aspartate and glutamine/glutamate ratios that lead to more balanced amino acid metabolism in the LA medium. Flux through pyruvate carboxylase (PC) could not be precisely resolved in our study due to uncertainties associated with pyruvate recycling through malic enzyme (ME). However,

the net anaplerotic flux of pyruvate entering the CAC (i.e., the difference between PC and ME fluxes) was estimated with good precision (Table A- 4-8). The results indicate net outflow (i.e., cataplerosis) of pyruvate leaving the CAC, suggesting that amino acids provided the major source of anaplerotic carbon to support mitochondrial metabolism in all media conditions.

4.5 Discussion

Ammonia toxicity is a well-documented effect of excess amino acid metabolism in CHO cell cultures [14]. Sanofi successfully engineered a proprietary media variant that maintained cell growth, viability, and mAb production while dramatically reducing ammonia production in industrial CHO cell cultures. ^{13}C MFA revealed that decreasing media concentrations of glutamine, asparagine, and serine while increasing media availability of glutamate and aspartate had significant effects on ammonia-producing fluxes while largely preserving central carbon metabolism unchanged. There was only a 2% difference in the total molar mass between the two formulations as a result of the amino acid manipulations. Therefore, changes in byproduct formation were not simply due to a leaner medium.

Reducing glutamine availability is a natural first step for eliminating excess ammonia production. This has generally been achieved by adapting CHO cells to glutamine-independent growth or through genetic engineering to introduce glutamine synthetase (GS) to host cells [18,39–41]. Asparagine and serine have also been identified as tunable amino acids for the reduction of byproduct formation while maintaining cellular requirements for biosynthesis and energy production [11]. While asparagine is essential to cell survival [11], it is also a source of ammonia when metabolized through asparaginase [9]. For this reason, the LA media variant limits asparagine availability to meet the cellular requirements of proliferating cells while minimizing excess flux to aspartate through asparaginase. As a result, aspartate consumption

increases in order to compensate for reduced asparagine availability [11]. In this study, the LA medium contained increased aspartate levels to counteract asparagine limitation and to supply sufficient OAA to support CAC anaplerosis (Figure 4-13). Aspartate utilization to form OAA was increased in the LA medium such that excretion of aspartate was decreased (Table A- 4-4). The conversion of serine to pyruvate is another notable source of ammonia in CHO cell cultures [19]. Serine is the major supplier of one-carbon units for methylation reactions along with its role in protein, nucleotide, and lipid biosynthesis [11]. Complete removal of serine in CHO cell cultures reportedly limits cell growth and causes metabolic shifts that ultimately increase ammonia production through heavy dependence on asparagine consumption [11]. Tight regulation of serine concentrations to match cellular metabolic demands has been shown to effectively minimize ammonia formation [11]. Due to these previous findings, serine was limited to biologically required levels in the LA medium with flux analysis indicating a trend toward increased serine consumption in the LA and LA+ media conditions (Table A- 4-4). This could indicate a more efficient metabolism of serine when its availability is limited along with glutamine and asparagine.

As further evidence of improved metabolic efficiency, less pyruvate was converted to alanine via ALT (Table A- 4-4) in the LA medium compared to CM or LA+ cultured cells. LA+ cultured cells increased their flux to alanine as a result of increased ammonia stress [38]. Cells cultured in CM exhibited an alanine flux that was intermediate between that of the LA and LA+ conditions. This trend corroborates the concept that alanine production results from ammonia stress, since the CM cultured cells experienced a gradual increase in ammonia levels over the course of the experiment while the LA+ cultured cells were exposed to high levels of ammonia throughout the experiment.

By elucidating the metabolic phenotype induced by nutrient alterations, this study demonstrates the effectiveness of ^{13}C MFA in media development efforts. While directly observable extracellular measurements can provide useful information to guide media optimization, they do not describe the intracellular metabolic responses induced by altering the carbon and nitrogen sources available to CHO cells. In the current study, the effects of media alterations on CAC anaplerotic sources and amino acid metabolism might have been overlooked in the absence of ^{13}C MFA. These changes could potentially impact bioprocess operations or product attributes, even though cell growth and specific productivity were not significantly altered. On the other hand, ^{13}C MFA confirmed that many central metabolic pathways were completely unaffected by the media switch, confirming that amino acid metabolism could be effectively manipulated without significantly altering important bioenergetic fluxes. Understanding which metabolic pathways are altered by media changes, and which are not, can thus provide important information for decision-making in industrial cell culture applications. To our knowledge, this is the first study that has applied ^{13}C MFA to assess intracellular metabolic effects resulting from media reformulation. This study provides a valuable example of how flux analysis can be applied to obtain intracellular metabolic readouts that would be otherwise unavailable to industrial researchers.

4.6 Appendix

Table A- 4-4 Flux maps of the three media conditions with 95% confidence intervals; CM=control medium, LA=low ammonia medium, LA+=low ammonia medium with added ammonia. LB-lower bound of 95% confidence interval, UB-upper bound of 95% confidence interval. An '.e' indicates an extracellular metabolite pool; '.m' indicates a mitochondrial metabolite pool; '.u' indicates an unlabeled metabolite pool; and a '.l' indicates a labeled metabolite pool.

Rxn ID	Reaction	CM (umol/Mcell/day)			LA (umol/Mcell/day)			LA+ (umol/Mcell/day)		
		Flux	**LB**	**UB**	**Flux**	**LB**	**UB**	**Flux**	**LB**	**UB**
GUR	Glc.e → Glc	2.30	2.00	2.50	2.30	1.90	2.70	2.30	1.70	2.90
Glc.l IN	Glc.l → Glc.e	2.30	1.90	2.50	2.30	1.80	2.70	2.10	1.60	2.90
Glc.u IN	Glc.u → Glc.e	0.00	0.00	0.24	0.00	0.00	0.35	0.16	0.00	0.38
HK	Glc → G6P	2.30	2.00	2.50	2.30	1.90	2.70	2.30	1.70	2.90
PGI	G6P ↔ F6P	2.00	1.60	2.40	1.90	1.40	2.40	2.00	1.30	2.80
PFK	F6P → DHAP + GAP	2.10	1.90	2.40	2.10	1.70	2.70	2.10	1.50	2.80
TPI	DHAP ↔ GAP	2.10	1.80	2.40	2.10	1.70	2.60	2.10	1.50	2.80
GAPDH	GAP ↔ 3PG	4.30	3.80	4.80	4.30	3.40	5.30	4.30	3.20	5.60
PGM	3PG ↔ PEP	4.30	3.70	4.80	4.40	3.50	5.40	4.50	3.30	5.70
AGXT	3PG ↔ Ser	0.01	-0.19	0.21	-0.07	-0.18	0.04	-0.12	-0.26	0.01
PK	PEP → Pyr	4.30	3.70	4.80	4.40	3.50	5.40	4.50	3.30	5.70
LDH	Pyr ↔ Lac	2.10	1.80	2.40	2.10	1.80	2.40	1.90	1.80	2.00
PDH	Pyr → AcCoA.m + CO2	2.30	1.80	2.90	2.40	1.40	3.40	2.70	1.40	4.00
CS	OAA + AcCoA.m → Cit	2.30	1.80	3.00	2.40	1.40	3.50	2.80	1.50	4.10
IDH	Cit ↔ aKG + CO2	2.00	1.50	2.70	2.00	0.97	3.10	2.40	1.10	3.80
AKGDH	aKG → Suc + CO2	2.30	1.80	3.00	2.00	1.00	3.10	2.50	1.10	3.90
SDH	Suc ↔ Fum	2.30	1.80	3.00	2.00	1.00	3.20	2.50	1.10	4.00
FH	Fum ↔ Mal	2.30	1.80	3.20	2.00	1.00	3.20	2.50	1.20	4.00
MDH	Mal ↔ OAA	1.90	0.46	2.60	1.70	-1.50	2.80	2.10	-0.44	3.40
G6PDH	G6P → Ru5P + CO2	0.23	0.00	0.59	0.33	0.00	0.68	0.31	0.00	0.94
PPE	Ru5P ↔ X5P	0.14	-0.02	0.37	0.19	0.19	0.43	0.18	-0.03	0.60
PPI	Ru5P ↔ R5P	0.10	0.02	0.22	0.13	0.13	0.25	0.12	0.02	0.34
TKT1	X5P ↔ EC2 + GAP	0.14	-0.02	0.37	0.19	0.19	0.43	0.18	-0.03	0.60
TKT2	EC2 + E4P ↔ F6P	0.07	-0.01	0.19	0.10	0.09	0.21	0.09	-0.01	0.30
TKT3	EC2 + R5P ↔ S7P	0.07	-0.01	0.19	0.10	0.09	0.21	0.09	-0.01	0.30
TAL1	EC3 + GAP ↔ F6P	0.07	-0.01	0.19	0.10	0.09	0.21	0.09	-0.01	0.30
TAL2	S7P ↔ EC3 + E4P	0.07	-0.01	0.19	0.10	0.09	0.21	0.09	-0.01	0.30
ME	Mal → Pyr + CO2	0.41	0.18	1.70	0.29	0.10	3.00	0.42	0.15	2.90
PC	Pyr + CO2 → OAA	0.00	0.00	1.30	0.00	0.00	2.90	0.00	0.00	2.50
ACL	Cit → AcCoA.c + OAA	0.32	0.26	0.37	0.40	0.35	0.46	0.35	0.28	0.42
AS	Asn ↔ Asp	0.34	0.21	0.47	0.34	0.25	0.43	0.38	0.29	0.47
PCC	ProCoA + CO2 → Suc	0.00	0.00	0.03	0.01	0.00	0.05	0.03	0.00	0.08
GS	Gln ↔ Glu	0.68	0.60	0.76	0.26	0.21	0.31	0.21	0.16	0.26
PYCR	Glu ↔ Pro	0.06	-0.04	0.17	0.00	-0.09	0.09	-0.04	-0.17	0.08
Gly syn	CO2 + C1 ↔ Gly	0.14	0.12	0.16	0.10	0.08	0.12	0.12	0.10	0.15
His cat	His → C1 + Glu	0.00	0.00	0.03	0.00	0.00	0.04	0.01	0.00	0.05
PAH	Phe → Tyr	0.01	0.00	0.27	0.00	0.00	0.01	0.00	0.00	0.03

SHMT	Ser ↔ Gly + C1	0.17	0.14	0.19	0.14	0.12	0.16	0.15	0.11	0.17
Thr cat	Thr → Pyr + CO2	0.00	0.00	0.02	0.00	0.00	0.02	0.00	0.00	0.04
Trp cat	Trp → 2 CO2 + Ala + aKA	0.00	0.00	0.01	0.00	0.00	0.01	0.00	0.00	0.01
aKA cat	aKA → 2 CO2 + 2 AcCoA.m	0.00	0.00	0.04	0.00	0.00	0.04	0.01	0.00	0.07
GDH	Glu ↔ aKG	0.30	0.14	0.46	0.05	-0.07	0.18	0.09	-0.08	0.26
ALT	Pyr ↔ Ala	0.29	0.25	0.33	0.24	0.21	0.27	0.33	0.29	0.37
Ile cat	Ile → AcCoA.m + CO2 + ProCoA	0.00	0.00	0.02	0.00	0.00	0.03	0.01	0.00	0.04
Leu cat	Leu + CO2 → CO2 + 3 AcCoA.m	0.00	0.00	0.02	0.00	0.00	0.03	0.01	0.00	0.05
Tyr cat	Tyr → CO2 + Fum + 2 AcCoA.m	0.00	0.00	0.25	0.00	0.00	0.03	0.01	0.00	0.05
Val cat	Val → 2 CO2 + ProCoA	0.00	0.00	0.03	0.01	0.00	0.04	0.02	0.00	0.06
Lys cat	Lys → aKA	0.00	0.00	0.04	0.00	0.00	0.04	0.01	0.00	0.06
AST	Asp ↔ OAA	0.11	-0.06	0.28	0.23	0.09	0.36	0.29	0.12	0.46
ARG	Arg → Glu + Urea	0.00	0.00	0.03	0.00	0.00	0.03	0.02	0.00	0.06
Cys cat	Cys → Pyr	0.04	0.02	0.07	0.02	0.00	0.03	0.02	0.00	0.04
Met cat	Met + Ser → C1 + Cys + ProCoA + CO2	0.00	0.00	0.01	0.00	0.00	0.01	0.00	0.00	0.01
Lys IN	Lys.e → Lys	0.10	0.09	0.14	0.12	0.10	0.15	0.12	0.09	0.17
Thr IN	Thr.e → Thr	0.08	0.07	0.10	0.09	0.08	0.11	0.09	0.08	0.12
Phe IN	Phe.e → Phe	0.05	0.04	0.31	0.05	0.04	0.06	0.05	0.04	0.07
Tyr IN	Tyr.e → Tyr	0.03	0.00	0.06	0.05	0.04	0.07	0.05	0.03	0.08
Val IN	Val.e → Val	0.09	0.08	0.12	0.11	0.09	0.14	0.11	0.09	0.15
Leu IN	Leu.e → Leu	0.10	0.09	0.13	0.12	0.11	0.15	0.12	0.10	0.15
Ile IN	Ile.e → Ile	0.05	0.04	0.07	0.07	0.05	0.09	0.07	0.05	0.09
Trp IN	Trp.e → Trp	0.01	0.01	0.02	0.02	0.01	0.02	0.02	0.01	0.03
His IN	His.e → His	0.03	0.02	0.05	0.03	0.03	0.07	0.04	0.02	0.08
Met IN	Met.e → Met	0.02	0.02	0.03	0.03	0.02	0.03	0.03	0.02	0.04
Ser IN	Ser.e ↔ Ser	0.27	0.07	0.47	0.33	0.22	0.44	0.39	0.25	0.52
Ala OUT	Ala ↔ Ala.e	0.19	0.16	0.23	0.13	0.10	0.15	0.23	0.20	0.26
Arg IN	Arg.e ↔ Arg	0.06	0.05	0.09	0.07	0.06	0.10	0.08	0.06	0.13
Asp OUT	Asp ↔ Asp.e	0.15	0.03	0.26	0.02	-0.08	0.12	0.01	-0.14	0.15
Cys IN	Cys.e ↔ Cys	0.07	0.05	0.10	0.05	0.04	0.06	0.05	0.03	0.06
Glu OUT	Glu ↔ Glu.e	0.25	0.17	0.33	0.13	0.07	0.20	0.12	0.03	0.20
Gln IN	Gln.e ↔ Gln	0.74	0.66	0.81	0.33	0.28	0.38	0.27	0.22	0.32
Gly OUT	Gly ↔ Gly.e	0.20	0.15	0.24	0.11	0.08	0.14	0.15	0.11	0.19
Pro IN	Pro.e ↔ Pro	0.00	-0.11	0.11	0.08	-0.01	0.16	0.11	-0.01	0.24
Asn IN	Asn.e ↔ Asn	0.39	0.26	0.52	0.40	0.31	0.49	0.44	0.35	0.53
Lac OUT	Lac ↔ Lac.e	2.10	1.80	2.40	2.10	1.80	2.40	1.90	1.80	2.00
Gln.l IN	Gln.l → Gln.e	0.72	0.64	0.80	0.33	0.25	0.38	0.27	0.22	0.32
Gln.u IN	Gln.u → Gln.e	0.02	0.00	0.02	0.00	0.00	0.05	0.00	0.00	0.02

Table A- 4-5 Growth (day^{-1}) and antibody (nmol/Mcell/day) fluxes for the three media conditions.

Reaction	CM			LA			LA+		
	Flux	**LB**	**UB**	**Flux**	**LB**	**UB**	**Flux**	**UB**	**LB**
Specific growth rate	0.43	0.36	0.51	0.55	0.47	0.62	0.48	0.39	0.57
Antibody production rate	0.55	0.49	0.62	0.52	0.44	0.61	0.57	0.51	0.63

Table A- 4-6 Metabolite fragments measured by GC-MS for analysis of intracellular metabolite labeling.

Metabolite	Mass	Carbon atoms	Fragment Formula
Lactate	233	2 3	$C_{10}H_{25}O_2Si_2$
Lactate	261	1 2 3	$C_{11}H_{25}O_3Si_2$
Pyruvate	174	1 2 3	$C_6H_{12}O_3NSi$
Alanine	232	2 3	$C_{10}H_{26}ONSi_2$
Alanine	260	1 2 3	$C_{11}H_{26}O_2NSi_2$
Serine	288	2 3	$C_{12}H_{34}NOSi_2$
Serine	302	1 2	$C_{12}H_{32}NO_2Si_2$
Serine	362	2 3	$C_{14}H_{40}NO_2Si_3$
Serine	390	1 2 3	$C_{17}H_{40}O_3NSi_3$
Aspartate	302	1 2	$C_{12}H_{32}NO_2Si_2$
Aspartate	376	1 2	$C_{14}H_{38}NO_3Si_3$
Aspartate	390	2 3 4	$C_{14}H_{40}NO_3Si_3$
Asparagine	417	1 2 3 4	$C_{14}H_{41}N_2O_3Si_3$
Glutamate	330	2 3 4 5	$C_{16}H_{36}O_2NSi_2$
Glutamate	358	1 2 3 4 5	$C_{12}H_{36}NO_3Si_2$
Glutamine	431	1 2 3 4 5	$C_{19}H_{43}O_3N_2Si_3$
Malate	419	1 2 3 4	$C_{18}H_{39}O_5Si_3$
Glycine	218	2	$C_8H_{24}NO_2Si_2$
Glycine	246	1 2	$C_{10}H_{24}O_2NSi_2$

Table A- 4-7 Model goodness-of-fit assessment.

Model	Degrees of freedom	SSR expected range	Best-fit SSR
CM	19	8.9, 32.9	25.4
LA	19	8.9, 32.9	15.6
LA+	19	8.9, 32.9	5.4

Table A- 4-8 Pyruvate contribution to anaplerosis. PC=pyruvate carboxylase, ME=malic enzyme, PC-ME=difference between PC and ME fluxes (i.e., net anaplerotic flux from pyruvate). CM=control medium, LA=low ammonia medium, LA+=low ammonia medium with added ammonia. SE=standard error of flux estimate, LB=lower bound of 95% confidence interval, UB=upper bound of 95% confidence interval, CI=confidence interval.

Rxn	CM (umol/Mcell/day)					LA (umol/Mcell/day)					LA+ (umol/Mcell/day)				
	Flux	SE	LB	UB	CI width	Flux	SE	LB	UB	CI width	Flux	SE	LB	UB	CI width
PC	1E-4	0.33	0.00	1.30	1.30	9.9E-2	-0.84	0.00	3.30	3.30	1E-4	0.66	0.00	2.60	2.60
ME	0.41	0.39	0.19	1.70	1.52	0.39	0.87	-0.11	3.50	3.39	0.42	0.73	0.16	3.00	2.85
PC-ME	-0.41	0.16	-0.81	-0.18	0.62	-0.29	0.10	-0.49	-9.6E-2	0.40	-0.42	0.14	-0.69	-0.16	0.53

Table A- 4-9. Biomass composition.

Metabolite	Coefficient (mmol/Mcell)
Alanine	1.78E-04
Arginine	1.12E-04
Asparagine	1.40E-04
Aspartate	8.53E-05
Cysteine	4.29E-05
Glutamine	9.53E-05
Glutamate	1.14E-04
Glycine	1.95E-04
Histidine	4.23E-05
Isoleucine	9.59E-05
Leucine	1.67E-04
Lysine	1.69E-04
Methionine	4.09E-05
Phenylalanine	6.49E-05
Proline	9.27E-05
Serine	1.31E-04
Threonine	1.14E-04
Tryptophan	1.31E-05
Tyrosine	5.39E-05
Valine	1.23E-04
G6P	8.54E-05
R5P	6.89E-05
MEETHF	7.55E-05
DHAP	3.60E-05
AcCoA.c	7.33E-04

Table A- 4-10 Antibody composition (mol/mol).

Amino Acid	Coefficient
Alanine	38
Cysteine	18
Aspartate	26
Glutamate	33
Phenylalanine	21
Glycine	46
Histidine	14
Isoleucine	15
Lysine	47
Leucine	55
Methionine	8
Asparagine	24
Proline	48
Glutamine	30
Arginine	20
Serine	90
Threonine	55
Valine	67
Tryptophan	13
Tyrosine	34

Equation A- 4-1 Average percent enrichments (APE) were calculated according to the following equation (after correction for natural isotope abundance):

$$APE = \frac{\sum_{i=1}^{n}(M_i \times i)}{n}$$

$n = number\ of\ carbons\ in\ fragment\ ion$
$M_i = abundance\ of\ the\ i\text{-}th\ mass\ isotopomer$

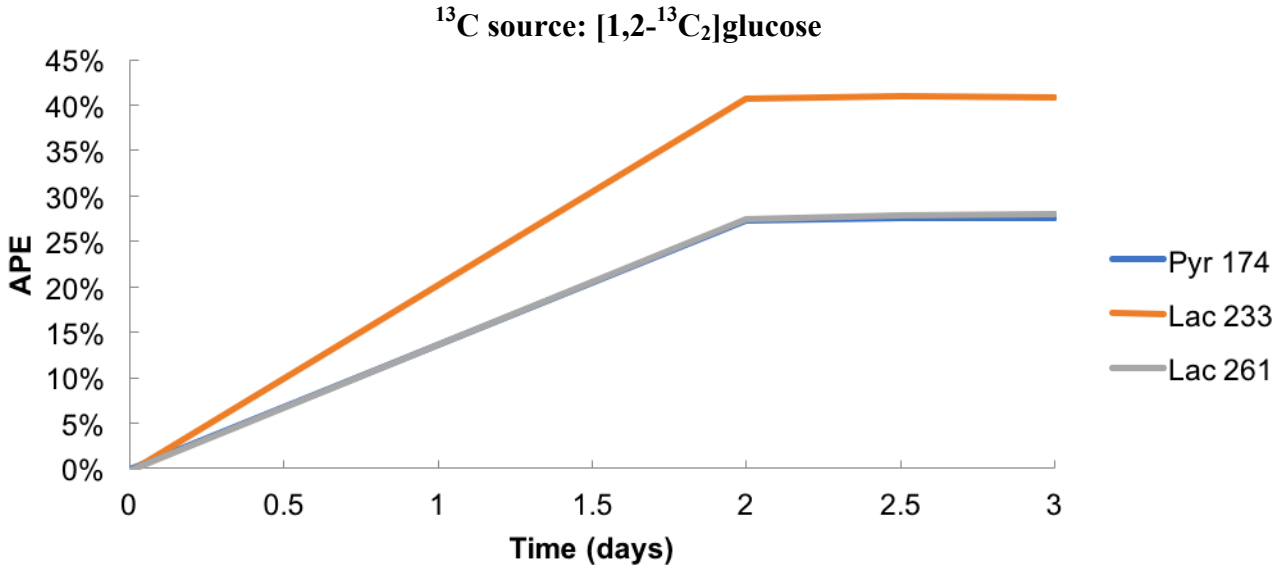

Figure A- 4-13 Average percent enrichments (APEs) of pyruvate and lactate for CM fed cells labeled with [1,2-$^{13}C_2$]glucose.

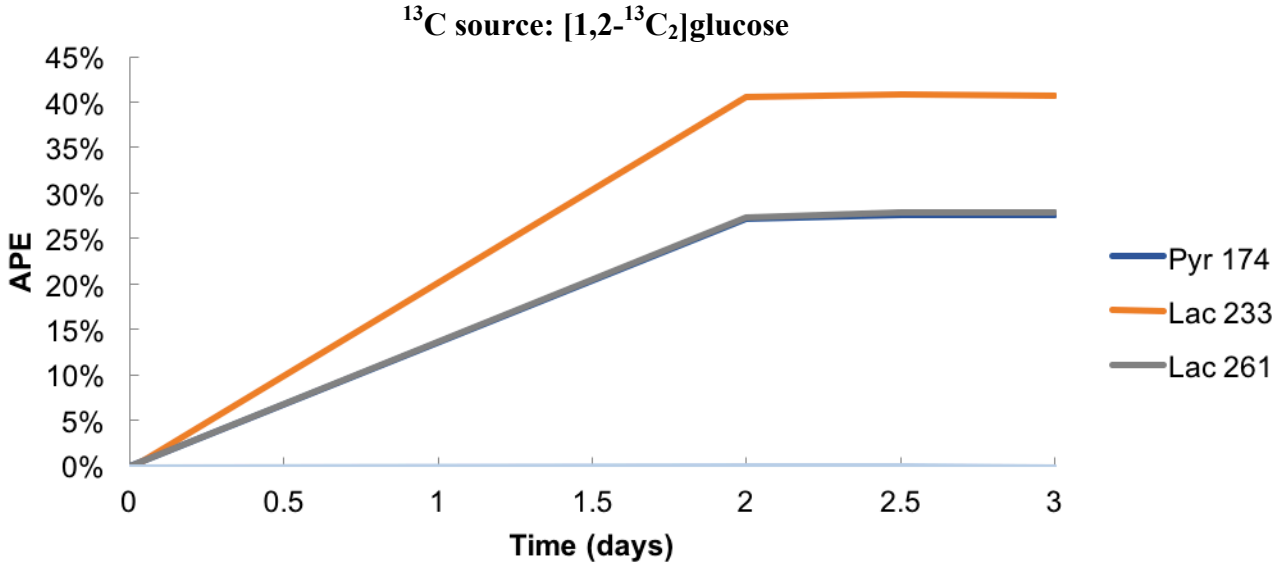

Figure A- 4-14 APEs of pyruvate and lactate for LA fed cells labeled with [1,2-$^{13}C_2$]glucose.

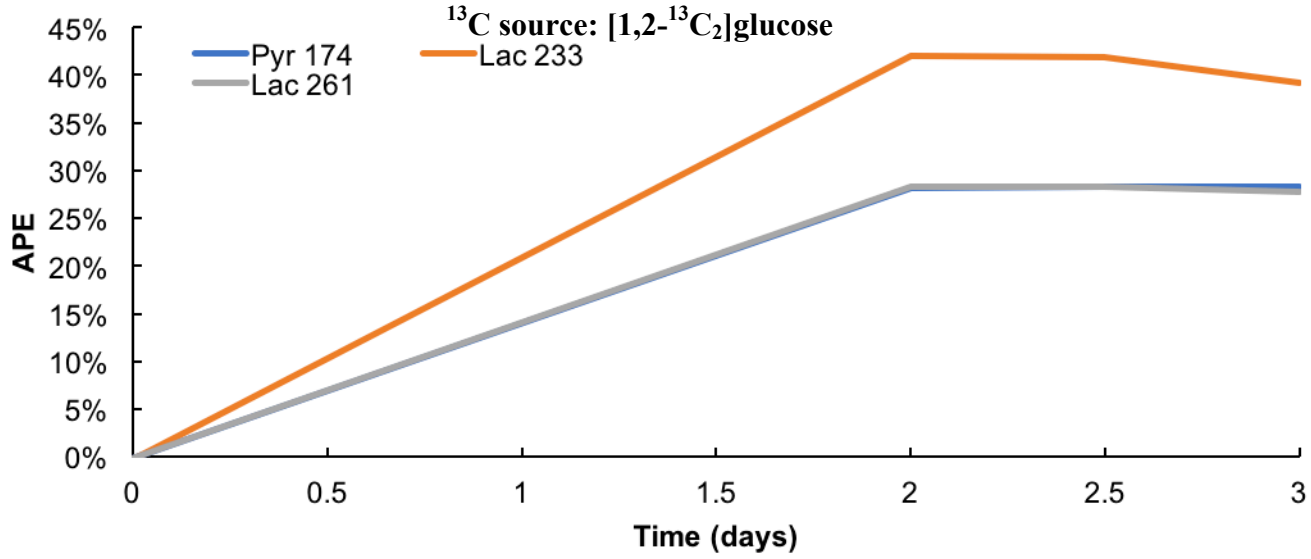

Figure A- 4-15 APEs of pyruvate and lactate for LA+ fed cells labeled with [1,2-$^{13}C_2$]glucose.

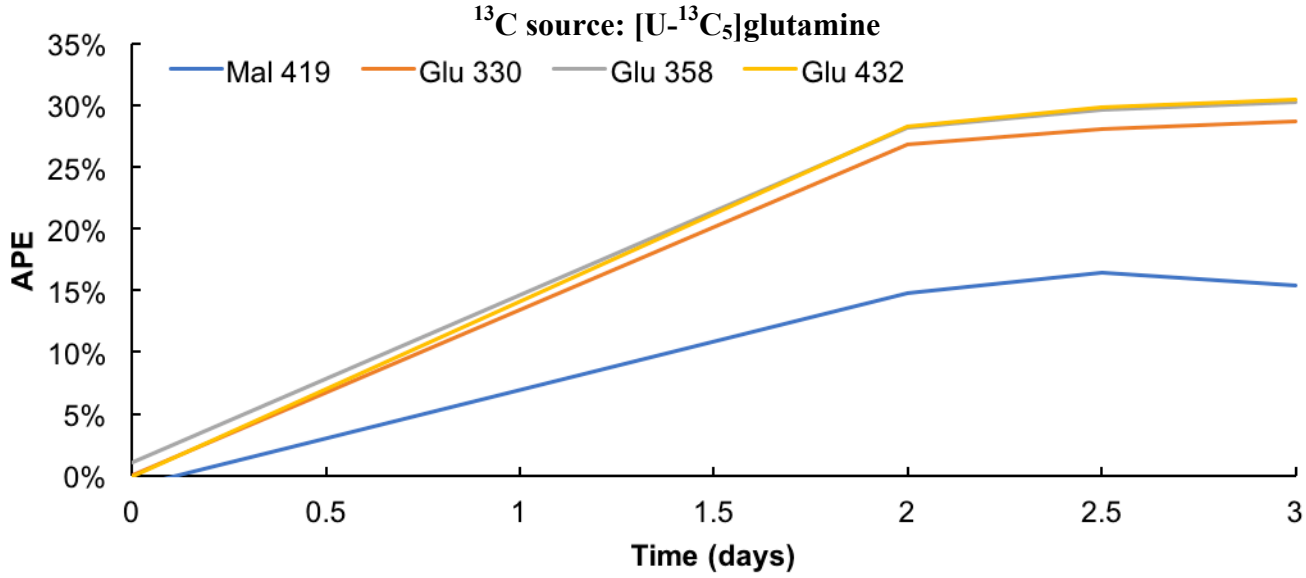

Figure A- 4-16 APEs of malate and glutamate for CM fed cells labeled with [U-$^{13}C_5$]glutamine.

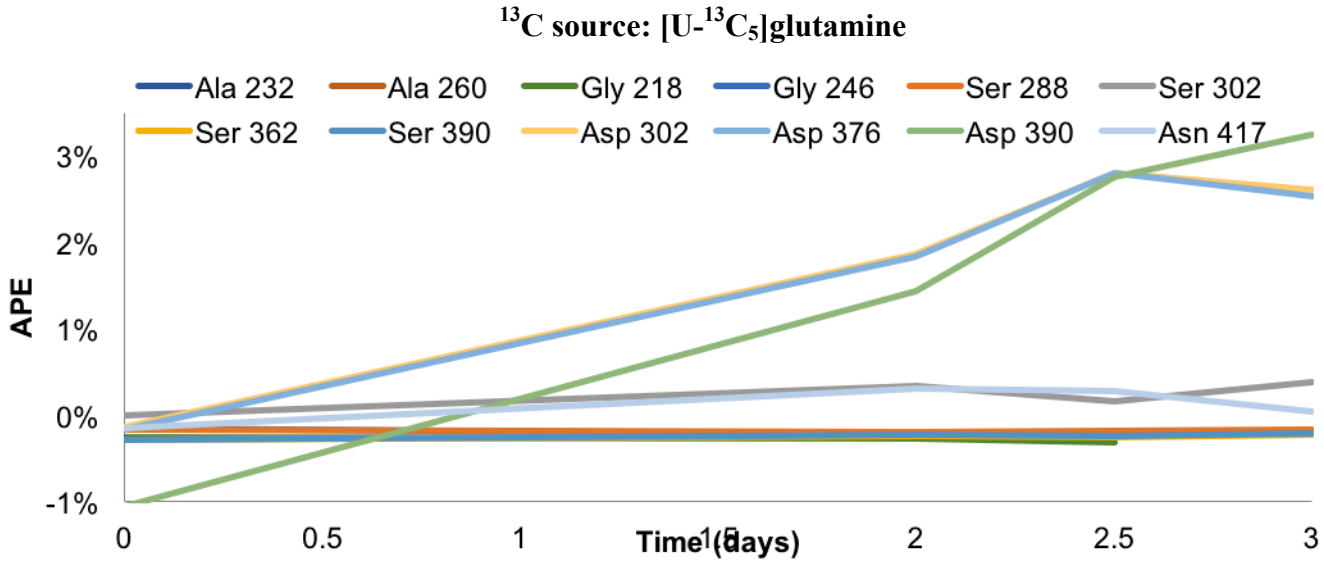

Figure A- 4-17 APEs of alanine, glycine, serine, aspartate, and asparagine for CM fed cells labeled with [U-$^{13}C_5$]glutamine.

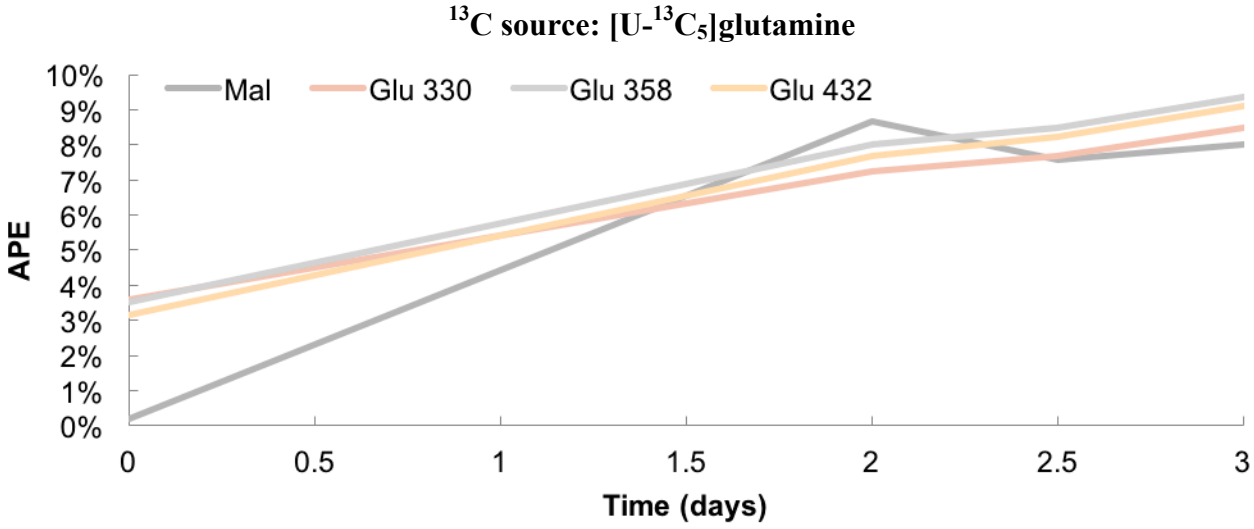

Figure A- 4-18 APEs of malate and glutamate for LA grown cells labeled with [U-$^{13}C_5$]glutamine.

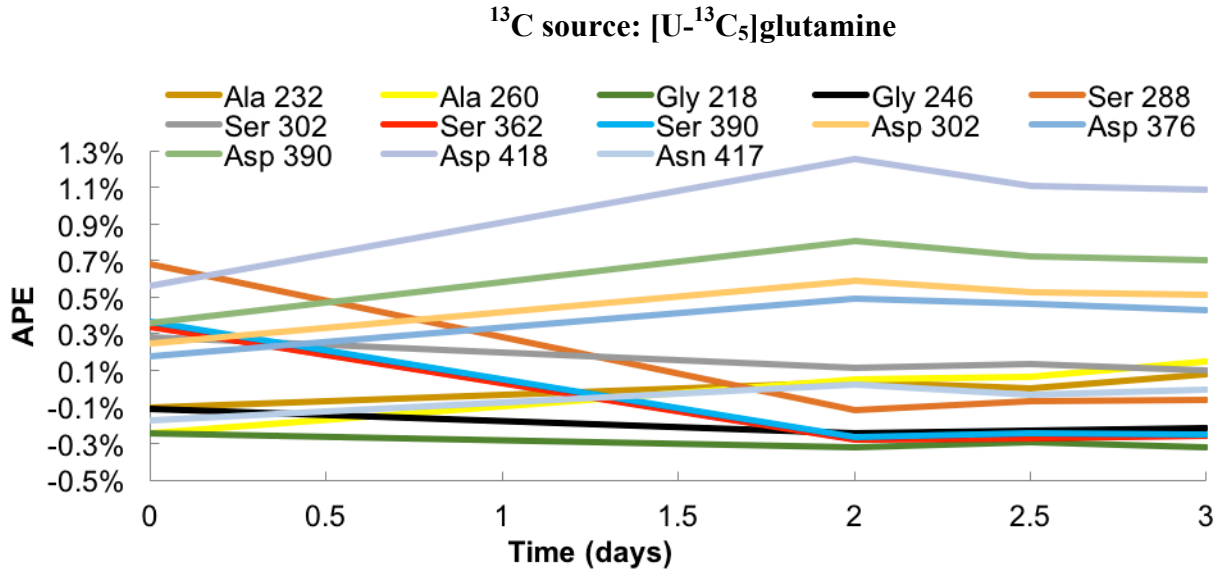

Figure A- 4-19 APEs of alanine, glycine, serine, aspartate, and asparagine for LA grown cells labeled with [U-$^{13}C_5$]glutamine.

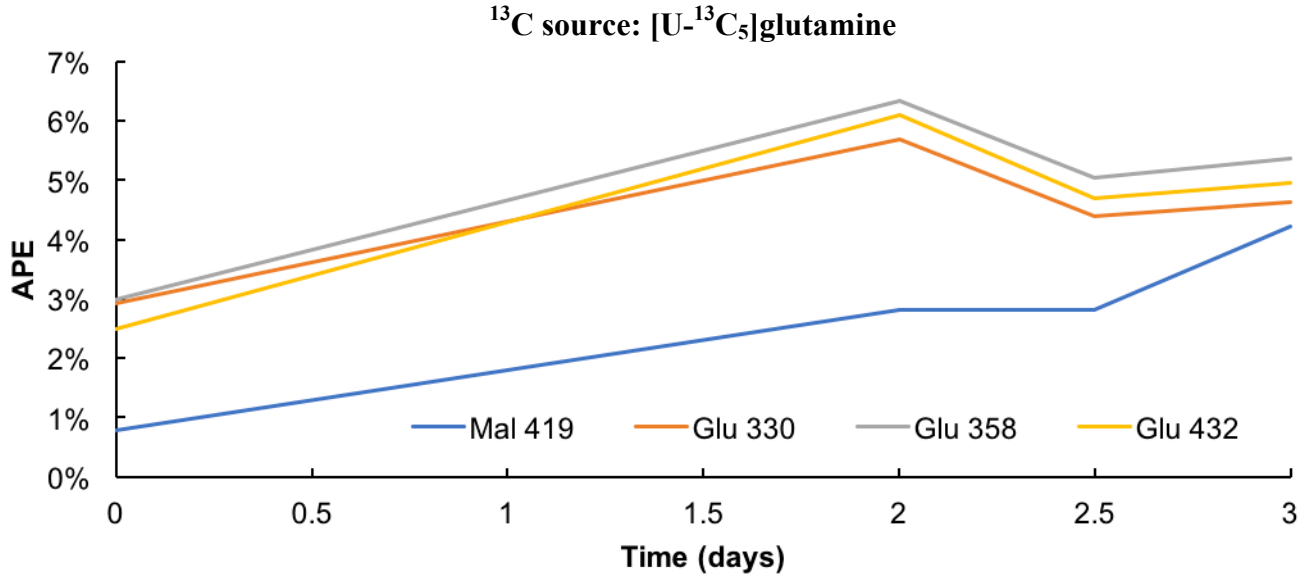

Figure A- 4-20 APEs of malate and glutamate for LA+ fed cells labeled with [U-$^{13}C_5$]glutamine.

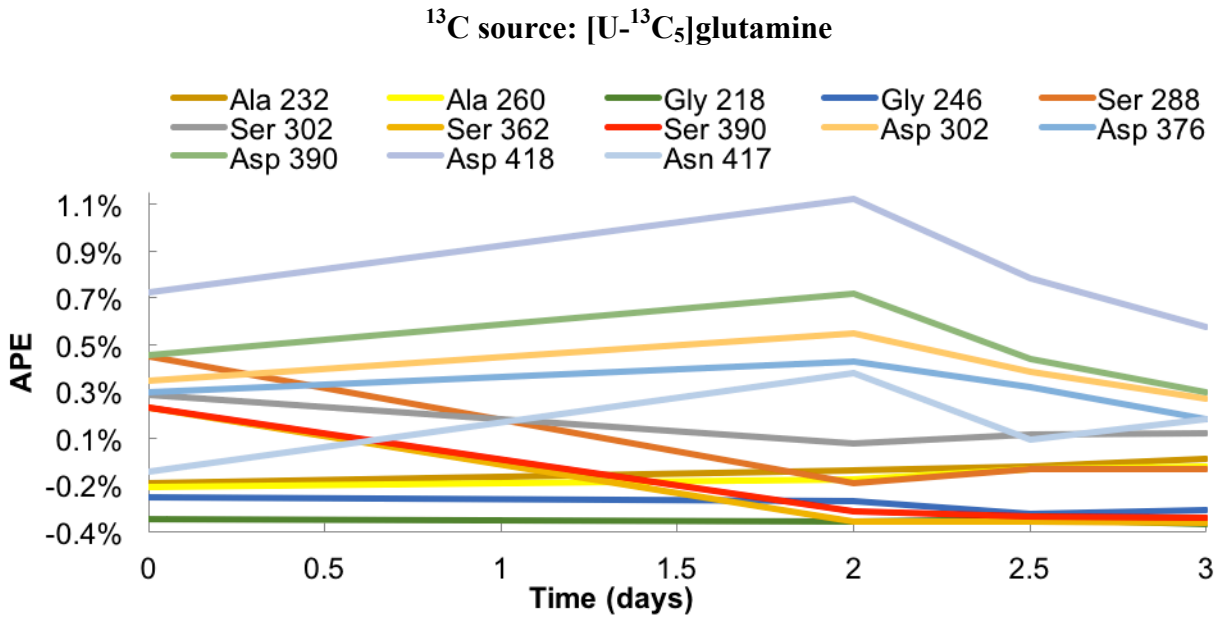

Figure A- 4-21 APEs of alanine, glycine, serine, aspartate, and asparagine for LA+ fed cells labeled with [U-$^{13}C_5$]glutamine.

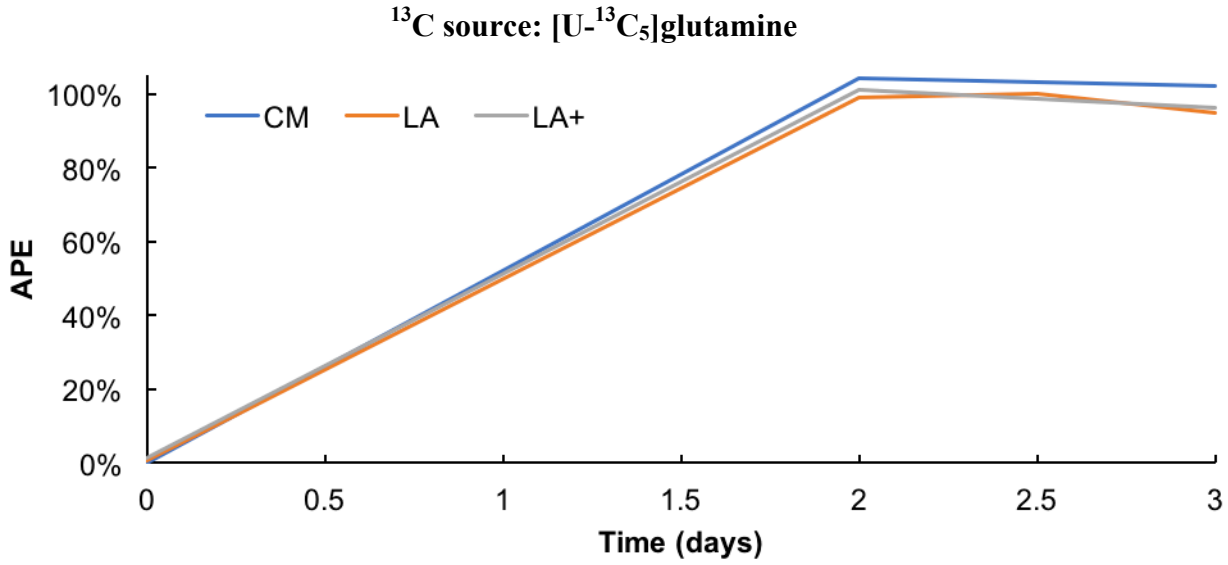

Figure A- 4-22 APEs of glutamine for cells cultured in each media variant. 100% of the intracellular glutamine was labeled by day 2.

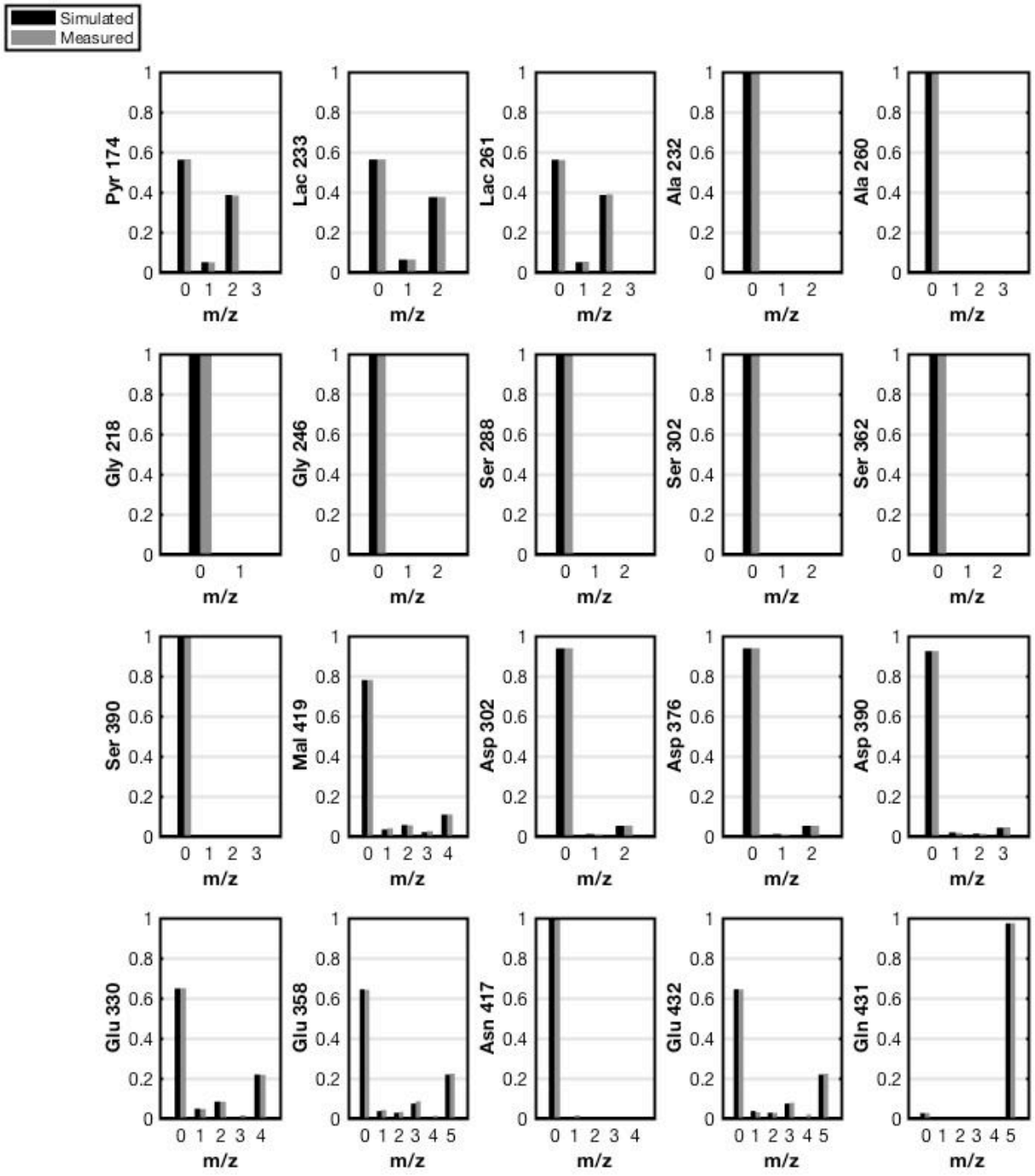

Figure A- 4-23 MIDs of labeled intracellular metabolites as measured (gray bars) by GC-MS and simulated (black bars) by the best-fit model for the CM condition.

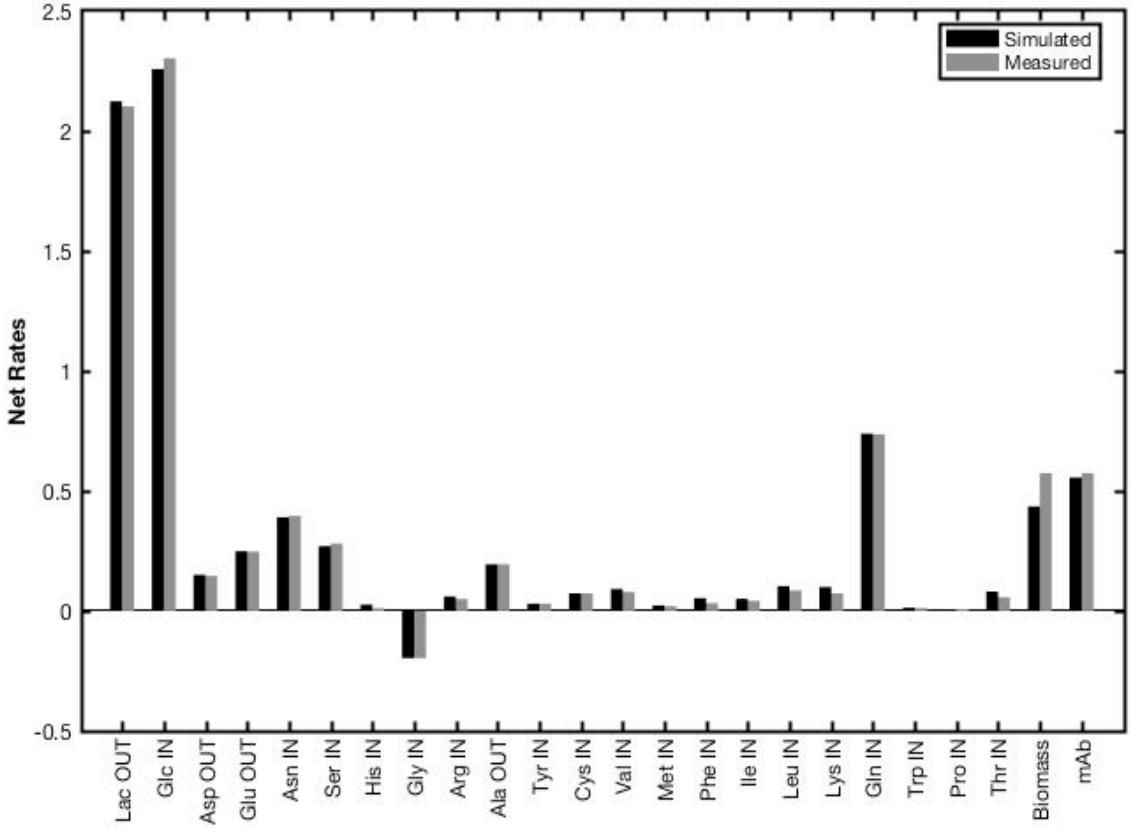

Figure A- 4-24 Fluxes of extracellular metabolites as measured (gray bars) and simulated (black bars) by the best-fit model for the CM condition.

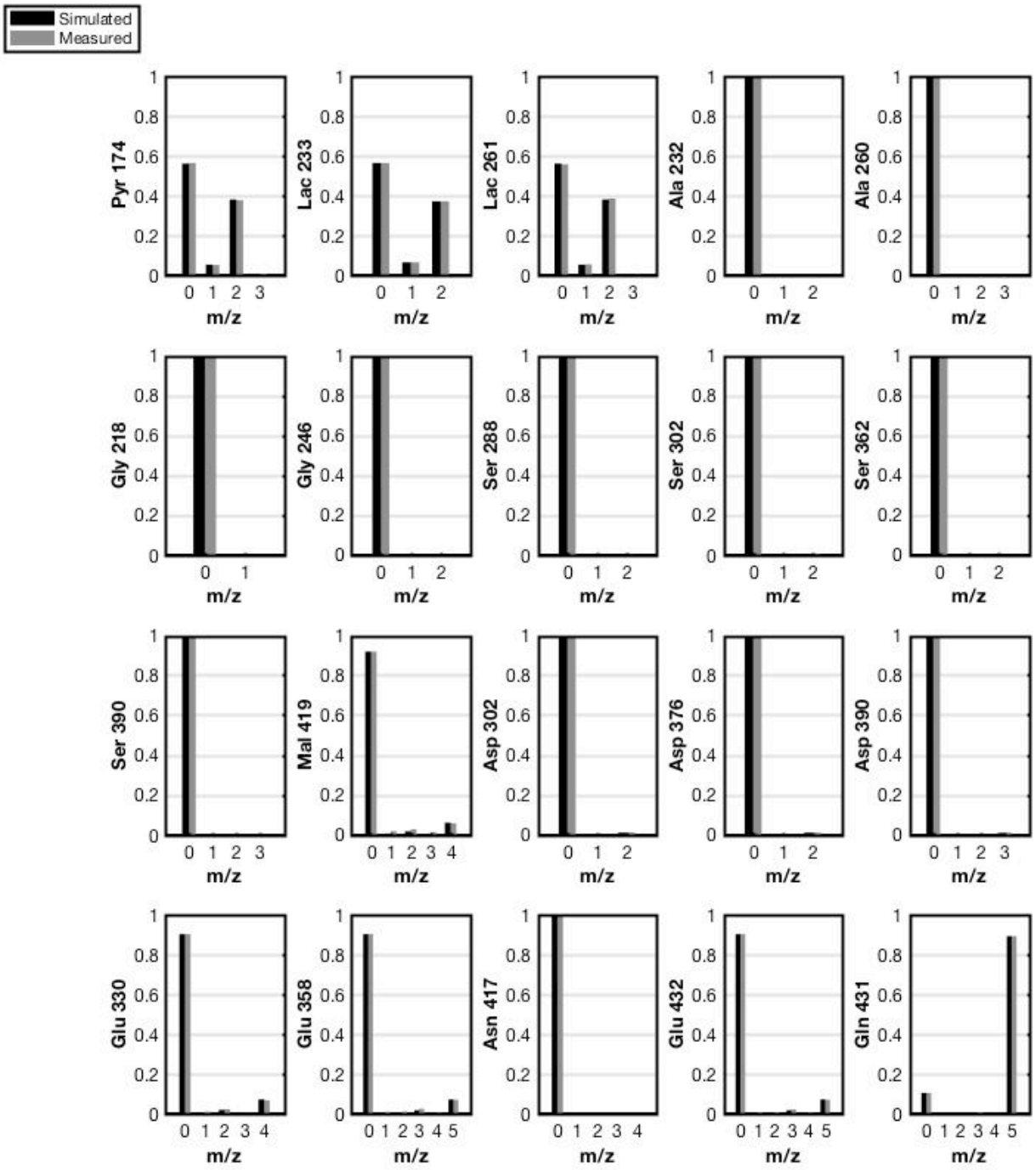

Figure A- 4-25 MIDs of labeled intracellular metabolites as measured (gray bars) by GC-MS and simulated (black bars) by the best-fit model for the LA condition.

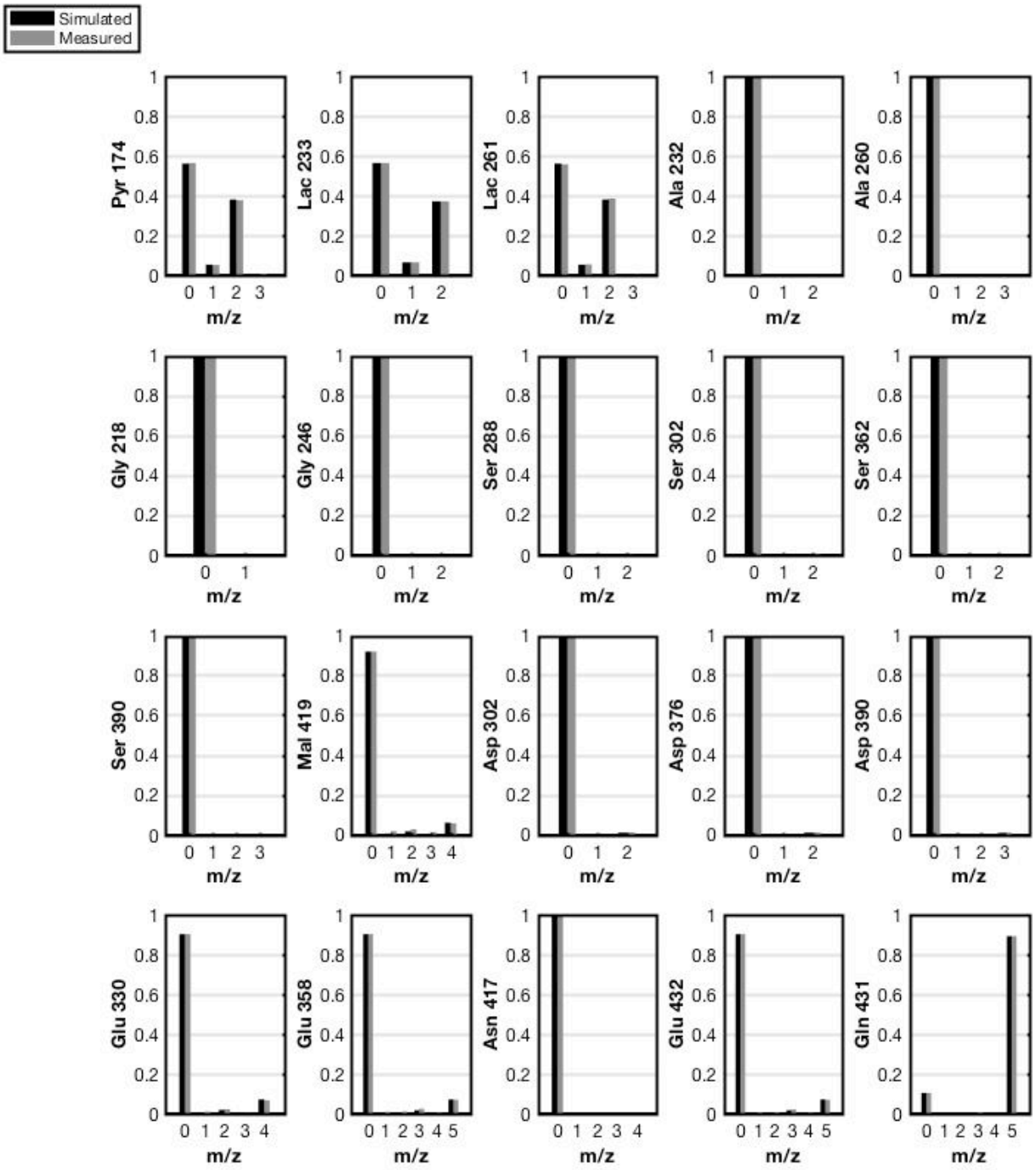

Figure A- 4-26 Fluxes of extracellular metabolites as measured (gray bars) and simulated (black bars) by the best-fit model for the LA medium condition.

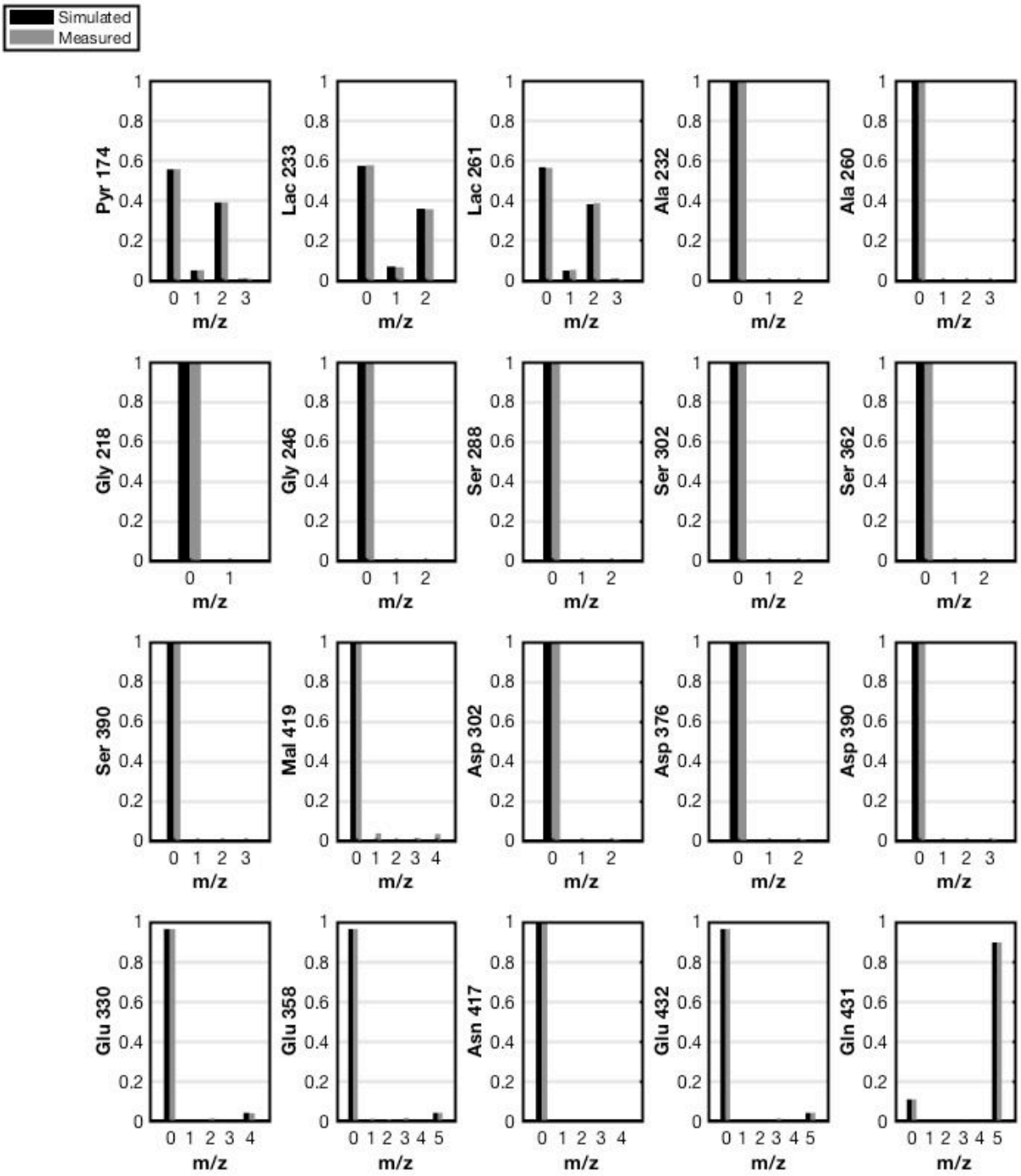

Figure A- 4-27 MIDs of labeled intracellular metabolites as measured (gray bars) by GC-MS and simulated (black bars) by the best-fit model for the LA+ condition.

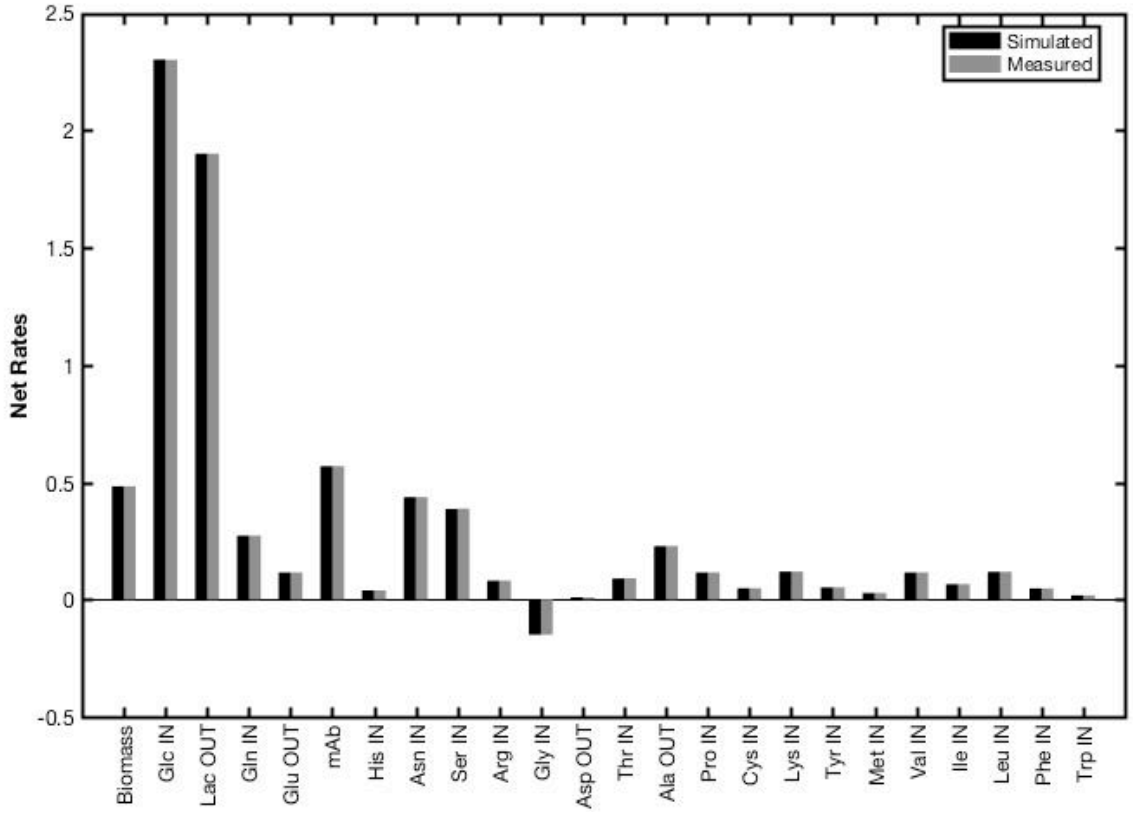

Figure A- 4-28 Fluxes of extracellular metabolites as measured (gray bars) and simulated (black bars) by the best-fit model for the LA+ medium condition.

4.7 References

[1] G. Walsh, Biopharmaceutical benchmarks 2010, Nat. Biotechnol. 28 (2010) 1–10. doi:10.1038/nbt.3040.

[2] M.S. Lao, D. Toth, Effects of ammonium and lactate on growth and metabolism of a recombinant Chinese hamster ovary cell culture., Biotechnol. Prog. 13 (1997) 688–91. doi:10.1021/bp9602360.

[3] F. Zagari, M. Jordan, M. Stettler, H. Broly, F.M. Wurm, Lactate metabolism shift in CHO cell culture: the role of mitochondrial oxidative activity., N. Biotechnol. 30 (2013) 238–245. doi:10.1016/j.nbt.2012.05.021.

[4] H. Dorai, Y.S. Kyung, D. Ellis, C. Kinney, C. Lin, D. Jan, G. Moore, M.J. Betenbaugh, Expression of anti-apoptosis genes alters lactate metabolism of Chinese Hamster Ovary cells in culture., Biotechnol. Bioeng. 103 (2009) 592–608. doi:10.1002/bit.22269.

[5] N. Templeton, A. Lewis, H. Dorai, E. a Qian, M.P. Campbell, K.D. Smith, S.E. Lang, M.J. Betenbaugh, J.D. Young, The impact of anti-apoptotic gene Bcl-2Δ expression on CHO central metabolism., Metab. Eng. 25 (2014) 92–102. doi:10.1016/j.ymben.2014.06.010.

[6] M. Zhou, Y. Crawford, D. Ng, J. Tung, A.F.J. Pynn, A. Meier, I.H. Yuk, N. Vijayasankaran, K. Leach, J. Joly, B. Snedecor, A. Shen, Decreasing lactate level and increasing antibody production in Chinese Hamster Ovary cells (CHO) by reducing the expression of lactate dehydrogenase and pyruvate dehydrogenase kinases., J. Biotechnol. 153 (2011) 27–34. doi:10.1016/j.jbiotec.2011.03.003.

[7] M. Gagnon, G. Hiller, Y.-T. Luan, A. Kittredge, J. DeFelice, D. Drapeau, High-end pH-controlled delivery of glucose effectively suppresses lactate accumulation in CHO fed-

batch cultures., Biotechnol. Bioeng. 108 (2011) 1328–37. doi:10.1002/bit.23072.

[8] K.B. Konstantinov, Tsai Yeong-shou, D. Moles, R. Matanguihan, Control of long-term perfusion Chinese hamster ovary cell culture by glucose auxostat, Biotechnol. Prog. 12 (1996) 100–109. doi:10.1021/bp950044p.

[9] C. Altamirano, C. Paredes, a Illanes, J.J. Cairó, F. Gòdia, Strategies for fed-batch cultivation of t-PA producing CHO cells: substitution of glucose and glutamine and rational design of culture medium., J. Biotechnol. 110 (2004) 171–9. doi:10.1016/j.jbiotec.2004.02.004.

[10] D.Y. Kim, M.A. Chaudhry, M.L. Kennard, M.A. Jardon, K. Braasch, B. Dionne, M. Butler, J.M. Piret, Fed-batch CHO cell t-PA production and feed glutamine replacement to reduce ammonia production, Biotechnol. Prog. 29 (2013) 165–175. doi:10.1002/btpr.1658.

[11] T.M. Duarte, N. Carinhas, L.C. Barreiro, M.J.T. Carrondo, P.M. Alves, A.P. Teixeira, Metabolic responses of CHO cells to limitation of key amino acids, Biotechnol. Bioeng. 111 (2014) 2095–2106. doi:10.1002/bit.25266.

[12] Y. Genzel, J.B. Ritter, S. König, R. Alt, U. Reichl, Substitution of glutamine by pyruvate to reduce ammonia formation and growth inhibition of mammalian cells., Biotechnol. Prog. 21 (2005) 58–69. doi:10.1021/bp049827d.

[13] E. Pacis, M. Yu, J. Autsen, R. Bayer, F. Li, Effects of cell culture conditions on antibody N-linked glycosylation-what affects high mannose 5 glycoform, Biotechnol. Bioeng. 108 (2011) 2348–2358. doi:10.1002/bit.23200.

[14] M. Schneider, I.W. Marison, U. von Stockar, The importance of ammonia in mammalian cell culture., J. Biotechnol. 46 (1996) 161–85.

[15] S.C. Burleigh, T. van de Laar, C.J.M. Stroop, W.M.J. van Grunsven, N. O'Donoghue, P.M. Rudd, G.P. Davey, Synergizing metabolic flux analysis and nucleotide sugar metabolism to understand the control of glycosylation of recombinant protein in CHO cells., BMC Biotechnol. 11 (2011) 95. doi:10.1186/1472-6750-11-95.

[16] M. Taschwer, M. Hackl, J.A. Hernández Bort, C. Leitner, N. Kumar, U. Puc, J. Grass, M. Papst, R. Kunert, F. Altmann, N. Borth, Growth, productivity and protein glycosylation in a CHO EpoFc producer cell line adapted to glutamine-free growth., J. Biotechnol. 157 (2012) 295–303. doi:10.1016/j.jbiotec.2011.11.014.

[17] J. a H. Bort, B. Stern, N. Borth, CHO-K1 host cells adapted to growth in glutamine-free medium by FACS-assisted evolution., Biotechnol. J. 5 (2010) 1090–7. doi:10.1002/biot.201000095.

[18] A.G. McAtee, N. Templeton, J.D. Young, Role of Chinese hamster ovary central carbon metabolism in controlling the quality of secreted biotherapeutic proteins, Pharm. Bioprocess. 2 (2014) 63–74.

[19] P. Chen, S.W. Harcum, Effects of amino acid additions on ammonium stressed CHO cells., J. Biotechnol. 117 (2005) 277–86. doi:10.1016/j.jbiotec.2005.02.003.

[20] C. Altamirano, A. Illanes, S. Becerra, J.J. Cairó, F. Gòdia, Considerations on the lactate consumption by CHO cells in the presence of galactose., J. Biotechnol. 125 (2006) 547–56. doi:10.1016/j.jbiotec.2006.03.023.

[21] P.M. Castro, P.M. Hayter, a P. Ison, a T. Bull, Application of a statistical design to the optimization of culture medium for recombinant interferon-gamma production by Chinese hamster ovary cells., Appl. Microbiol. Biotechnol. 38 (1992) 84–90. doi:10.1007/BF00169424.

[22] C.F. Mandenius, A. Brundin, Bioprocess optimization using design-of-experiments methodology, Biotechnol. Prog. 24 (2008) 1191–1203. doi:10.1002/btpr.67.

[23] A. Parampalli, K. Eskridge, L. Smith, M.M. Meagher, M.C. Mowry, A. Subramanian, Developement of serum-free media in CHO-DG44 cells using a central composite statistical design, Cytotechnology. 54 (2007) 57–68. doi:10.1007/s10616-007-9074-3.

[24] W.S. Ahn, M.R. Antoniewicz, Metabolic flux analysis of CHO cells at growth and non-growth phases using isotopic tracers and mass spectrometry., Metab. Eng. 13 (2011) 598–609. doi:10.1016/j.ymben.2011.07.002.

[25] N. Templeton, K.D. Smith, A.G. McAtee-Pereira, H. Dorai, M.J. Betenbaugh, S.E. Lang, J.D. Young, Application of 13C flux analysis to identify high-productivity CHO metabolic phenotypes, Metab. Eng. 29 (2017) 53–62. doi:10.1016/j.ymben.2017.01.008.

[26] P.G. Slade, R.G. Caspary, S. Nargund, C.-J. Huang, Mannose metabolism in recombinant CHO cells and its effect on IgG glycosylation, Biotechnol. Bioeng. (2016) n/a-n/a. doi:10.1002/bit.25924.

[27] A.G. McAtee, L.J. Jazmin, J.D. Young, Application of isotope labeling experiments and 13C flux analysis to enable rational pathway engineering, Curr. Opin. Biotechnol. 36 (2015) 50–56. doi:10.1016/j.copbio.2015.08.004.

[28] W. Suk Ahn, M.R. Antnoniewicz, Parallel labeling experiments with [1,2-(13)C]glucose and [U-(13)C]glutamine provide new insights into CHO cell metabolism., Metab. Eng. 15 (2013) 34–47. doi:10.1016/j.ymben.2012.10.001.

[29] N. Templeton, J. Dean, P. Reddy, J.D. Young, Peak antibody production is associated with increased oxidative metabolism in an industrially relevant fed-batch CHO cell culture., Biotechnol. Bioeng. 110 (2013) 2013–2024. doi:10.1002/bit.24858.

[30] C. a Sellick, R. Hansen, A.R. Maqsood, W.B. Dunn, G.M. Stephens, R. Goodacre, A.J. Dickson, Effective quenching processes for physiologically valid metabolite profiling of suspension cultured Mammalian cells., Anal. Chem. 81 (2009) 174–83. doi:10.1021/ac8016899.

[31] J. Folch, M. Lees, G.. H. Sloane Stanley, A simple method for the isolation and purification of total lipides from animal tissues, J. Biol. Chem. 226 (1957) 497–509. doi:10.1016/j.ultrasmedbio.2011.03.005.

[32] K. Sheikh, J. Fo, L.K. Nielsen, Modeling Hybridoma Cell Metabolism Using a Generic Genome-Scale Metabolic Model of Mus musculus, Biotechnol. Prog. 21 (2005) 112–121. doi:10.1021/bp0498138.

[33] M.R. Antoniewicz, J.K. Kelleher, G. Stephanopoulos, Elementary metabolite units (EMU): a novel framework for modeling isotopic distributions., Metab. Eng. 9 (2007) 68–86. doi:10.1016/j.ymben.2006.09.001.

[34] J.D. Young, J.L. Walther, M.R. Antoniewicz, H. Yoo, An Elementary Metabolite Unit (EMU) Based Method of Isotopically Nonstationary Flux Analysis, Biotechnol. Bioeng. 99 (2008) 686–699. doi:10.1002/bit.

[35] H. Brunengraber, J.K. Kelleher, C. Des Rosiers, Applications of Mass Isotopomer Analysisto Nutrition Research, Annu. Rev. Nutr. 17 (1997) 559–96. doi:10.1146/annurev.nutr.17.1.559.

[36] T.A. Murphy, J.D. Young, ETA: robust software for determination of cell specific rates from extracellular time courses., Biotechnol. Bioeng. 110 (2013) 1748–58. doi:10.1002/bit.24836.

[37] M.R. Antoniewicz, J.K. Kelleher, G. Stephanopoulos, Determination of confidence

intervals of metabolic fluxes estimated from stable isotope measurements, Metab. Eng. 8 (2006) 324–37. doi:10.1016/j.ymben.2006.01.004.

[38] J. Wahrheit, A. Nicolae, E. Heinzle, Dynamics of growth and metabolism controlled by glutamine availability in Chinese hamster ovary cells., Appl. Microbiol. Biotechnol. 98 (2014) 1771–83. doi:10.1007/s00253-013-5452-2.

[39] F.M. Wurm, Production of recombinant protein therapeutics in cultivated mammalian cells., Nat. Biotechnol. 22 (2004) 1393–8. doi:10.1038/nbt1026.

[40] J.D. Young, Metabolic flux rewiring in mammalian cell cultures, Curr. Opin. Biotechnol. (2013) 1–8. doi:10.1016/j.copbio.2013.04.016.

[41] C. Paredes, E. Prats, J.J. Cairó, F. Azorín, L. Cornudella, F. Gòdia, Modification of glucose and glutamine metabolism in hybridoma cells through metabolic engineering., Cytotechnology. 30 (1999) 85–93. doi:10.1023/A:1008012518961.

5 ^{13}C METABOLIC FLUX ANALYSIS IN LABELING CHO CELL STATIONARY GROWTH PHASE

5.1 Summary

Chinese hamster ovary (CHO) cell cultures are extensively used in industry for the production of complex recombinant proteins (e.g., biotherapeutics, vaccines, and monoclonal antibodies) in bioreactors. Programmed cell death, or apoptosis, is inevitable as a result of nutrient or growth factor depletion, byproduct accumulation, and other stressors inherent to bioreactor growth conditions. Apoptosis is a highly regulated signaling cascade that has been successfully combatted by cell engineering techniques with the result of prolonged culture viabilities and increased recombinant protein production. However, few previous studies have investigated the effects of anti-apoptotic protein engineering on CHO cell central carbon metabolism. Here, we utilized ^{13}C metabolic flux analysis (MFA) to analyze the effects of four anti-apoptotic genes (Bcl-2Δ, E1B-19K, Aven, and XIAP) on CHO cells in culture during stationary growth phase. CHO cell metabolism naturally shifts from producing predominantly biomass to producing predominantly recombinant protein with cell density remaining relatively constant during stationary growth phase. Bcl-2Δ was studied and a similar protein, E1B-19K was studied in concert with Aven and XIAP and compared to the parental control cell line with no anti-apoptotic gene expression. Favorable shifts in lactate consumption, an altered amino acid metabolism, and an elevated utilization of mitochondrial metabolism were observed in the apoptosis-resistant cells. Specifically, the Bcl-2Δ clone consumed roughly 85% more lactate than the parental clone during stationary phase, a highly advantageous metabolic phenotype.

5.2 Background and Introduction

Chinese hamster ovary (CHO) cells are the prevailing cell line used by the pharmaceutical industry to produce biotherapeutic drugs, such as the monoclonal antibodies (mAbs) used to treat cancer and immunological disorders [1]. The metabolism of CHO cells is complex and generally consists of two main growth phases: exponential and stationary. During the exponential growth phase, typically the first two to three days of batch or the first four to five days of fed-batch culture, the cells are heavily glycolytic and double in biomass approximately every 24 hours. When CHO cells enter the stationary growth phase, the cells have partially exhausted their glucose supply and subsequently switch from primarily biomass production to protein production. This is the phase when cells produce and secrete the majority of their recombinant products such as mAbs or other industrially relevant proteins [2].

CHO cell metabolism is generally characterized by an energy inefficient phenotype. They produce excessive quantities of ammonia and lactate that not only demonstrate a wasteful metabolic phenotype, but can also have toxic side effects to the culture [3]. Scientists often combat high ammonia producing strains by genetically modifying the CHO cells to express glutamine synthetase (GS) which enables CHO cells to produce their own glutamine for biological requirements [4–7]. This allows cells to metabolically bypass glutaminolysis, the major source of culture ammonia. While extensive metabolic engineering has been performed on CHO cell lines to combat lactate production [8–10], some CHO cell clones, like the clones studied here, consume excess lactate at the onset of stationary phase [8,9,11]. Since glucose is virtually depleted at this point in the culture's growth, the otherwise toxic lactate serves as the major carbon source during stationary growth phase. There is no conclusively agreed upon reason for this phenomenon in literature since not all cultures that experience this shift are

glucose depleted, or otherwise nutrient starved. However, in the clones studied here, the switch from lactate production to consumption signifies the onset of stationary phase. Interestingly, anti-apoptotic gene overexpression in CHO cells has been previously reported to alter their lactate metabolism so they do not accumulate inhibitory levels of lactate as seen in control cell lines [8].

Anti-apoptosis engineering of industrial producer lines is a well-established technique to prolong cell culture life and, therefore, volumetric protein production [12–14]. Since the volumetric protein production of a culture is directly proportional to the integrated viable cell density (IVCD) [15], the more cells that survive for longer periods of time, the more product protein that will be produced. Apoptosis is reported to cause up to 80% of cell death in normal bioreactor cultures [16]. Here, we study the stationary phase metabolism of two cell lines expressing either Bcl-2Δ, a combination of three other anti-apoptotic proteins, E1B-19K, AVEN, and XIAP, and the parental, non-modified cell line. Bcl-2 (B-cell lymphoma 2) is localized at the outer membrane of the mitochondria, nuclear envelope, and portions of the endoplasmic reticulum (ER) and has been shown to suppress programmed cell death, also known as apoptosis [17,18]. Bcl-2Δ, a more stable and efficacious truncated version of Bcl-2 [14,19], has been associated with reduced lactate accumulation, increased IVCD, increased biomass yield, increased peak VCD, and increased isocitrate dehydrogenase (IDH) and NADH oxidase activities in a previous study performed in this lab [9]. E1B-19K is a functional and structural homolog of Bcl-2—both anti-apoptotic proteins have been shown to disable p53 function [20]. Aven, another anti-apoptotic gene studied here, has been shown to suppress cell death in multiple cell types including CHO cells in previous studies [21,22]. Aven's anti-apoptotic effects are due to its ability to inhibit the apoptosome complex early in the apoptotic process [8]. XIAP (X-linked inhibitor of apoptosis protein), the final anti-apoptotic gene used in this study,

accumulates in the cytosol and acts by inhibiting the activation of caspases, which are a family of protease enzymes that play a critical role in the late stages of apoptosis [8,23].

XIAP has been shown to significantly protect HEK 293 cells against nutrient deprivation and virus infection induced apoptosis [23]. The action of the three anti-apoptotic genes studied in this experiment are detailed in Figure 5-1. Previous studies of anti-apoptosis engineering have mainly used apoptotic DNA laddering [23,24], percent viability analysis [9,14,23,24], caspase activity screening [9,14], titer, and extracellular metabolic rates such as lactate production [14] to determine the effects of anti-apoptotic genes in various cell types. While utilizing the aforementioned metrics gives a general picture of cellular metabolism, they do not quantitatively elucidate the effects of anti-apoptotic genes on intracellular central carbon metabolism. Instead, these metrics confirm anti-apoptotic activity, extracellular changes in metabolism, and even intracellular indicators of anti-apoptotic gene activity but are unable to elucidate the effects of anti-apoptotic genes on the critical intracellular metabolism of the cells. However, ^{13}C metabolic flux analysis (MFA) allows for rigorous quantification of intracellular carbon metabolism in a way that is not possible with extracellular metabolic flux measurements alone. MFA opens up the black box of intracellular metabolism to enable identification of metabolic bottlenecks, underutilized pathways, possible feedback mechanisms, etc. by tracing ^{13}C atoms through intracellular metabolism as they are rearranged and shuffled through various metabolic pathways [25]. In this study, we performed ^{13}C MFA on CHO cell lines constitutively expressing zero, one, or three anti-apoptotic gene(s) during their stationary growth phase. Since stationary phase is the peak recombinant protein production phase for industrial CHO cell lines, the metabolic phenotype during this growth phase is of utmost interest to pharmaceutical researchers [2].

The experiment detailed in this chapter utilized ^{13}C MFA to elucidate the intracellular metabolism of three industrial CHO cell lines: two clones over expressing anti-apoptotic gene(s) and a control clone during stationary growth phase. From this work, we determined a fed-batch experimental protocol for future use in analyzing CHO cell metabolism during stationary phase. Furthermore, it was determined that the anti-apoptotic genes did affect overall metabolic phenotype even with the alteration of substrate preference. One anti-apoptotic clone preferred lactate whereas the other preferred amino acids as primary fuel sources during stationary growth.

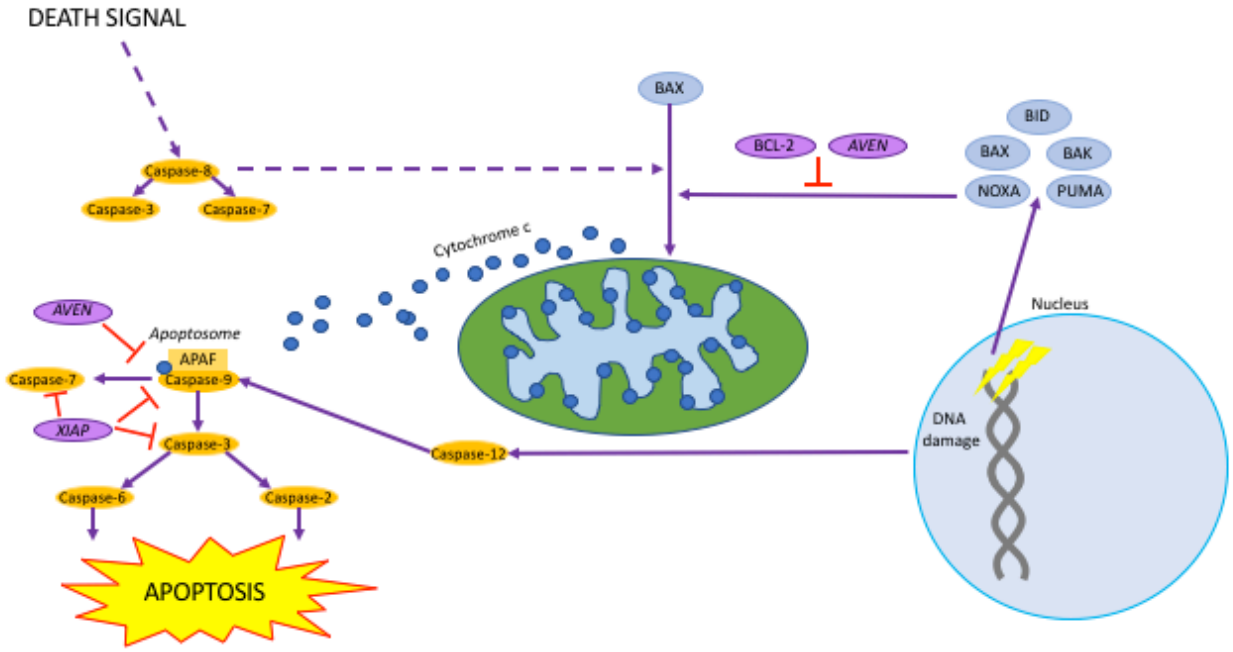

Figure 5-1 Apoptosis signaling cascade in mammalian cells. The anti-apoptotic genes studied in this paper are shown in purple ovals. Bcl-2Δ and AVEN inhibit the signaling cascade that triggers apoptosis due to DNA damage while AVEN also inhibits the apoptosome complex early in the apoptotic process as shown. XIAP inhibits the activation of caspases 3, 7, and 9 which play a critical role in the late stages of apoptosis. Bcl-2Δ and E1B-19K are homologous.

5.3 Materials and Methods

5.3.1 Cell Culture

Three proprietary cell lines from Janssen Pharmaceuticals, C1013A, C1013H, and C1013K, were seeded in Janssen's proprietary MACH-1 media at 0.3 Mcell/mL in 125 mL shake

with 50 mL working volume at 37°C, 130 RPM, and 5% CO_2. Five flasks (designated A-E) of each cell line were cultivated for this experiment. C1013A served as the control cell line with no anti-apoptotic genes expressed. C1013H signified C1013A with Bcl-2Δ overexpressed, and C1013K denoted C1013A with E1B-19K, Aven, and XIAP overexpressed. The cells were grown for twelve total days in fed-batch cultivation with a glucose feed at day five, the onset of stationary growth phase. Medium lactate levels were measured twice daily until the lactate profile switched from production to consumption, indicating the onset of stationary growth phase. At this point, a bolus of 35 mM ^{13}C glucose tracer was spiked into flasks D and E of each cell line such that the ^{13}C glucose would account for approximately 50% of the overall glucose concentration in each labeled flask. At the same time, a bolus of 35 mM natural glucose was spiked into flasks A, B, and C. The 35 mM ^{13}C glucose media were comprised of a 50:50 mixture of [1,2-$^{13}C_2$] glucose and [U-$^{13}C_6$] glucose in flasks D and E.

5.3.2 Analytical techniques

Cell culture samples from flasks A-C were taken every 12 hours starting at culture day two and analyzed via a YSI 2300 STAT Plus (YSI Bioanalytical Products) for glucose and lactate concentrations. Cell culture samples from flasks A-C of each cell line were collected every 12 hours starting at day zero and analyzed for viable cell density (VCD) and percent viability via CEDEX, and amino acid concentrations were measured via high performance liquid chromatography (HPLC) as previously described [2]. Flasks D and E of each cell line were measured for VCD, percent viability, and amino acid concentrations every 24 hours from day zero. After the spike of ^{13}C-glucose at day five in flasks D and E, cell culture aliquots were collected containing approximately 10 million viable cells at days six, seven, eight, ten, and eleven. These aliquots were immediately cold-quenched with 5x volumes of 60/40 (v/v) solution

of methanol and ammonium bicarbonate (AMBIC) pre-cooled to -40°C [26]. The samples were centrifuged and the supernatant was immediately removed. Following the cold-quench, intracellular metabolites were extracted via the Folch method [27]. Once extracted, the intracellular metabolites were derivatized via methoxamine (MOX) and tert-butyldimethylsilyl chloride (TBDMS) reagents for analysis via gas chromatography-mass spectrometry (GC-MS) [2]. Samples taken after the ^{13}C bolus feed on day five were derivatized with di-*O*-isopropylidene propionate as previously described [28]. The enrichment of each ^{13}C glucose tracer was determined as reported in Table 5-1. The highest total percent enrichment (obtained from the combination of the two tracers) of ^{13}C tracer was 48% in C1013K with the lowest being 43% in C1013H. Genes over expressed in each cell line and ^{13}C tracer fractional enrichment data for each cell line used is detailed below.

Table 5-1 Description of each cell line studied. Genes overexpressed in each cell line and ^{13}C tracer fractional enrichment data for each cell line are detailed below.

Cell line	Genes overexpressed	[1,2-$^{13}C_2$] glucose	[U-$^{13}C_6$] glucose
C1013A	-	0.2239	0.2239
C1013H	Bcl-2Δ	0.2153	0.2153
C1013K	E1B-19K, AVEN, XIAP	0.2424	0.2424

5.3.3 ^{13}C Metabolic flux analysis

GC/MS analysis of the aforementioned quenched samples from flasks D and E of each cell line provided ^{13}C isotope enrichment data which were analyzed using the MATLAB-based software package isotopomer network compartmental analysis (INCA) (publicly available at http://mfa.vueinnovations.com) [15]. Mass and isotopomer balances were simulated for CHO cell central carbon metabolism using an elementary metabolite unit (EMU) decomposition of the metabolic reaction network to model variations in ^{13}C isotope labeling caused by changes in metabolic fluxes [29,30]. Cultures were verified to be at metabolic steady state by observing

constant rates of change in extracellular metabolite concentrations. Isotopic steady state was verified by measuring the equilibration of mass isotopomer distributions (MIDs) over time through the calculations of the average percent enrichment (APE) of each ^{13}C labeled metabolite [31]. The change in isotopic enrichment over time fell within the range of the measurement's uncertainty at isotopic steady state. Extracellular fluxes were calculated using the MATLAB-based software package extracellular time course analysis (ETA) to regress the changes in extracellular metabolite concentrations over the experimental time course [32]. Stationary ^{13}C MFA was applied at the day eight time point to calculate intracellular metabolic fluxes. Experimentally measured extracellular fluxes and intracellular MIDs were regressed using a Levenberg-Marquardt optimization algorithm [9]. One flux map was generated for each of the three cell lines studied. Fluxes were calculated using a minimum of 50 unique restarts from randomized start values to ensure a global minimum was achieved. A chi-square statistical test was applied to assess the goodness-of-fit and 95% confidence intervals were calculated for each flux value [33]. A summary of the best-fit solutions, 95% confidence intervals, and goodness-of-fit metrics can be found in Table A- 5-1.

5.3.4 Statistical analysis

The regressed fluxes and other experimentally calculated data from the three cell lines were compared by one-way ANOVA with a significance level threshold of 5%. Where there was no significance found at the 5% confidence threshold, a 10% threshold was used as indicated by the graphs that follow. Standard error of the mean (SEM) was calculated from 95% confidence intervals by dividing the difference of the upper and lower bounds by 3.92.

5.4 Results

5.4.1 CHO cells overexpressing anti-apoptotic genes survive longer with higher VCDs

During exponential phase (days 0-5), all three cell lines experienced comparable VCD and fractional viability measurements as shown in Figure 5-2A and B. However, beginning at day 8, the C1013A cell line began to die significantly faster than cell lines engineered with the anti-apoptotic gene(s) as detailed in Figure 5-2C and D. The C1013H and C1013K lines maintained mean viabilities over 70% through the completion of the experiment at day 12, whereas the control line plummeted to 52% viability by the conclusion of the experiment.

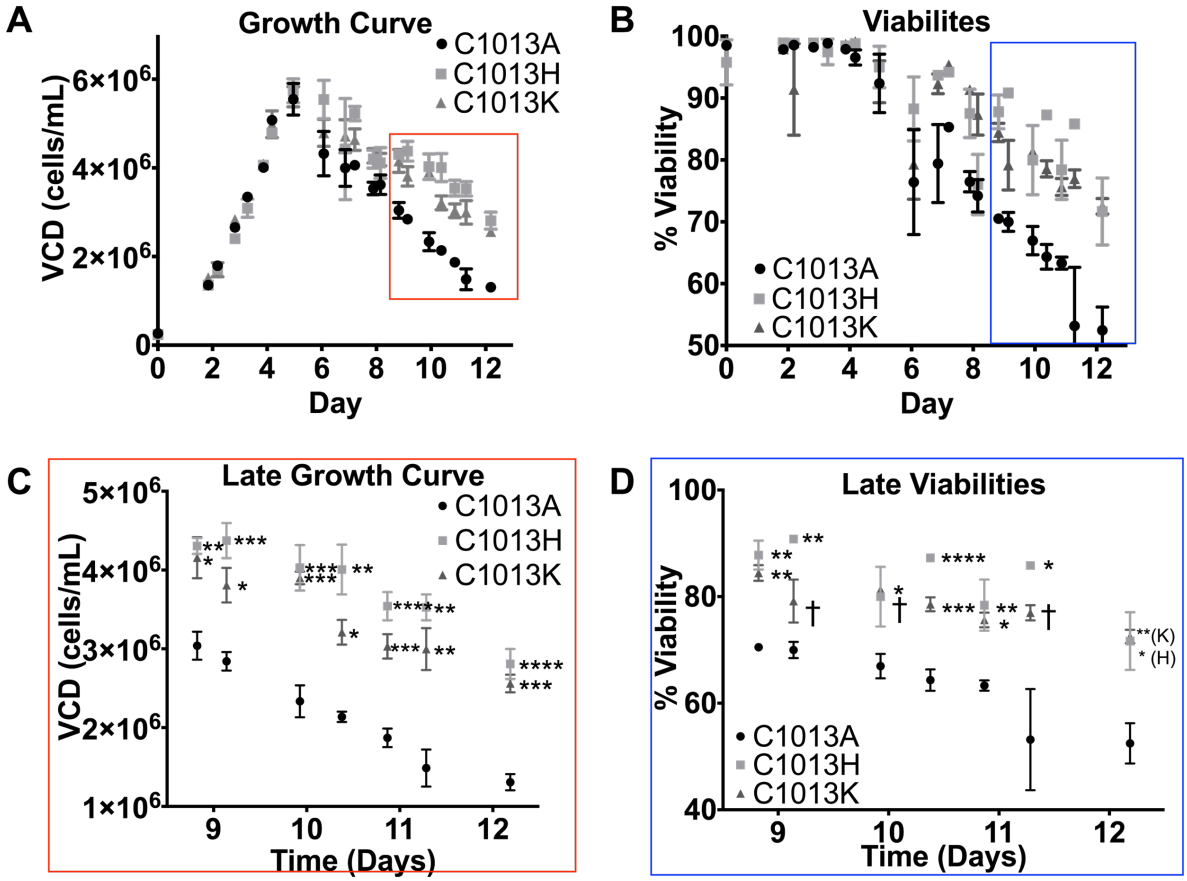

Figure 5-2 (A) Viable cell densities and (B) percent viabilities over time. (C) Zoomed in data from boxed region in (A). (D) Zoomed in data from boxed region of (B). Means ± SEM plotted, n=5. *indicates significance relative to control (C1013A) at $\alpha<0.05$, ** $\alpha<0.01$, *** $\alpha<0.001$, and **** $\alpha<0.0001$.

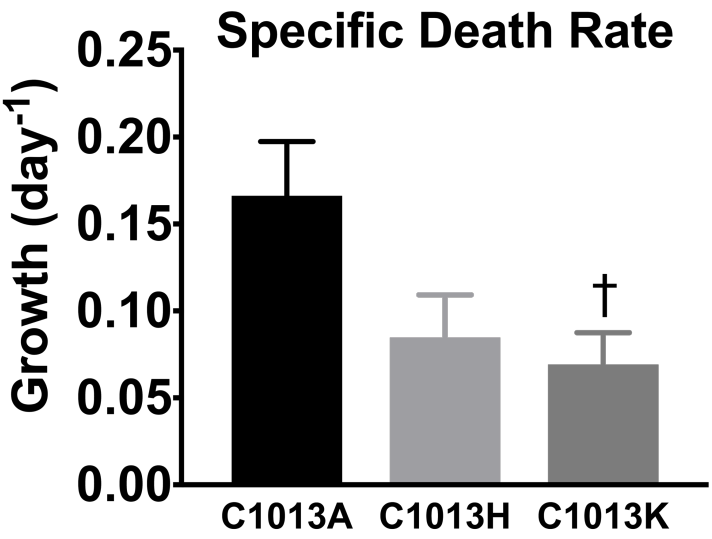

Figure 5-3 Specific death rate of the studied cell lines during stationary growth phase. Means ± SEM plotted, n=5. † indicates significance from the control (C1013A) at α<0.1.

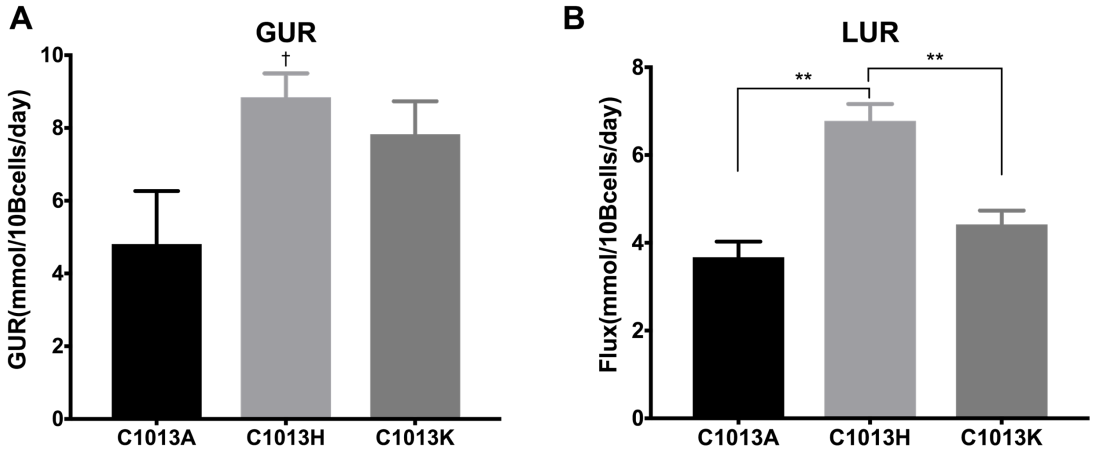

Figure 5-4 (A) Glucose and (B) lactate uptake rates of the three cell lines during stationary phase. Means ± SEM plotted, n=5. ** indicates significance at α<0.01, and † α<0.1. (Unless noted by brackets, significance relative to control (C1013A).

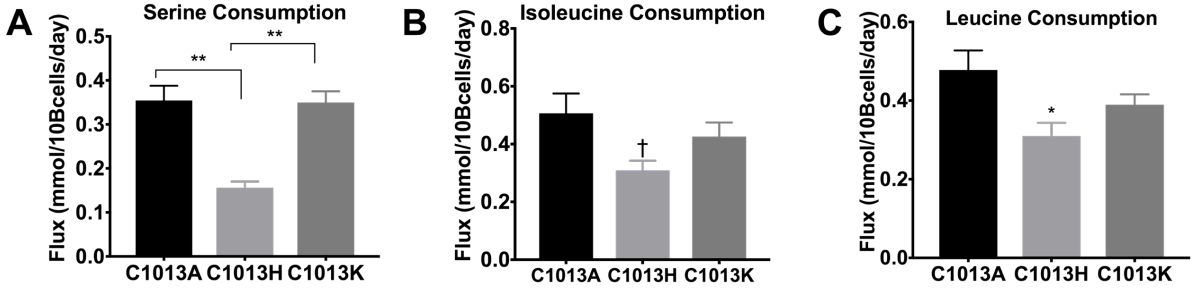

Figure 5-5 (A) Serine, (B) threonine, (C) isoleucine, and (D) leucine consumption rates. Means ± SEM plotted, n=5. * indicates significance from control (C1013A) unless indicated by brackets at α<0.05, ** α<0.01, and † α<0.1.

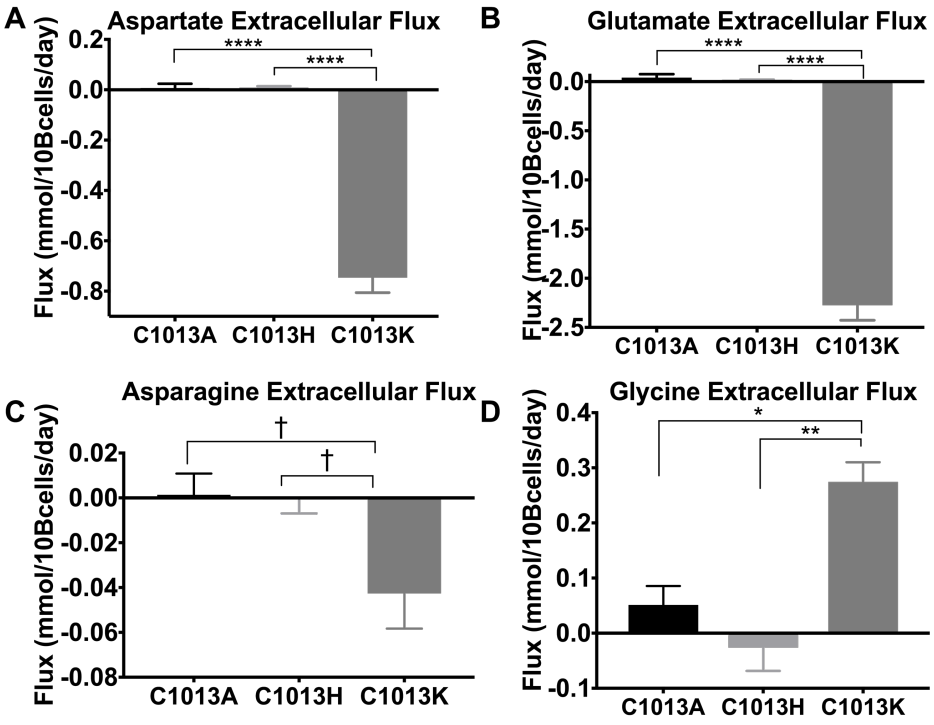

Figure 5-6(A) Aspartate, (B) glutamate, (C) asparagine, and (D) glycine extracellular fluxes. Negative flux indicates net consumption. Means ± SEM plotted, n=3. *indicates significance at $\alpha<0.05$, ** $\alpha<0.01$, **** $\alpha<0.0001$, † $\alpha<0.1$.

5.4.2 Anti-apoptotic gene overexpression altered extracellular CHO cell fluxes during stationary phase

The glucose uptake rates (GURs) trended upward in the anti-apoptotic gene expressing CHO cell lines studied (Figure 5-4A). The lactate uptake rate (LUR) was significantly increased in the Bcl-2Δ- expressing C1013H line over that of both the control (C1013A) and the triple anti-apoptotic gene overexpressing cell line, C1013K, as shown in Figure 5-4B. (Glucose and lactate profiles are reported in Figure A- 5-1.) This trend of C1013H being statistically different holds true with serine, threonine, isoleucine, and leucine extracellular fluxes as well (Figure 5-5). This trend flipped to C1013K being the statistically significant clone with aspartate, glutamate, asparagine, and glycine extracellular fluxes (Figure 5-6).

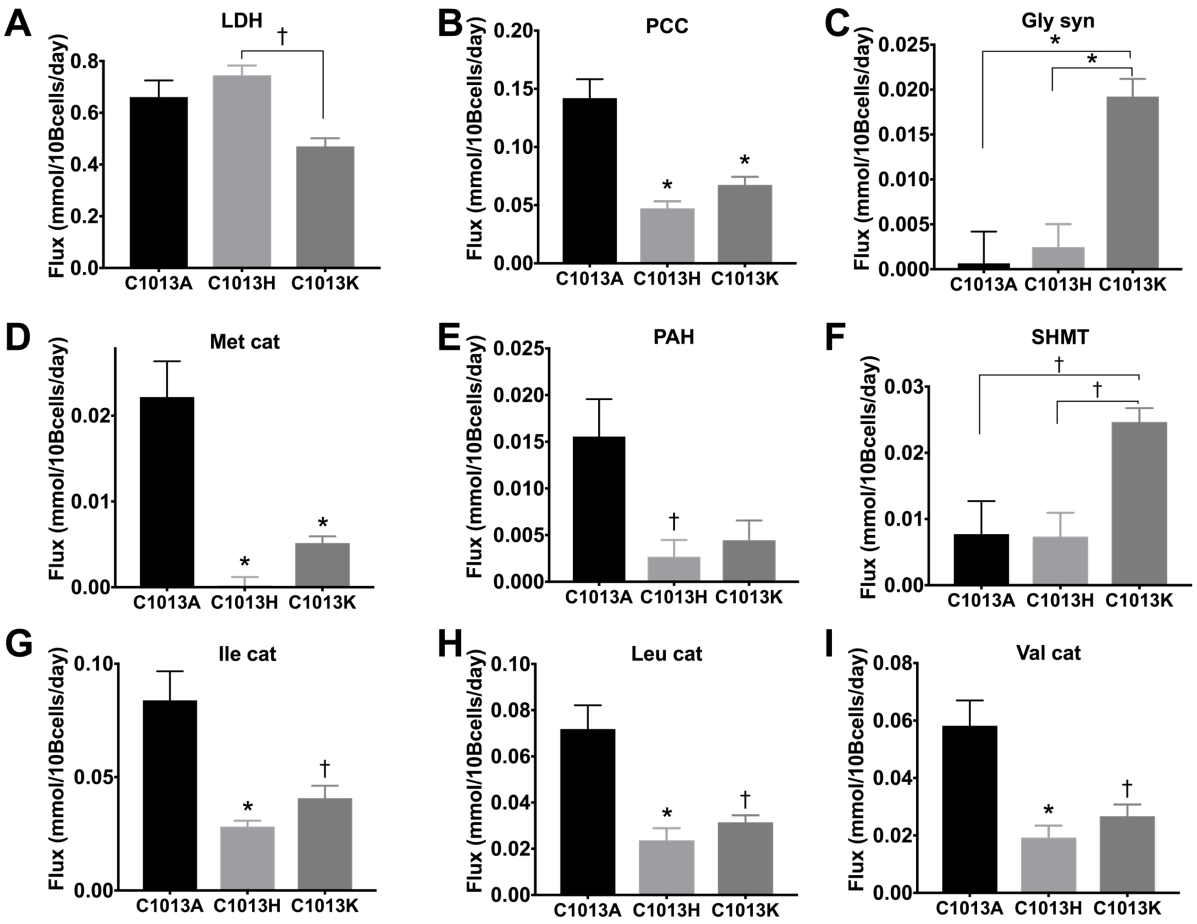

Figure 5-7 Intracellular fluxes where significant differences were calculated. (A) Lactate dehydrogenase (LDH), (B) propionyl-CoA carboxylase (PCC), (C) glycine synthase (Gly syn), (D) methionine catabolism (Met cat), (E) phenylalanine hydroxylase (PAH), (F) serine hydroxymethyl transferase (SHMT), (G) isoleucine catabolism (Ile cat), (H) leucine catabolism (Leu cat), and (I) valine catabolism (Val cat). For reaction details corresponding to each enzyme reported, see the complete flux map in Table A- 5-3. Means ± SEM plotted, n=3. * indicates significance $\alpha<0.05$ and † $\alpha<0.1$. Significance reported relative to control (C1013A) unless otherwise noted by brackets.

5.4.3 Anti-apoptotic gene overexpression led to trends in increased mitochondrial metabolism

The intracellular flux rates with statistically different fluxes are detailed in Figure 5-7. Comprehensive flux maps detailing central carbon metabolism are shown in Figure 5-8 with quantitative fluxes and 95% confidence intervals detailed in Table A- 5-3. The apoptosis-resistant C1013H and C1013K cell lines demonstrated a definite shift toward a highly oxidative metabolic phenotype with increased carbon flux through the mitochondrial TCA cycle.

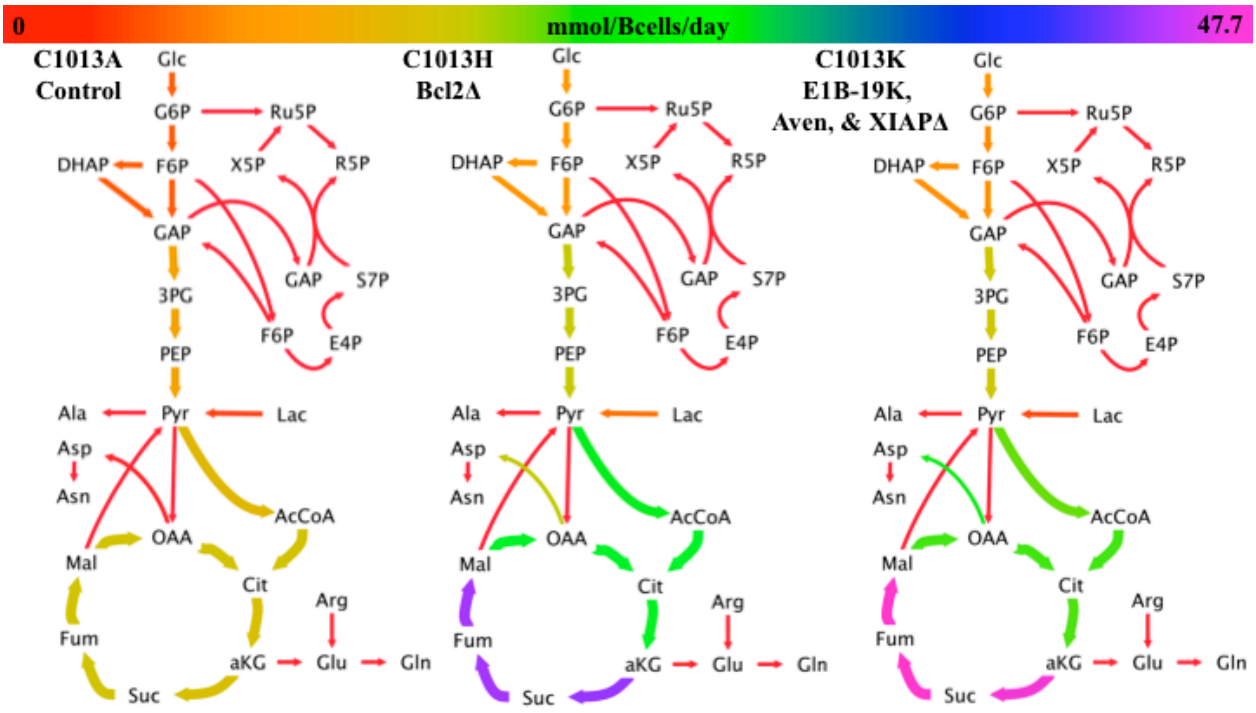

Figure 5-8 Metabolic flux maps of the apoptosis resistant clones compared to the parental. Arrow width and color corresponds to flux value.

5.5 Discussion

Anti-apoptotic genes are primarily engineered into industrial host cells to prolong cell life by inhibiting programmed cell death through a variety of biochemical mechanisms. Previous studies on apoptosis-resistant CHO cells reported sustained VCDs for longer times than parental controls and an increased reliance on lactate to fuel an upregulated oxidative mitochondrial metabolism [8,9,34]. This heavily oxidative metabolic phenotype consistently appears in high producer clones as well as apoptosis-resistant clones [9,34]. While ^{13}C MFA has been previously utilized to study Bcl2Δ CHO cells during stationary phase [9], the study presented here applied a true fed-batch isotopic labeling study to characterize apoptosis-resistant CHO cell metabolism achieved by the expression of anti-apoptotic genes.

Here, similar peak VCDs were achieved by the apoptosis-resistant clones as the control, but the engineered cell lines maintained high VCDs for a longer duration than the parental line

(Figure 5-2). Further mirroring previous work, both anti-apoptotic clones had LURs that trended higher than the control (Figure 5-4). Heavy reliance on lactate consumption is an advantageous phenotype in industrial hosts due to the elimination of the toxic byproduct from the culture. This lactate provides a direct fuel source for the increased rates of mitochondrial oxidative metabolism observed in the anti-apoptotic engineered cells.

In this study, C1013H and C1013K do not behave identically—indicating the different anti-apoptotic genes act on CHO cell metabolism in unique ways. Through a decreased reliance on serine, isoleucine, and leucine consumption (Figure 5-5) to fuel the oxidative TCA cycle, we conclude that C1013H preferentially oxidized lactate to fuel mitochondrial metabolism while C1013K preferred amino acid oxidation. C1013K cultures consumed increased amounts of aspartate, asparagine, and glutamate over C1013H and the control (Figure 5-6). These amino acids provide nitrogen and carbon for TCA cycle metabolism. Bcl-2Δ expression has reportedly increased flux through isocitrate dehydrogenase (IDH)—a rate-limiting step in the TCA cycle [9]—a finding corroborated by our findings of IDH flux trending upward in both apoptosis-resistant clones (Figure 5-8). Quantitative flux maps with 95% confidence intervals of all three studied clones are detailed in Table A- 5-3.

Taken together, these results indicate a rewiring of TCA cycle metabolism to run on alternative carbon and nitrogen sources as a result of anti-apoptotic engineering. Regardless of fuel source, both anti-apoptotic clones experience an upregulated mitochondrial metabolism (Figure 5-8), a metabolic phenotype consistent with that of high producing CHO cell clones.

The fed-batch study presented here improves upon a ^{13}C MFA study previously performed in this lab of a Bcl-2Δ expressing CHO cell line. By introducing the stable isotope tracer at the onset of stationary growth phase, we successfully eliminated secondary ^{13}C-labeled

tracers. In Templeton, et al (2014), ^{13}C substrate was introduced at the onset of the culture growth; therefore, the large amount of lactate produced during exponential growth was isotopically labeled with ^{13}C glucose as well [9]. When this ^{13}C labeled lactate was consumed by the cells in stationary phase, it introduced a secondary source of ^{13}C into cellular metabolism. Since the available analytic techniques did not allow for accurate analysis of positional ^{13}C labeling of metabolites, assumptions were required about the ^{13}C lactate labeling distribution. However, the fed-batch protocol employed by the study presented here introduced ^{13}C substrate when lactate was being net consumed. This ensured that the fed ^{13}C glucose was the single source of labeled carbon, thus eliminating the need for positional enrichment assumptions for accurate MFA. This fed-batch method was successfully implemented by Templeton, et al. (2017) in a large-scale bioreactor study of industrial Bcl-2Δ + mAb expressing CHO cell clones [34]. This large-scale study further confirmed that the highly oxidative metabolic phenotype found in apoptosis resistant CHO cell clones supports increased specific productivities [34].

5.6 Appendix

Table A- 5-1 Model goodness-of-fit assessment, where SSR is the sum of squares residual.

Model	Degrees of Freedom	SSR expected Range	Best-fit SSR
C1013A	30	16.8-47.0	41.7
C1013H	27	14.6-43.2	19.2
C1013K	35	20.6-53.2	44.2

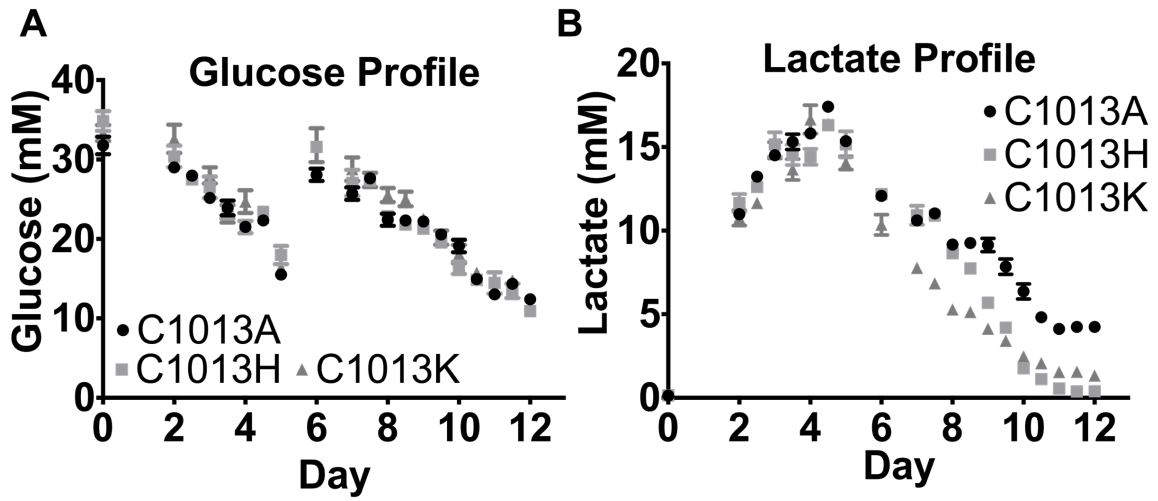

Figure A- 5-1 (A) Glucose and (B) lactate profiles.

Table A- 5-2 Precursor requirements for growth.

Metabolite	Coefficient (mmol/10Bcells/day)
Alanine	0.1974
Arginine	0.124
Asparagine	0.0948
Aspartate	0.1552
Cysteine	0.0477
Glutamine	0.1059
Glutamate	0.127
Glycine	0.2165
Histidine	0.047
Isoleucine	0.1066
Leucine	0.1856
Lysine	0.1875
Methionine	0.0454
Phenylalanine	0.0721
Proline	0.103
Serine	0.1451
Threonine	0.127
Tryptophan	0.0145
Tyrosine	0.0599
Valine	0.1369
G6P	0.0949
R5P	0.0766
MEETHF	0.0839
DHAP	0.04
CO_2	0.0766
AcCoA.c	0.8143

Table A- 5-3 Flux maps of each cell line with overall flux value in (mmol/10Bcells/day) with 95% confidence intervals reported as a lower bound (LB) and upper bound (UB) for each reported flux value.

		C1013A			C1013H			C1013K		
#	Reaction	Flux	LB	UB	Flux	LB	UB	Flux	LB	UB
1	Glc.e → Glc	5.4699	3.5972	7.9812	9.02	7.7575	10.2875	8.958	7.4537	10.5417
2	Glc → G6P	5.4699	3.5972	7.9812	9.02	7.7575	10.2875	8.958	7.4537	10.5417
3	G6P ↔ F6P	3.6456	-0.477	7.1211	8.6512	-1.9419	10.2345	7.923	3.8633	10.2775
4	F6P → DHAP + GAP	4.8092	2.8719	7.3569	8.8373	5.4299	10.2076	8.5467	6.7938	10.2556
5	DHAP ↔ GAP	4.7907	0.1431	7.3381	8.8165	1.2211	10.1883	8.5236	5.8598	10.2324
6	DHAP → GLP	1.00E-07	0	6.1462	1.00E-07	0	7.4841	1.00E-07	0	2.8241
7	GAP ↔ 3PG	10.1817	6.0605	15.1226	17.7469	10.1017	20.3843	17.3822	14.2523	20.4806
8	3PG ↔ 2PG	7.3721	3.2113	11.6759	16.7296	8.2974	19.7817	15.199	12.2105	18.148
9	2PG ↔ PEP	10.3058	6.1892	15.2477	17.747	9.7464	20.3916	17.3807	13.7417	20.4817
11	3PG + Glu → Ser + aKG	1.8658	0	8.3618	0.472	0	9.9516	1.0949	0	4.473
12	PEP → Pyr	10.3058	6.1892	15.2477	17.747	9.7464	20.3916	17.3807	13.7417	20.4817
13	Lac ↔ Pyr	3.6147	2.9234	4.3053	6.7148	6.0711	7.4157	4.2084	3.717	4.8254
10	Ser + Pyr → 2PG + Ala	2.9337	0	8.4835	1.0173	0	9.9635	2.1818	0	4.4692
14	Pyr → AcCoA.m + CO2	1.922	0.2209	4.3055	6.224	0	8.803	5.022	2.0735	7.5321
15	OAA.m + AcCoA.m → Cit	4.0327	2.3724	6.4094	7.3021	0.9932	9.8814	6.4041	3.4573	8.9178
16	Cit → aKG + CO2	3.6579	1.9941	6.0529	6.877	0.5252	9.5541	5.9322	2.985	8.4581
17	aKG → Suc + CO2	3.6087	0.2272	7.3271	5.0506	0	18.8177	4.9201	0	11.7633
18	Suc ↔ Fum	4.5068	1.1176	8.2337	5.4774	0.3456	19.2481	5.5701	0.6027	12.4147
19	Fum ↔ Mal	4.5068	1.1176	8.2337	5.4774	0.3456	19.2481	5.5701	0.6027	12.4147
20	Mal ↔ OAA.c	12.4438	5.9495	19.6451	16.9973	6.5524	40.2712	16.3523	7.2549	28.3495
21	Mal ↔ OAA.m	-7.8091	-12.9896	-4.1674	-11.4781	-28.6811	-6.0907	-10.7202	-16.3277	-6.4606
22	G6P → Ru5P + CO2	1.7806	0	6.2447	0.3193	0	11.0227	0.9801	0	5.4938
23	Ru5P ↔ X5P	1.1636	-0.0338	4.1406	0.1862	-0.04	7.3256	0.6238	-0.0335	3.6325
24	Ru5P ↔ R5P	0.617	0.0137	2.1041	0.1331	0.0054	3.5376	0.3563	0.0233	1.8582
25	X5P + R5P ↔ GAP + S7P	0.5818	-0.0169	2.0703	0.0931	-0.02	3.6628	0.3119	-0.0167	1.8162
26	S7P + GAP ↔ E4P + F6P	0.5818	-0.0169	2.0703	0.0931	-0.02	3.6628	0.3119	-0.0167	1.8162
27	X5P + E4P ↔ GAP + F6P	0.5818	-0.0169	2.0703	0.0931	-0.02	3.6628	0.3119	-0.0167	1.8162
28	Mal → Pyr + CO2	1.00E-07	0	3.9509	1.00E-07	0	16.4422	1.00E-07	0	1.5054
29	Pyr + CO2 → OAA.m	11.8418	8.312	17.5908	18.7802	12.7592	35.6727	17.1243	13.7976	20.6601
30	Cit → AcCoA.c + OAA.c	0.3748	0.1471	0.6062	0.4251	0.0853	0.6387	0.4718	0.3648	0.5371
31	Asp ↔ Asn	0.045	0.0126	0.0777	0.0493	0.0079	0.0785	0.0123	-0.0194	0.044
32	ProCoA + CO2 → Suc	0.7768	0.6027	0.9503	0.4259	0.3298	0.5438	0.6038	0.4828	0.7249
33	Gln ↔ Glu	-0.0377	-0.0883	0.0124	-0.0992	-0.1397	-0.0487	-0.0879	-0.1134	-0.0623
34	Glu ↔ Pro	-2.06E-15	-4.718	5.1276	1.654	-16.6765	9.4367	3.1815	-5.9856	10.4453
35	CO2 + MEETHF ↔ Gly	0.0036	-0.0335	0.0422	0.0221	-0.024	0.0669	0.1721	0.1382	0.2077
36	His → FormTHF + Glu	0.0285	0.0023	0.0545	1.00E-07	0	0.0196	0.0244	0	0.0801
37	Met + Ser → Methyl + Cys + Suc	0.1213	0.0766	0.1661	8.11E-04	0	0.0385	0.0461	0.0324	0.06
38	Phe → Tyr	0.0851	0.042	0.1279	0.0239	0	0.0647	0.0397	0.0019	0.077
39	Ser ↔ Gly + MEETHF	0.0422	-0.0103	0.0966	0.0659	-0.0036	0.1247	0.2207	0.1837	0.2579
40	Thr → Pyr + CO2	0.1549	0	0.3197	1.00E-07	0	3.8379	0.0895	0	0.1906
41	Trp → CO2 + CO2 + Ala + aKetoadi	0.0464	0.0223	0.0705	0.0271	0.0042	0.0499	0.0238	0.0029	0.0449
42	aKetoadi → CO2 + CO2 + AcCoA.m + AcCoA.m	0.1088	0.0338	0.1836	0.0513	0.0045	0.1454	0.0238	0.0029	0.0579
43	aKG ↔ Glu	11.5735	8.0939	16.5824	17.9904	12.0097	26.0774	16.3869	13.1664	20.9853
44	Ala + aKG ↔ Pyr + Glu	2.5354	-0.4521	8.0993	1.5464	0.1314	10.4945	2.6494	-0.0041	4.9514
45	Ile + aKG → AcCoA.m + CO2 + ProCoA + Glu	0.4586	0.3211	0.596	0.2531	0.2102	0.3052	0.3645	0.2678	0.4612
46	Leu + aKG + CO2 → CO2 + AcCoA.m + AcCoA.m + AcCoA.m + Glu	0.3929	0.282	0.5024	0.2129	0.1252	0.3123	0.2819	0.2277	0.3349
47	Tyr + aKG → CO2 + Mal + AcCoA.m + AcCoA.m + Glu	0.128	0.0695	0.1859	0.0418	0	0.1056	0.0621	0.0215	0.1026
48	Val + aKG → Glu + CO2 + CO2 + ProCoA	0.3182	0.2232	0.4129	0.1728	0.1012	0.2513	0.2393	0.1678	0.3109
49	Lys + aKG + aKG → Glu + Glu + aKetoadi	0.0625	0	0.1301	0.0243	0	0.1105	1.00E-07	0	0.0268
50	OAA.c + Glu ↔ Asp + aKG	12.8186	6.3444	20.0009	17.4224	7.0004	40.5576	16.8242	7.7249	28.8187
51	Arg + aKG → Glu + Urea + Glu	0.0593	0	0.1291	1.00E-07	0	0.083	0.0354	0	0.1521
52	3PG + Glu → Ser + aKG	0.9439	0	8.3609	0.5452	0	9.9551	1.0883	0	4.4722
53	Cys + aKG → Pyr + Glu	0.0867	0.0313	0.1421	1.00E-07	0	0.1078	1.00E-07	0	0.0212
54	Ser → Pyr	1.00E-07	0	2.6626	0.0134	0	6.3104	1.00E-07	0	2.719
55	Lys.e → Lys	0.1488	0.1059	0.1917	0.1222	0.0841	0.1611	0.1086	0.0937	0.1236
56	Thr.e → Thr	0.2133	0.0536	0.3742	0.0663	0.0133	3.9034	0.1631	0.0691	0.2636
57	Phe.e → Phe	0.1183	0.0805	0.1561	0.0615	0.033	0.0905	0.0815	0.0441	0.1189
58	Tyr.e → Tyr	0.0705	0.0465	0.0945	0.0492	0.0308	0.0676	0.0571	0.0453	0.0689
59	Val.e → Val	0.3812	0.2946	0.4682	0.2442	0.1873	0.3011	0.3187	0.248	0.3894
60	Leu.e → Leu	0.4783	0.3809	0.5758	0.3097	0.2436	0.3759	0.3895	0.3373	0.4417
61	Ile.e → Ile	0.5076	0.3735	0.6417	0.3088	0.2798	0.3378	0.4263	0.33	0.5226
62	Trp.e → Trp	0.053	0.0293	0.0768	0.0346	0.0124	0.0569	0.0323	0.0115	0.0532
63	His.e → His	0.0501	0.0277	0.0727	0.0245	0.0054	0.0435	0.0516	0.0222	0.1072
64	Met.e → Met	0.1422	0.0994	0.1851	0.0245	0.007	0.0587	0.0725	0.0585	0.0868
65	Ser.e ↔ Ser	0.3544	0.2888	0.4199	0.1559	0.1279	0.1839	0.3495	0.2998	0.3994
66	Ala ↔ Ala.e	0.3538	-0.0641	0.7708	-0.6051	-0.9997	-0.229	-0.5581	-1.2692	-0.0131
67	Arg.e ↔ Arg	0.1164	0.0559	0.177	0.0647	0.0187	0.1359	0.1073	0.0575	0.2235
68	Asp ↔ Asp.e	12.7022	6.2172	19.8887	17.2921	6.8654	40.54	16.7219	7.625	28.7182
69	Cys.e ↔ Cys	-0.0126	-0.0361	0.0109	0.0241	-0.0246	0.1269	-0.0185	-0.0337	7.54E-05
70	Glu ↔ Glu.e	0.0409	-0.0276	0.1096	0.0068	-0.014	0.0275	-2.271	-2.5701	-1.976
71	Gln.e ↔ Gln	0.011	0	0.0517	-0.0439	-0.07	-0.0178	-0.0265	-0.0506	-0.0024
72	Gly.e ↔ Gly	0.0538	-0.0135	0.1189	0.0251	-0.0528	0.105	-0.2674	-0.3377	-0.2002
73	Pro.e ↔ Pro	0.0474	-5.0827	4.7653	-1.6003	-9.4027	16.7293	-3.1218	-10.3853	6.0453
74	Asn.e ↔ Asn	-0.0013	-0.02	0.0173	2.08E-04	-0.013	0.0134	0.0426	0.0119	0.0734
75	Lac ↔ Lac.e	-3.6147	-4.3053	-2.9234	-6.7148	-7.4157	-6.0711	-4.2084	-4.8254	-3.717
76	Biomass production	0.4603	0.1806	0.7445	0.522	0.1048	0.7844	0.5795	0.448	0.6596

Table A- 5-4 Metabolite fragments measured by GC-MS for analysis of intracellular metabolite labeling.

Metabolite	Mass	Carbon atoms	Fragment formula
Lactate	233	2 3	$C_{10}H_{25}O_2Si_2$
Lactate	261	1 2 3	$C_{11}H_{25}O_3Si_2$
Alanine	232	2 3	$C_{10}H_{26}O_2NSi_2$
Alanine	260	1 2 3	$C_{11}H_{26}O_2NSi_2$
Serine	288	2 3	$C_{12}H_{34}ONSi_2$
Serine	302	1 2	$C_{12}H_{32}O_2NSi_2$
Serine	362	2 3	$C_{14}H_{40}O_2NSi_3$
Serine	390	1 2 3	$C_{17}H_{40}O_3NSi_3$
Malate	419	1 2 3 4	$C_{18}H_{39}O_5Si_3$
Glycine	218	2	$C_8H_{24}O_2NSi_2$
Glycine	246	1 2	$C_{10}H_{24}O_2NSi_2$
Glycerol 3 phosphate	571	1 2 3	$C_{20}H_{56}O_6Si_4P$

5.7 References

[1] Walsh G. Biopharmaceutical benchmarks 2010. Nat Biotechnol 2010;28:1–10. doi:10.1038/nbt.3040.

[2] Templeton N, Dean J, Reddy P, Young JD. Peak antibody production is associated with increased oxidative metabolism in an industrially relevant fed-batch CHO cell culture. Biotechnol Bioeng 2013;110:2013–24. doi:10.1002/bit.24858.

[3] Lao MS, Toth D. Effects of ammonium and lactate on growth and metabolism of a recombinant Chinese hamster ovary cell culture. Biotechnol Prog 1997;13:688–91. doi:10.1021/bp9602360.

[4] McAtee AG, Templeton N, Young JD. Role of Chinese hamster ovary central carbon metabolism in controlling the quality of secreted biotherapeutic proteins. Pharm Bioprocess 2014;2:63–74.

[5] Wurm FM. Production of recombinant protein therapeutics in cultivated mammalian cells. Nat Biotechnol 2004;22:1393–8. doi:10.1038/nbt1026.

[6] Young JD. Metabolic flux rewiring in mammalian cell cultures. Curr Opin Biotechnol 2013;24:1–8. doi:10.1016/j.copbio.2013.04.016.

[7] Paredes C, Prats E, Cairó JJ, Azorín F, Cornudella L, Gòdia F. Modification of glucose and glutamine metabolism in hybridoma cells through metabolic engineering. Cytotechnology 1999;30:85–93. doi:10.1023/A:1008012518961.

[8] Dorai H, Kyung YS, Ellis D, Kinney C, Lin C, Jan D, et al. Expression of anti-apoptosis genes alters lactate metabolism of Chinese Hamster Ovary cells in culture. Biotechnol Bioeng 2009;103:592–608. doi:10.1002/bit.22269.

[9] Templeton N, Lewis A, Dorai H, Qian E a, Campbell MP, Smith KD, et al. The impact of

anti-apoptotic gene Bcl-2Δ expression on CHO central metabolism. Metab Eng 2014;25:92–102. doi:10.1016/j.ymben.2014.06.010.

[10] Zhou M, Crawford Y, Ng D, Tung J, Pynn AFJ, Meier A, et al. Decreasing lactate level and increasing antibody production in Chinese Hamster Ovary cells (CHO) by reducing the expression of lactate dehydrogenase and pyruvate dehydrogenase kinases. J Biotechnol 2011;153:27–34. doi:10.1016/j.jbiotec.2011.03.003.

[11] Zagari F, Stettler M, Broly H, Wurm M, Jordan M. High expression of the aspartate–glutamate carrier Aralar1 favors lactate consumption in CHO cell culture. Pharm Bioprocess 2013;1:19–27.

[12] Majors BS, Betenbaugh MJ, Chiang GG. Links between metabolism and apoptosis in mammalian cells: Applications for anti-apoptosis engineering. Metab Eng 2007;9:317–26. doi:10.1016/j.ymben.2007.05.003.

[13] Arden N, Betenbaugh MJ. Life and death in mammalian cell culture: Strategies for apoptosis inhibition. Trends Biotechnol 2004;22:174–80. doi:10.1016/j.tibtech.2004.02.004.

[14] Dorai H, Ellis D, Keung YS, Campbell M, Zhuang M, Lin C, et al. Combining high-throughput screening of caspase activity with anti-apoptosis genes for development of robust CHO production cell lines. Biotechnol Prog 2010;26:1367–81. doi:10.1002/btpr.426.

[15] Altamirano C, Paredes C, Illanes a, Cairó JJ, Gòdia F. Strategies for fed-batch cultivation of t-PA producing CHO cells: substitution of glucose and glutamine and rational design of culture medium. J Biotechnol 2004;110:171–9. doi:10.1016/j.jbiotec.2004.02.004.

[16] Goswami J, Sinskey AJ, Steller H, Stephanopoulos GN, Wang DIC. Apoptosis in Batch

Cultures of Chinese Hamster Ovary Cells. Biotechnol Bioeng 1999;62:632–40. doi:10.1002/(SICI)1097-0290(19990320)62:6<632::AID-BIT2>3.0.CO;2-I.

[17] Hanada M, Aime-Sempe C, Sato T, Reed JC. Structure-function analysis of Bcl-2 protein. Identification of conserved domains important for homodimerization with Bcl-2 and heterodimerization with bax. J Biol Chem 1995;270:11962–9. doi:10.1074/jbc.270.20.11962.

[18] Dietmair S, Nielsen LK, Timmins NE. Engineering a mammalian super producer. J Chem Technol Biotechnol 2011;86:905–14. doi:10.1002/jctb.2576.

[19] Figueroa B, Sauerwald TM, Mastrangelo AJ, Hardwick JM, Betenbaugh MJ. Comparison of Bcl-2 to a Bcl-2 deletion mutant for mammalian cells exposed to culture insults. Biotechnol Bioeng 2001;73:211–22. doi:10.1002/bit.1053.

[20] Han J, Sabbatini P, Perez D, Rao L, Modha D, White E. The E1B 19K protein blocks apoptosis by interacting with and inhibiting the p53-inducible and death-promoting Bax protein. Genes Dev 1996;10:461–77. doi:10.1101/gad.10.4.461.

[21] Figueroa Jr B, Ailor E, Osborne D, Hardwick JM, Reff M, Betenbaugh MJ. Enhanced Cell Culture Performance Using Inducible Anti-Apoptotic Genes E1B-19K and Aven in the Production of a Monoclonal Antibody With Chinese Hamster Ovary Cells. Biotechnol Bioeng 2007;97:877–92. doi:10.1002/bit.

[22] Chau BN, Cheng EHY, Kerr DA, Hardwick JM. Aven, a novel inhibitor of caspase activation, binds Bcl-x(L) and Apaf-1. Mol Cell 2000;6:31–40. doi:10.1016/S1097-2765(05)00021-3.

[23] Sauerwald TM, Betenbaugh MJ, Oyler GA. Inhibiting apoptosis in mammalian cell culture using the caspase inhibitor XIAP and deletion mutants. Biotechnol Bioeng

2002;77:704–16. doi:10.1002/bit.10154.

[24] Figueroa B, Chen S, Oyler GA, Hardwick JM, Betenbaugh MJ. Aven and Bcl-xL Enhance Protection Against Apoptosis for Mammalian Cells Exposed to Various Culture Conditions. Biotechnol Bioeng 2004;85:589–600. doi:10.1002/bit.10913.

[25] McAtee AG, Jazmin LJ, Young JD. Application of isotope labeling experiments and 13C flux analysis to enable rational pathway engineering. Curr Opin Biotechnol 2015;36:50–6. doi:10.1016/j.copbio.2015.08.004.

[26] Sellick C a, Hansen R, Maqsood AR, Dunn WB, Stephens GM, Goodacre R, et al. Effective quenching processes for physiologically valid metabolite profiling of suspension cultured Mammalian cells. Anal Chem 2009;81:174–83. doi:10.1021/ac8016899.

[27] Folch J, Lees M, Sloane Stanley GHH. A simple method for the isolation and purification of total lipides from animal tissues. J Biol Chem 1957;226:497–509. doi:10.1016/j.ultrasmedbio.2011.03.005.

[28] Hasenour CM, Wall ML, Ridley DE, Hughey CC, James FD, Wasserman DH, et al. Mass spectrometry-based microassay of ^{2}H and ^{13}C plasma glucose labeling to quantify liver metabolic fluxes in vivo. Am J Physiol - Endocrinol Metab 2015;309:E191–203. doi:10.1152/ajpendo.00003.2015.

[29] Antoniewicz MR, Kelleher JK, Stephanopoulos G. Elementary metabolite units (EMU): a novel framework for modeling isotopic distributions. Metab Eng 2007;9:68–86. doi:10.1016/j.ymben.2006.09.001.

[30] Young JD, Walther JL, Antoniewicz MR, Yoo H. An Elementary Metabolite Unit (EMU) Based Method of Isotopically Nonstationary Flux Analysis. Biotechnol Bioeng 2008;99:686–99. doi:10.1002/bit.

[31] Brunengraber H, Kelleher JK, Des Rosiers C. Applications of Mass Isotopomer Analysisto Nutrition Research. Annu Rev Nutr 1997;17:559–96. doi:10.1146/annurev.nutr.17.1.559.

[32] Murphy TA, Young JD. ETA: robust software for determination of cell specific rates from extracellular time courses. Biotechnol Bioeng 2013;110:1748–58. doi:10.1002/bit.24836.

[33] Antoniewicz MR, Kelleher JK, Stephanopoulos G. Determination of confidence intervals of metabolic fluxes estimated from stable isotope measurements. Metab Eng 2006;8:324–37. doi:10.1016/j.ymben.2006.01.004.

[34] Templeton N, Smith KD, McAtee-Pereira AG, Dorai H, Betenbaugh MJ, Lang SE, et al. Application of 13C flux analysis to identify high-productivity CHO metabolic phenotypes. Metab Eng 2017;29:53–62. doi:10.1016/j.ymben.2017.01.008.

6 ^{13}C FLUX ANALYSIS IN DETERMINING OXIDATIVE PENTOSE PHOSPHATE PATHWAY ACTIVITY IN INDUSTRIAL CHINESE HAMSTER OVARY (CHO) CELL LINES

6.1 Summary

Monoclonal antibody (mAb) protein therapeutics are used to treat a variety of diseases including cancer. Chinese hamster ovary (CHO) cells are the most commonly utilized host cell for mAb biomanufacturing. Light and heavy chains of mAbs are linked by disulfide (DS) bonds. The therapeutic efficacy of mAbs is highly dependent upon the maintenance of their three-dimensional configurations. In this study, ^{13}C metabolic flux analysis (MFA), a rigorous quantitative approach for intracellular metabolic flux elucidation, was used to study two CHO cell lines producing a mAb product. Cell line A produced mAb product with reduced DS bonds while B produced intact mAb product. Previous studies have linked an active thioredoxin (Trx) system in cell culture medium with DS reduction. The Trx system is fueled by the reductant NADPH produced by the oxidative pentose phosphate pathway (OPPP) and other pathways. Our ^{13}C study of the metabolic byproduct, lactate, revealed that both cell lines have statistically equivalent rates of OPPP flux utilization. Therefore, any DS bond reduction was not fueled by an increased intracellular OPPP metabolism.

6.2 Background and Introduction

The pharmaceutical industry commonly relies on mammalian host cells, predominantly Chinese hamster ovary (CHO) cells, to produce biotherapeutic drugs such as monoclonal antibodies (mAbs) often used for the treatment of cancer and immunological disorders [1]. Maintaining protein conformation is imperative in industrial production as a compromised physical protein structure leads to decreased or destroyed efficacy. When the proteins lose their

proper three-dimensional conformation in the media, it is costly to perform the required downstream processing necessary to gather and produce product with proper efficacy.

CHO cell central carbon metabolism has previously been shown to impact disulfide (DS) bonds, and therefore, mAb quality [2]. Inter-chain DS bonds are mainly responsible for bonding together the light and heavy chains of an antibody, forming its functional three-dimensional structure [3–6]. These DS bonds are formed in the oxidizing environment of the endoplasmic reticulum of the cells and are responsible for structural stability. Cell lysing can release intracellular enzymatic systems during downstream mechanical harvesting causing a significant DS bond reduction event [4–6]. DS bond reductions cause proteins to dissociate and lose their functionality, rendering them therapeutically useless. This reduction process is not specific to one particular product protein or class of product proteins and it can occur during both manufacturing-scale and laboratory-scale production runs [5,6].

DS bonds are formed from the oxidation of the thiol side groups of two cysteine residues. Re-oxidizing the reduced proteins downstream is difficult to control and may cause unwanted oxidation of other amino acid residues in the extracellular media, further compromising protein quality [5]. Previous studies have determined that an active thioredoxin (Trx) system is often present in reducing cell culture medium [2,6]. An active Trx system consists of Trx, thioredoxin reductase (TrxR), and NADPH operating as shown in **Error! Reference source not found.**[4,6,7]. It is thought that the NADPH required for the Trx system to function properly is provided through the conversion of $NADP^+$ and glucose-6-phosphate (G6P) via the G6P dehydrogenase (G6PD) enzyme to form NADPH and 6-phosphoglucono-lactone. G6PDH is located in the oxidative pentose phosphate pathway (OPPP) of intact cells [4].

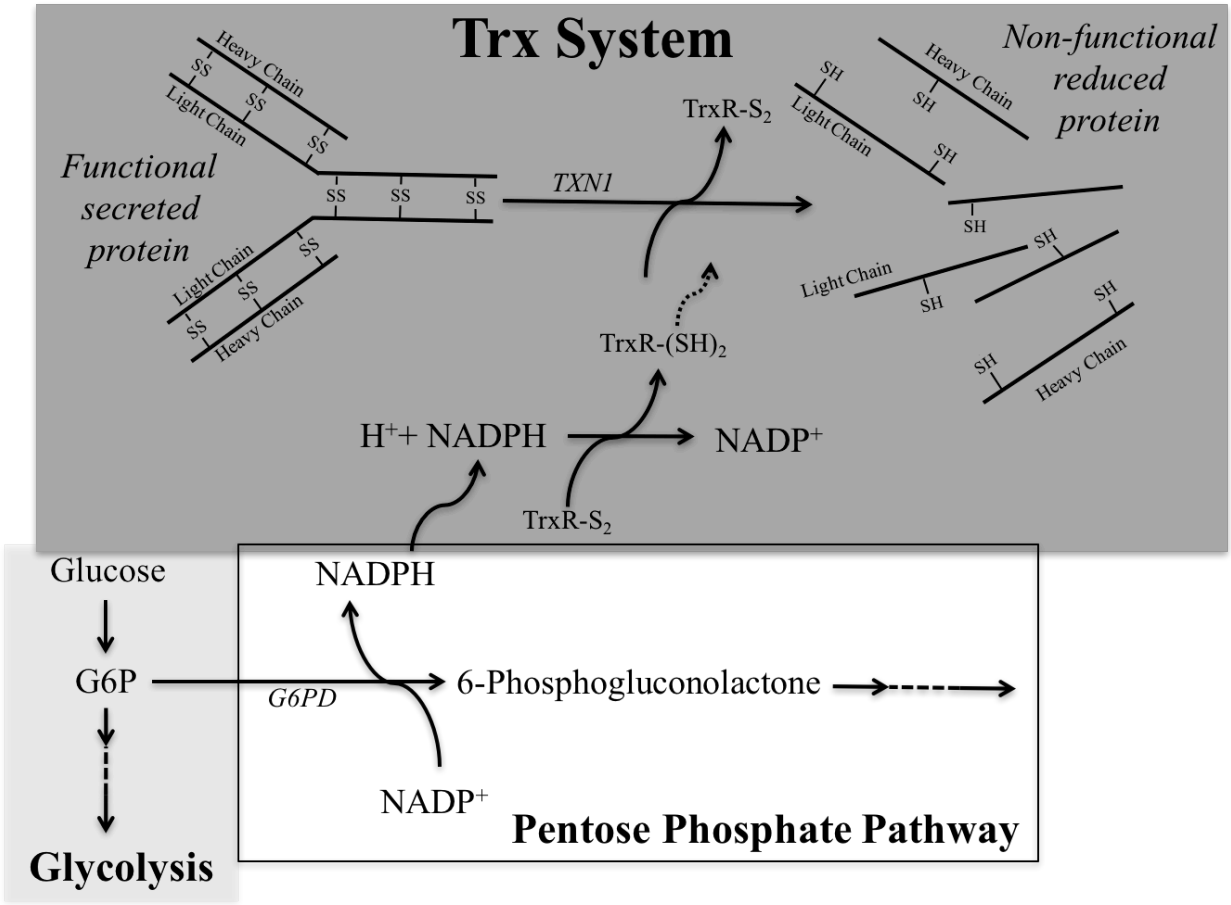

Figure 6-1 The Thioredoxin (Trx) system is responsible for the disulfide (DS) bond reduction mechanismthat can occur in the harvested cell medium. The NADPH that initiates the Trx system is created from the first steps of glycolysis and the pentose phosphate pathway. Thioredoxin reductase (TrxR) reduces Trx using that NADPH. The reduced Trx then reduces the DS bonds of the protein. The terminal enzyme has been identified as mammalian thioredoxin 1 (TXN1).

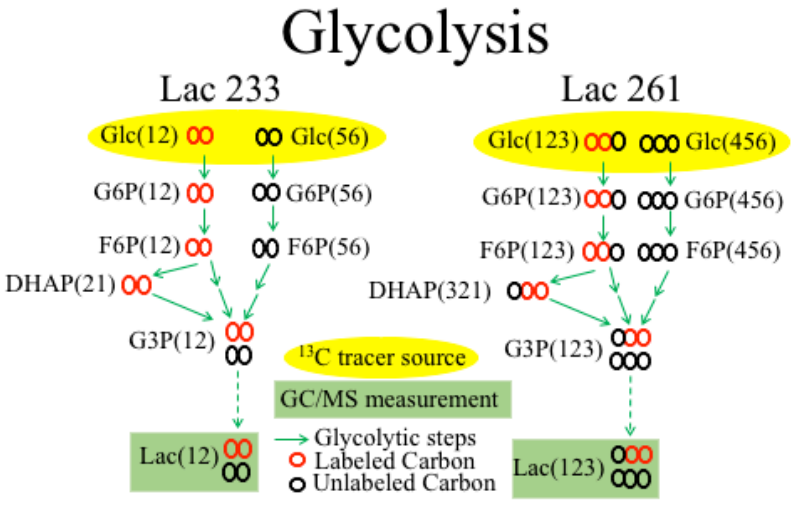

Figure 6-2 Carbon rearrangement of each lactate fragment as analyzed by GC/MS if a [1,2-$^{13}C_2$]Glucose molecule is metabolized through glycolysis. Dashed lines indicate intermediate reactions not shown.

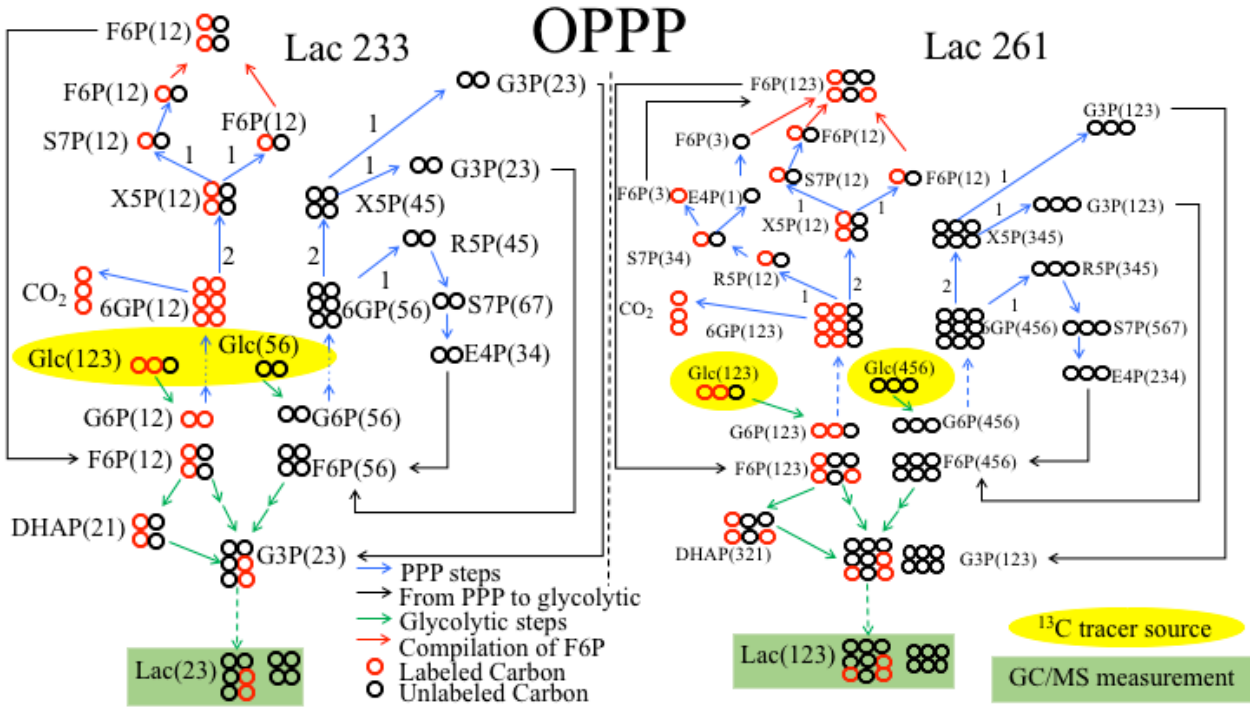

Figure 6-3 Carbon rearrangement of lactate fragments as analyzed by GC/MS if a [1,2-$^{13}C_2$]Glucose molecule was metabolized through the OPPP. Dashed lines indicate intermediate reactions not shown. A 1 or 2 on an arrow indicates number of molecules shunted down that reaction.

^{13}C MFA allowed us to determine the fraction of [1,2-$^{13}C_2$] glucose metabolized by the OPPP. When derivatized and analyzed via gas chromatography-mass spectroscopy (GC-MS) as described in the Materials and Methods section, lactate produces two unique ions with masses of 233 and 261. Lactate 233 only contains two of the three carbons contained in lactate's carbon backbone. When lactate is produced from glucose via the OPPP, it undergoes the carbon rearrangements shown in Figure 6-3. Since the first carbon of glucose exits the cell as CO_2 during the first enzymatic step of the OPPP, when the labeled carbon is metabolized to become lactate, only one labeled carbon from each glucose remains. Therefore, if the lactate was produced via OPPP metabolism, the lactate will be singly labeled (M1) in the lactate 233 fragment ion (Figure 6-3). However, if a lactate molecule is produced from glucose metabolized

through glycolysis, it undergoes no carbon loss or rearrangements as shown in Figure 6-2. If the lactate was produced through glycolysis, the lactate will have zero (M0) or two labeled carbons (M2) since there is no carbon loss or rearrangement in glycolysis that would lead to another arrangement of carbon in either lactate fragment (Figure 6-2). These unique labeling patterns produced by the two unique mass fragments of lactate generate enough information to determine the ratio of OPPP to glycolytic metabolism occurring in CHO cells by analyzing the ratio of M1/M2 lactate found in the two cell lines. From this analysis, we determined from our ^{13}C MFA study that neither cell line had a significantly higher rate of OPPP metabolism. Therefore, the reduction events occurring in the mAb were not due to NADPH produced via intracellular OPPP.

This study examines two mAb-producing proprietary CHO cell lines, denoted A and B, used by Genentech for the production of biotherapeutic mAbs. Cell line A produced a product that did not properly maintain DS bond integrity after secretion. Genentech scientists hypothesized that cell line A experienced higher production of NADPH via OPPP metabolism. We employed ^{13}C metabolic flux analysis (MFA) to quantify the fraction of glucose metabolized via glycolysis and OPPP in each cell line. Ultimately, we determined that the cell lines had similar levels of OPPP activity, therefore, DS bond reduction was not due to a difference in OPPP-generated NADPH.

6.3 Materials and Methods

6.3.1 Cell Culture

Two mAb-producing CHO cell lines (A and B) were cultivated in duplicate 25 mL shake flasks at 37°C by Genentech scientists on site. Each cell line was grown in duplicate for 12 days and fed at days zero and three. 100% [1,2-$^{13}C_2$] glucose was added to glucose-free media for seeding on day zero and feeding on day three of fed-batch cultivation of both cell lines.

6.3.2 Analytical techniques

Cell culture samples (1 mL) were collected on days 0, 3 (before feed), 3.5 (after feed), 7, 9, 11, and 12 for viable cell density (VCD), percent viability, pH, glucose, glutamate, and lactate concentrations to monitor culture health and extracellular metabolism. Supernatant aliquots were collected on days 1, 2, 3, 3.5, 4, 6, 8, 10, and 12 for ^{13}C labeling analysis of lactate. The supernatant samples were immediately frozen at -80°C and shipped on dry ice to Vanderbilt University for testing at the conclusion of the experiment. Upon receipt of the samples at Vanderbilt University, the extracellular media samples were deproteinated using acetone as previously described [8]. Once the ^{13}C-labeled extracellular metabolites were deproteinated, they were dried overnight and derivatized via methoxamine (MOX) and tert-butyldimethylsilyl (TBDMS) reagents for analysis via gas chromatography-mass spectrometry (GC/MS) [9]. Spent media from comparable cells grown in the absence of ^{13}C tracer were harvested from a previous experiment to use as unlabeled controls for the MFA analysis.

6.3.3 ^{13}C Metabolic flux analysis

^{13}C MFA was performed at each time point where ^{13}C labeled supernatant samples were collected throughout the experiment in order to track the distribution of glucose carbons entering or bypassing the OPPP over the course of the experiment. The ^{13}C isotope labeling data generated by GC/MS analysis were analyzed using the MATLAB-based software package isotopomer network compartmental analysis (INCA) (publicly available at http://mfa.vueinnovations.com) [10]. Isotopomer balances were simulated for CHO cell glycolytic and OPPP metabolism using an elementary metabolite unit (EMU) decomposition of the reaction network to simulate perturbations in isotope labeling induced by changes in

metabolic fluxes [11,12]. Table 6-1 details the network used here. All intracellular fluxes were calculated as a percentage of glucose uptake rate which was set to 100. Experimentally measured mass isotopomer distributions (MIDs) were regressed using a Levenberg-Marquardt optimization algorithm [13]. Fluxes were calculated from at least 50 unique restarts from random initial values to ensure a global minimum was obtained. Flux results were subjected to a chi-square statistical test to assess the goodness-of-fit, and 95% confidence intervals were calculated for each estimated flux [14].

Table 6-1 Metabolic model used for ^{13}C MFA with carbon rearrangements shown as lowercase letters. H6P represents six-carbon molecules G6P and F6P. T3P represents three-carbon molecules DHAP and GAP. P5P represents five-carbon Ru5P, R5P, and X5P. Lac.u is unlabeled lactate.

Reaction ID	Reactant(s)		Product(s)
R1	Glc (abcdef)	→	H6P (abcdef)
R2	H6P (abcdef)	→	T3P (cba) + T3P (def)
R3	H6P (abcdef)	→	CO_2 (a) + P5P (bcdef)
R4	P5P (abcde) + P5P (fghij)	→	T3P (hij) + S7P (fgabcde)
R5	S7P (abcdefg) + T3P (hij)	→	E4P (defg) + H6P (abchij)
R6	P5P (abcde) + E4P (fghi)	←→	T3P (cde) + H6P (abfghi)
R7	T3P (abc)	→	Lac (abc)
R8	Lac.u (abc)	→	Lac (abc)

6.3.4 Statistical analysis

The regressed fluxes from cell lines A and B were compared using Student's t-tests with a significance threshold of 5%. Where there was no significance found at the 5% confidence threshold, a 10% threshold was used.

6.4 Results

The raw lactate MIDs (Figure A- 6-1) were imported into a simplified metabolic model shown in Table 6-1 encompassing glycolytic and the OPPP metabolism. ^{13}C MFA revealed that

both cell lines A and B utilized the OPPP approximately equally throughout the experiment as shown in Figure 6-6. Cell line B trended toward a higher utilization of the OPPP than did cell line A; however, this trend was not statistically significant. The ratio of M1/M2 lactate labeling is constant between the two cell lines at each time point as shown in Figure 6-5. Reaction three (R3) (Table 6-1) flux indicated that the percentage of total glucose metabolized by the OPPP over time does not differ between the cell lines as shown by Figure 6-6.

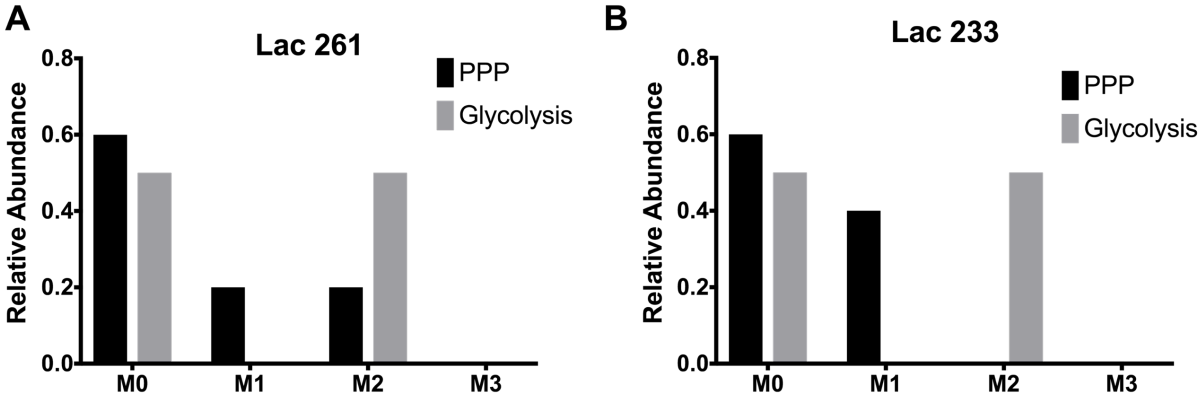

Figure 6-4 Predicted labeling of (A) Lac 261 and (B) Lac 233 fragments if [1,2-$^{13}C_2$] glucose is metabolized through glycolysis or OPPP to generate lactate.

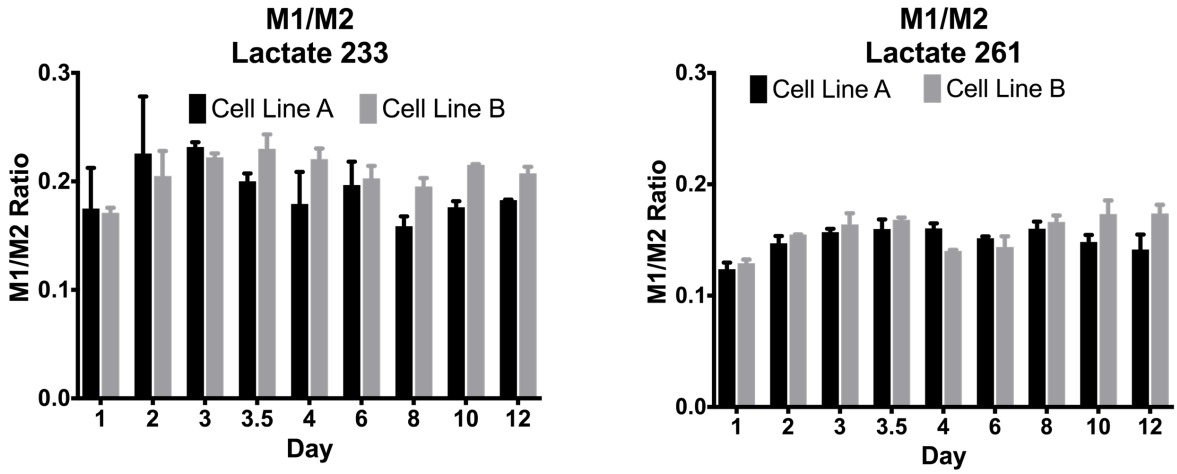

Figure 6-5 The ratio of M1 lactate over M2 lactate for both lactate fragments. There were no statistically significant differences between the two cell lines at any time.

6.5 Discussion and Future Directions

When glucose is consumed by CHO cells, it is primarily metabolized through glycolysis or the OPPP. CHO cell metabolism is inefficient, resulting in large quantities of lactate excreted as a metabolic waste product [15]. When CHO cells are fed a [1,2-$^{13}C_2$] glucose tracer, lactate produced by the cells will exhibit unique labeling patterns depending on which metabolic pathway metabolized the parent glucose molecule. If a glucose molecule is metabolized via glycolysis, no carbon atoms are lost resulting in lactate that mirrors the two halves of the consumed glucose—unlabeled (M0) if it originated from the last three carbons of glucose, or doubly labeled (M2) if it originated from the first three carbons of glucose (Figure 6-2). However, if a [1,2-$^{13}C_2$] glucose molecule is metabolized by the OPPP, the first carbon is lost as CO_2 in the first reaction of the OPPP. Only one ^{13}C atom per glucose molecule that enters the OPPP remained to produce lactate in later steps. Through the metabolic rearrangements depicted in Figure 6-3, lactate produced by this pathway may still contain two ^{13}C atoms; however, the fraction is lower (Figure 6-4). These distinctions in the lactate labeling yield a predictable labeling pattern of excreted lactate as shown in Figure 6-4. Therefore, ^{13}C MFA using the MID data of each cell line, the percentage of glucose metabolized through the OPPP was determined for each CHO cell line studied here (Figure 6-6). It is possible that both cell lines had excess capacity for $NADPH^+$ production, but that cell line A had increased Trx activity.

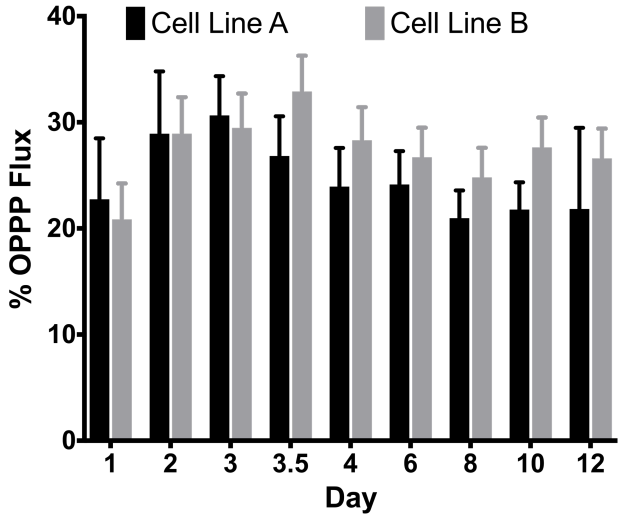

Figure 6-6 Utilization of oxidative pentose phosphate pathway (OPPP) metabolism as a percentage of overall glucose metabolism. Means +/- SEM plotted, n=2. SEM calculated by dividing reaction 3 (Table 6-1) flux's 95% confidence interval upper and lower bounds by 3.92.

Further study with either a combination of [1,2-$^{13}C_2$] glucose and [U-$^{13}C_6$] glucose, or if the cell lines are not using a glutamine synthetase (GS) expression system, parallel experiments with [1,2-$^{13}C_2$] glucose and [U-$^{13}C_5$] glutamine would yield a clearer metabolic model depicting the cell lines' central carbon metabolism. These tracer combinations, along with ample extracellular measurements would allow for comprehensive flux maps of central carbon metabolism. Furthermore, high ammonia production is a common metabolic inefficiency of CHO cell metabolism and high ammonia concentrations in the extracellular environment have also been linked to decreased quality metrics in protein products in mammalian cell culture [2,16]. The glutamate extracellular flux is significantly different between the two cell lines throughout the experiment. Glutamate excretion has been associated with high glutaminolysis and ammonia production [17]. This is corroborated by the trend in pH being lower in Cell Line A which has consistently higher glutamate excretion. This points to further metabolic discrepancies between the two cell lines, particularly in the TCA cycle.

Incomplete DS bond formation in the endoplasmic reticulum as a result of inefficient assembly of heavy and light chains could result in these reduced mAb species discovered in the cell culture medium of Cell Line A instead of degradation in the medium due to cellular components [5].

Furthermore, the pH differences in the two cell lines could contribute to product disruption. A more thorough analysis of extracellular fluxes would aid in building a more complete picture of cellular metabolism as well. Of the extracellular metabolites we have measurements for, they are not uniform between the two cell lines, indicating potential for greater metabolic variations between cell line A and cell line B than elucidated by our limited analysis.

6.6 Appendix

Table A- 6-1 Model goodness-of-fit assessment metrics as determined by INCA software and the best fit model at each time point. *indicates lack of fit in the model.

Day	Cell Line A			Cell Line B		
	DOF	SSR expected range	SSR best fit	DOF	SSR expected range	SSR best fit
0	2	0.1-7.4	3.87	2	0.1-7.4	5.37
1	2	0.1-7.4	0.09	2	0.1-7.4	0.22
2	2	0.1-7.4	0.92	2	0.1-7.4	7.21
3	2	0.1-7.4	0.44	2	0.1-7.4	2.41
3.5	2	0.1-7.4	0.68	2	0.1-7.4	7.9*
4	2	0.1-7.4	3.60	2	0.1-7.4	2.88
6	2	0.1-7.4	0.56	2	0.1-7.4	6.28
8	2	0.1-7.4	4.67	2	0.1-7.4	1.96
10	2	0.1-7.4	0.97	2	0.1-7.4	0.51
12	2	0.1-7.4	0.006	2	0.1-7.4	1.19

Table A- 6-2 Flux values at Day 0. Fluxes are reported as a percent of glucose uptake rate.

Reaction ID	Cell Line A			Cell Line B		
	Flux	LB	UB	Flux	LB	UB
R1	100	100	100	100	100	100
R2	0.903	1E-07	100	8.24	1.34	91.63
R3	297.29	3E-07	300	275.27	25.11	295.98
R4	99.10	1E-07	100	91.76	8.37	98.66
R5	99.10	1E-07	100	91.76	8.37	98.66
R6	99.10	1E-07	100	91.76	8.37	98.66
R7	1E-07	0	65535	176.91	0	6346.22
R8	1E-07	0	65535	235.01	0	65535

Table A- 6-3 Flux values at Day 1. Fluxes are reported as a percent of glucose uptake rate.

Reaction	Cell Line A			Cell Line B		
ID	Flux	LB	UB	Flux	LB	UB
R1	100	100	100	100	100	100
R2	92.42	88.10	95.83	93.06	90.74	95.19
R3	22.74	12.50	35.69	20.83	14.43	27.79
R4	7.58	4.17	11.90	6.94	4.81	9.26
R5	7.58	4.17	11.90	6.94	4.81	9.26
R6	7.58	4.17	11.90	6.94	4.81	9.26
R7	323.21	286.76	363.62	160.37	144.65	177.04
R8	11.46	0	76.15	24.45	7.40	80.77

Table A- 6-4 Flux values at Day 2. Fluxes are reported as a percent of glucose uptake rate.

Reaction	Cell Line A			Cell Line B		
ID	Flux	LB	UB	Flux	LB	UB
R1	100	100	100	100	100	100
R2	90.36	86.32	93.92	90.36	88.03	92.53
R3	28.92	18.23	41.03	28.91	22.42	35.90
R4	9.64	6.08	13.68	9.64	7.48	11.97
R5	9.64	6.08	13.68	9.64	7.48	11.97
R6	9.64	6.08	13.68	9.64	7.48	11.97
R7	177.37	153.91	202.72	116.92	104.22	130.35
R8	24.21	4.97	74.87	20.57	6.18	45.77

Table A- 6-5 Flux values at Day 3. Fluxes are reported as a percent of glucose uptake rate.

Reaction	Cell Line A			Cell Line B		
ID	Flux	LB	UB	Flux	LB	UB
R1	100	100	100	100	100	100
R2	89.78	87.29	92.10	90.18	88.01	92.21
R3	30.64	23.71	38.14	29.47	23.36	35.98
R4	10.22	7.90	12.71	9.82	7.79	11.99
R5	10.22	7.90	12.71	9.82	7.79	11.99
R6	10.22	7.90	12.71	9.82	7.79	11.99
R7	132.18	117.88	147.29	93.02	82.02	104.71
R8	26.85	10.14	57.97	38.26	16.88	90.65

Table A- 6-6 Flux values at Day 3.5. Fluxes are reported as a percent of glucose uptake rate.

Reaction	Cell Line A			Cell Line B		
ID	Flux	LB	UB	Flux	LB	UB
R1	100	100	100	100	100	100
R2	91.06	88.15	93.41	89.04	86.75	91.17
R3	26.82	19.77	34.48	32.89	26.50	39.74
R4	8.94	6.59	11.50	10.96	8.83	13.25
R5	8.94	6.59	11.50	10.96	8.83	13.25
R6	8.94	6.59	11.50	10.96	8.83	13.25
R7	149.68	133.34	167.12	94.17	83.08	105.83
R8	26.11	7.74	70.78	23.41	8.95	46.45

Table A- 6-7 Flux values at Day 4. Fluxes are reported as a percent of glucose uptake rate.

Reaction	Cell Line A			Cell Line B		
ID	Flux	LB	UB	Flux	LB	UB
R1	100	100	100	100	100	100
R2	92.02	89.52	94.30	90.57	88.47	92.54
R3	23.94	17.09	31.45	28.29	22.38	34.59
R4	7.98	5.70	10.48	9.43	7.46	11.53
R5	7.98	5.70	10.48	9.43	7.46	11.53
R6	7.98	5.70	10.48	9.43	7.46	11.53
R7	120.57	107.06	134.94	83.79	73.43	94.77
R8	36.42	14.44	121.39	25.46	9.67	56.51

Table A- 6-8 Flux values at Day 6. Fluxes are reported as a percent of glucose uptake rate.

Reaction	Cell Line A			Cell Line B		
ID	Flux	LB	UB	Flux	LB	UB
R1	100	100	100	100	100	100
R2	91.95	89.84	93.93	91.09	89.24	92.85
R3	24.24	18.21	30.48	26.72	21.46	32.29
R4	8.05	6.07	10.16	8.91	7.15	10.76
R5	8.05	6.07	10.16	8.91	7.15	10.76
R6	8.05	6.07	10.16	8.91	7.15	10.76
R7	90.13	79.46	101.34	67.45	59.22	76.06
R8	46.86	22.28	134.75	25.55	11.74	50.26

Table A- 6-9 Flux values at Day 8. Fluxes are reported as a percent of glucose uptake rate.

Reaction	Cell Line A			Cell Line B		
ID	Flux	LB	UB	Flux	LB	UB
R1	100	100	100	100	100	100
R2	93.01	91.24	94.68	91.73	89.85	93.48
R3	20.97	15.97	26.27	24.82	19.56	30.44
R4	6.99	5.32	8.76	8.27	6.52	10.15
R5	6.99	5.32	8.76	8.27	6.52	10.15
R6	6.99	5.32	8.76	8.27	6.52	10.15
R7	76.24	67.59	85.31	61.67	53.37	70.49
R8	37.30	16.66	112.23	54.22	25.22	182.79

Table A- 6-10 Flux values at Day 10. Fluxes are reported as a percent of glucose uptake rate.

Reaction	Cell Line A			Cell Line B		
ID	Flux	LB	UB	Flux	LB	UB
R1	100	100	100	100	100	100
R2	92.74	91.02	94.37	90.80	88.88	92.59
R3	21.78	16.89	26.95	27.61	22.22	33.35
R4	7.26	5.63	8.98	9.20	7.41	11.12
R5	7.26	5.63	8.98	9.20	7.41	11.12
R6	7.26	5.63	8.98	9.20	7.41	11.12
R7	57.55	49.62	65.96	58.53	50.27	67.28
R8	41.08	17.18	159.37	56.54	27.60	156.29

Table A- 6-11 Flux values at Day 12. Fluxes are reported as a percent of glucose uptake rate.

Reaction	Cell Line A			Cell Line B		
ID	Flux	LB	UB	Flux	LB	UB
R1	100	100	100	100	100	100
R2	92.72	86.10	96.79	91.13	89.24	92.90
R3	21.84	9.62	41.70	26.61	21.31	32.28
R4	7.28	3.21	13.90	8.87	7.10	10.76
R5	7.28	3.21	13.90	8.87	7.10	10.76
R6	7.28	3.21	13.90	8.87	7.10	10.76
R7	106.54	62.63	170.13	59.31	51.34	67.62
R8	36.16	9.18	65535	57.36	29.38	148.37

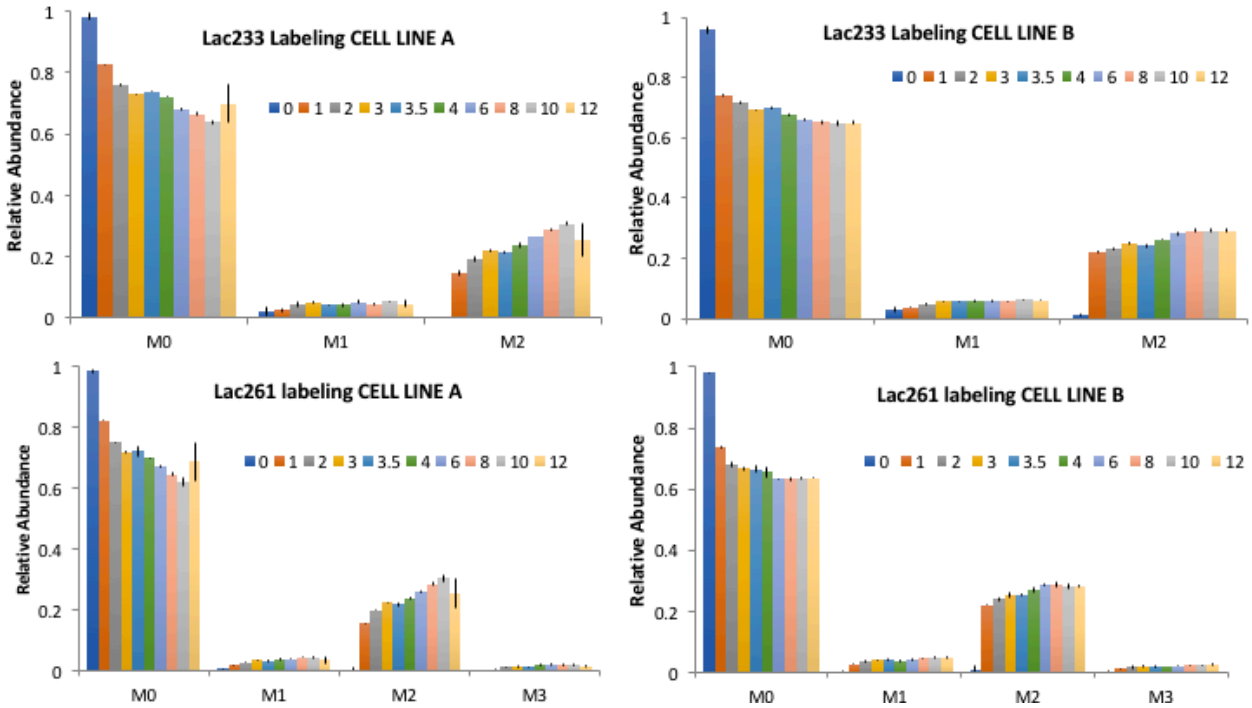

Figure A- 6-1 Lactate MIDs of both lactate fragments for each cell line. Labeling shown is corrected for natural ^{13}C abundances.

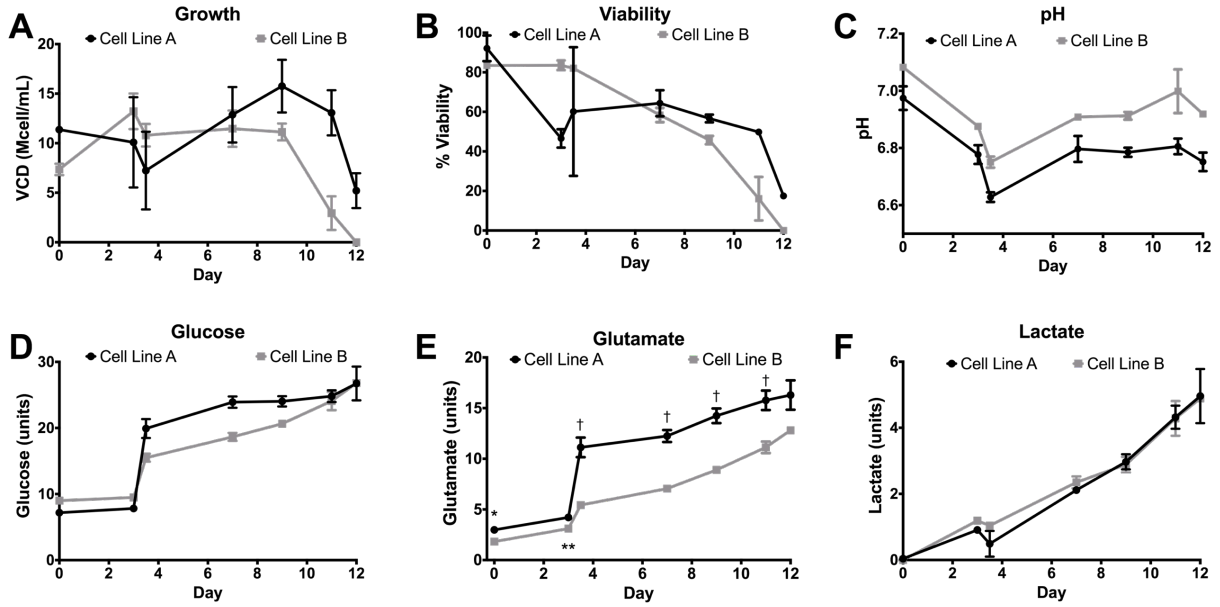

Figure A- 6-2 (A) Growth, (B) percent viability, (C) culture pH, (D) glucose profile, (E) lactate profile, and (F) glutamate profile over time. *Indicates significance at $\alpha<0.05$; ** $\alpha<0.01$; † $\alpha<0.1$.

6.7 References

[1] Walsh G. Biopharmaceutical benchmarks 2010. Nat Biotechnol 2010;28:1–10. doi:10.1038/nbt.3040.

[2] McAtee AG, Templeton N, Young JD. Role of Chinese hamster ovary central carbon metabolism in controlling the quality of secreted biotherapeutic proteins. Pharm Bioprocess 2014;2:63–74.

[3] Davies DR, Padlan E a, Segal DM. Three-dimensional structure of immunoglobulins. Annu Rev Biochem 1975;44:639–67. doi:10.1146/annurev.bi.44.070175.003231.

[4] Kao Y-H, Hewitt DP, Trexler-Schmidt M, Laird MW. Mechanism of antibody reduction in cell culture production processes. Biotechnol Bioeng 2010;107:622–32. doi:10.1002/bit.22848.

[5] Trexler-Schmidt M, Sargis S, Chiu J, Sze-Khoo S, Mun M, Kao Y-H, et al. Identification and prevention of antibody disulfide bond reduction during cell culture manufacturing. Biotechnol Bioeng 2010;106:452–61. doi:10.1002/bit.22699.

[6] Koterba KL, Borgschulte T, Laird MW. Thioredoxin 1 is responsible for antibody disulfide reduction in CHO cell culture. J Biotechnol 2012;157:261–7. doi:10.1016/j.jbiotec.2011.11.009.

[7] Gromer S, Urig S, Becker K. The Thioredoxin System - From Science to Clinic. Med Res Rev 2004;24:40–89. doi:10.1002/med.10051.

[8] Sheikholeslami Z, Jolicoeur M, Henry O. Elucidating the Effects of Postinduction Glutamine Feeding on the Growth and Productivity of CHO Cells. Biochem Eng J 2013;79:162–71. doi:10.1016/j.bej.2013.07.015.

[9] Templeton N, Dean J, Reddy P, Young JD. Peak antibody production is associated with

increased oxidative metabolism in an industrially relevant fed-batch CHO cell culture. Biotechnol Bioeng 2013;110:2013–24. doi:10.1002/bit.24858.

[10] Young JD. INCA: a computational platform for isotopically non-stationary metabolic flux analysis. Bioinformatics 2014;30:1333–5. doi:10.1093/bioinformatics/btu015.

[11] Antoniewicz MR, Kelleher JK, Stephanopoulos G. Elementary metabolite units (EMU): a novel framework for modeling isotopic distributions. Metab Eng 2007;9:68–86. doi:10.1016/j.ymben.2006.09.001.

[12] Young JD, Walther JL, Antoniewicz MR, Yoo H. An Elementary Metabolite Unit (EMU) Based Method of Isotopically Nonstationary Flux Analysis. Biotechnol Bioeng 2008;99:686–99. doi:10.1002/bit.

[13] Templeton N, Lewis A, Dorai H, Qian E a, Campbell MP, Smith KD, et al. The impact of anti-apoptotic gene Bcl-2Δ expression on CHO central metabolism. Metab Eng 2014;25:92–102. doi:10.1016/j.ymben.2014.06.010.

[14] Antoniewicz MR, Kelleher JK, Stephanopoulos G. Determination of confidence intervals of metabolic fluxes estimated from stable isotope measurements. Metab Eng 2006;8:324–37. doi:10.1016/j.ymben.2006.01.004.

[15] Lao MS, Toth D. Effects of ammonium and lactate on growth and metabolism of a recombinant Chinese hamster ovary cell culture. Biotechnol Prog 1997;13:688–91. doi:10.1021/bp9602360.

[16] Gawlitzek M, Ryll T, Lofgren J, Sliwkowski MB. Ammonium alters N-glycan structures of recombinant TNFR-IgG: degradative versus biosynthetic mechanisms. Biotechnol Bioeng 2000;68:637–46.

[17] Wahrheit J, Nicolae A, Heinzle E. Dynamics of growth and metabolism controlled by

glutamine availability in Chinese hamster ovary cells. Appl Microbiol Biotechnol 2013;98:1771–83. doi:10.1007/s00253-013-5452-2.

7 CONCLUSIONS

This dissertation provides several examples of the broad applicability of ^{13}C metabolic flux analysis (MFA) as a tool for biomanufacturing research. The literature has previously established that peak productivity in Chinese hamster ovary (CHO) cells occurs during stationary growth phase and involves up-regulation of oxidative mitochondrial metabolism [1,2]. This dissertation expands on these discoveries by utilizing ^{13}C MFA to quantify central carbon metabolism of industrial CHO cells under various experimental conditions related to oxidative metabolism. First, we engineered CHO cells to up-regulate oxidative metabolism to probe the link between high specific productivity (qP) and highly oxidative metabolic phenotype. We discovered that overexpressing a global regulator of mitochondrial biogenesis successfully increased the oxidative citric acid cycle (CAC) metabolic fluxes by roughly three-fold and increased qP by 2.6- to 5.2-fold over control cultures. Next, apoptosis-resistant CHO cells were discovered to shift their metabolism toward favorable lactate consumption, altered amino acid metabolism, and increased utilization of mitochondrial metabolism. Thirdly, CHO cells grown in a novel medium designed to significantly reduce the accumulation of the toxic byproduct ammonia, were studied and determined that the altered amino acid profile of the feed did not significantly alter central carbon metabolic phenotype while successfully decreasing ammonia accumulation by 40%. Lastly, CHO cells that were catalyzing product degradation in the extracellular culture medium were studied and determined that an increase in reducing power did not result from an increased utilization of oxidative pentose phosphate pathway (OPPP) metabolism. All of the studies described in this dissertation examine industrial CHO cell line metabolism as it relates to qP or product quality—both of central concern to the biomanufacturing industry.

7.1 Future Directions

CHO cells experience a fundamental shift in metabolic phenotype from exponential to stationary growth. This shift in metabolism signifies a switch in energy utilization from biomass production to mAb/product protein production. One hallmark of this phenotypic switch is an up-regulation of mitochondrial metabolism, specifically CAC flux. This dissertation details a study in which oxidative metabolism is constitutively up-regulated by the over-expression of the global regulator, PGC-1α. Constitutive overexpression of the mAb production phenotype seemingly inhibits culture VCD and overall volumetric productivity since the high productivity cultures are did not grow to equivalent high culture concentrations as that of the control. Therefore, efforts to induce the expression of the mAb production phenotype at the onset of stationary phase could benefit the culture both during exponential and stationary growth phases. Since the culture achieves maximum VCD during exponential phase, allowing the cultures to grow as normal without the burden of constitutive expression of an additional gene during the initial rapid growth phase would benefit overall possible volumetric titer potential. Therefore, an expression system that allows for induction of expression of the metabolic regulating protein would be ideal for turning on the desired peak production phenotype upon the switch to stationary phase—the phase naturally better equipped for peak production. One such inducible expression system is the cumate-gene switch which is activated by adding in cumate to the culture to activate the expression of the recombinant gene [3,4]. Alternatively, the self-regulated promoter *Txnip* has been used in CHO cells to express genes as culture growth slows [5]. It is currently unknown what exactly regulates *Txnip* promotion, but one study shows increased gene expression under the *Txnip* system increased over time, with certain clones activating at the onset of stationary phase [5]. This leads to the hypothesis that *Txnip* is regulated by some mechanism innately

programmed in CHO cells with a connection to the onset of stationary phase. More studies would be required to fully understand the mechanism of *Txnip* but it could potentially negate the requirement for small molecule addition for induction of regulatory gene expression in CHO cell cultures.

Furthermore, previous work shows that CHO cell metabolism directly affects the glycosylation profile of the mAbs they produce [6–9]. Glycosylation is an important post-translational modification required for proper folding, immunogenicity, protease sensitivity, efficacy, *in vivo* half-life, solubility, and thermal stability of recombinant therapeutic mAbs [6,10,11]. Current regulatory practices do permit product heterogeneity in glycan products, however demonstration of specific and reproducible glycosylation is required in order for approval to take a drug to market [12]. Due to the aforementioned importance of central carbon metabolism in mAb glycosylation profile and consistency, ^{13}C MFA can be used to characterize metabolic effects on glycosylation profile induced by expression of PGC-1α as described in Chapter 3 of this dissertation and any future studies of its inducible expression as proposed here. mAbs produced from the CHO cell clones studied can be purified via protein A affinity chromatography via HPLC and the purified mAb glycans can be labeled with 2-aminobenzamide (2-AB) for analysis on normal phase HPLC [8,13]. The structures can then be digested with specific enzymes and assigned to specific glycan structures found in the GlycoBase structure database. From this analysis, the glycan profiles of the mAbs produced via engineered CHO cell lines can be compared with those produced by control, non-engineered CHO cell lines. If differences in the resulting glycosylation profiles are detected as a direct result of recombinant PGC-1α expression, pool sizes of nucleotide precursors can be measured to determine if the PGC-1α over expression is responsible for altering the distribution of

nucleotides. If the pool sizes alter significantly due to recombinant PGC-1α expression, ^{13}C MFA can be utilized to determine how the labeling incorporation in the nucleotide-sugar precursors is altered and how it changes over time. This knowledge can provide rational engineering targets for further studies to regulate the glycosylation profiles of mAbs produced by CHO cell hosts.

7.2 Contribution

All studies presented within this dissertation demonstrate the usefulness of ^{13}C MFA in industrial CHO cells. The characterization of CHO cell metabolism under the influence of PGC-1α is perhaps this work's most valuable contribution to the field. This study provides evidence that researchers can induce a highly productive metabolic phenotype in producer CHO cell cultures to increase qP, and therefore, lower the cost of biotherapeutic drug production. Additionally, we performed the first ^{13}C MFA studies, to our knowledge, of media optimization and product degradation pathways in industrial CHO cells. Furthermore, this dissertation provides a unique example of how industrial-academic collaborations can investigate fundamental research questions while providing meaningful student training. All studies presented here were performed on industrial host CHO cell lines provided by an industrial partner for the purpose of studying a specific industrially relevant research question. Increasing CHO cell specific productivity is of utmost importance to the biopharmaceutical industry, and this work provides clear evidence for the usefulness of ^{13}C MFA in this endeavor.

7.3 References

[1] Templeton N, Smith KD, McAtee-Pereira AG, Dorai H, Betenbaugh MJ, Lang SE, et al. Application of 13C flux analysis to identify high-productivity CHO metabolic phenotypes. Metab Eng 2015;29:53–62. doi:10.1016/j.ymben.2017.01.008.

[2] Templeton N, Smith KD, McAtee-Pereira AG, Dorai H, Betenbaugh MJ, Lang SE, et al. Application of13C flux analysis to identify high-productivity CHO metabolic phenotypes. Metab Eng 2017;43:218–25. doi:10.1016/j.ymben.2017.01.008.

[3] Mullick A, Xu Y, Warren R, Koutroumanis M, Guilbault C, Broussau S, et al. The cumate gene-switch: a system for regulated expression in mammalian cells. BMC Biotechnol 2006;6:43. doi:10.1186/1472-6750-6-43.

[4] Gaillet B, Gilbert R, Broussau S, Pilotte A, Malenfant F, Mullick A, et al. High-level recombinant protein production in CHO cells using lentiviral vectors and the cumate gene-switch. Biotechnol Bioeng 2010;106:203–15. doi:10.1002/bit.22698.

[5] Le H, Vishwanathan N, Kantardjieff A, Doo I, Srienc M, Zheng X, et al. Dynamic gene expression for metabolic engineering of mammalian cells in culture. Metab Eng 2013;20:212–20. doi:10.1016/j.ymben.2013.09.004.

[6] Hossler P, Khattak SF, Li ZJ. Optimal and consistent protein glycosylation in mammalian cell culture. Glycobiology 2009;19:936–49. doi:10.1093/glycob/cwp079.

[7] Butler M. Optimisation of the Cellular Metabolism of Glycosylation for Recombinant Proteins Produced by Mammalian Cell Systems. Cytotechnology 2006;50:57–76. doi:10.1007/s10616-005-4537-x.

[8] Burleigh SC, van de Laar T, Stroop CJM, van Grunsven WMJ, O'Donoghue N, Rudd PM, et al. Synergizing metabolic flux analysis and nucleotide sugar metabolism to understand

the control of glycosylation of recombinant protein in CHO cells. BMC Biotechnol 2011;11:95. doi:10.1186/1472-6750-11-95.

[9] McAtee AG, Templeton N, Young JD. Role of Chinese hamster ovary central carbon metabolism in controlling the quality of secreted biotherapeutic proteins. Pharm Bioprocess 2014;2:63–74.

[10] Nam JH, Zhang F, Ermonval M, Linhardt RJ, Sharfstein ST. The effects of culture conditions on the glycosylation of secreted human placental alkaline phosphatase produced in Chinese hamster ovary cells. Biotechnol Bioeng 2008;100:1178–92. doi:10.1002/bit.21853.

[11] Wong NSC, Yap MGS, Wang DIC. Enhancing Recombinant Glycoprotein Sialylation Through CMP-Sialic Acid Transporter Over Expression in Chinese Hamster Ovary Cells. Biotechnol Bioeng 2006;93:1005–16. doi:10.1002/bit.

[12] Yuk IHY, Wang DIC. Changes in the overall extent of protein glycosylation by Chinese hamster ovary cells over the course of batch culture. Biotechnol Appl Biochem 2002;36:133–40. doi:10.1042/.

[13] Hong JK, Cho SM, Yoon SK. Substitution of glutamine by glutamate enhances production and galactosylation of recombinant IgG in Chinese hamster ovary cells. Appl Microbiol Biotechnol 2010;88:869–76. doi:10.1007/s00253-010-2790-1.